

WASHINGTON UNIVERSITY  
SEVER INSTITUTE OF TECHNOLOGY  
DEPARTMENT OF CIVIL ENGINEERING

---

ABSTRACT

---

TWO STRUCTURAL HEALTH MONITORING STRATEGIES BASED ON GLOBAL  
ACCELERATION RESPONSES: DEVELOPMENT, IMPLEMENTATION, AND VERIFICATION

by Juan Martin Caicedo

---

ADVISOR: Professor Shirley J. Dyke

---

May 2001

St. Louis, Missouri

---

In this thesis two structural health monitoring methodologies are developed and implemented. The first methodology uses the Natural Excitation Technique and the Eigensystem Realization Algorithm to identify the modal parameters of a structure. Then, a least squares solution of the eigenvalue problem is formulated for the calculation of the stiffness values. Damage is identified by comparing the stiffness of the undamaged structure with the damaged structure. Implementation issues are discussed herein. The method is verified through application of this method to the IASC-ASCE structural health monitoring benchmark problem.

The second methodology developed herein is based on component transfer functions. Interstory transfer functions of the structure are calculated using acceleration data. Damage in the structure is detected by identifying changes in these transfer functions. The extent of damage is obtained by comparing stiffness values of the damaged and undamaged structure. Stiffnesses are acquired using a nonlinear optimization technique. Experimental verification of this technique was performed in the Washington University Structural Control and Earthquake Engineering Lab.

Short Title: Structural Health Monitoring, Caicedo, M.S., 2001

To the people who always believe in me: my family.

# Contents

<b>Tables</b> .....	<b>vi</b>
<b>Figures</b> .....	<b>vii</b>
<b>Acknowledgments</b> .....	<b>ix</b>
<b>1 Structural Health Monitoring</b> .....	<b>1</b>
1.1 Natural Excitation Technique .....	3
1.2 Eigensystem Realization Algorithm .....	5
1.3 Benchmark Problem .....	7
1.4 Overview .....	9
<b>2 Background</b> .....	<b>12</b>
2.1 Stochastic processes .....	12
2.1.1 Classification of stochastic processes .....	14
2.1.2 Statistical properties of stochastic processes .....	15
2.1.3 Correlation function .....	18
2.1.4 Limit in the mean square .....	19
2.2 Natural Excitation Technique (NExT) .....	24
2.3 Eigensystem Realization Algorithm .....	27
2.4 Determination of the Stiffness Values .....	28
2.4.1 Least squares solution of eigenvalue problem .....	28
2.5 Summary .....	36
<b>3 Implementation of Proposed SHM Methodology</b> .....	<b>37</b>

3.1 Finite element models . . . . .	38
3.1.1 Structural model . . . . .	38
3.1.2 Generating data from analytical model . . . . .	41
3.1.3 Identification model . . . . .	43
3.2 Record length and number of points per frame . . . . .	45
3.2.1 Influence of record length on natural frequencies . . . . .	50
3.2.2 Influence of the records length on mode shapes . . . . .	52
3.2.3 Influence of the record length on damping . . . . .	53
3.2.4 Stiffness coefficients . . . . .	55
3.3 Spectral lines . . . . .	57
3.4 Sensor noise . . . . .	58
3.5 Modeling errors . . . . .	60
3.6 Summary . . . . .	61
<b>4 Application of Health Monitoring to Simulated Data . . . . .</b>	<b>63</b>
4.1 Benchmark problem definition . . . . .	64
4.1.1 Damage patterns . . . . .	64
4.1.2 Mass distribution . . . . .	67
4.1.3 Excitation cases . . . . .	68
4.1.4 Identification cases . . . . .	69
4.2 Solution to the benchmark problem . . . . .	70
4.3 Results . . . . .	71
4.3.1 Benchmark Problem Cases 1 through 3 . . . . .	72
4.3.2 Benchmark Problem Cases 4 and 5 . . . . .	76
4.3.3 Benchmark Problem Case 6 . . . . .	80
4.4 Summary . . . . .	83
<b>5 Component Transfer Function Technique . . . . .</b>	<b>85</b>
5.1 Motivation for the CTF Technique . . . . .	85

5.2 Component Transfer Function Technique.....	88
5.2.1 Determination of Experimental Component Transfer Functions .....	89
5.2.2 Identification of Natural Frequencies.....	90
5.2.3 Identification of stiffness coefficients .....	90
5.3 Experimental Verification.....	91
5.3.1 Experimental Results.....	92
5.4 Summary.....	97
<b>6 Conclusions and Future Work.....</b>	<b>98</b>
<b>References.....</b>	<b>102</b>
<b>Vita .....</b>	<b>106</b>

# Tables

TABLE 1-1.	Classification of Structural Health Monitoring Techniques. ....	2
TABLE 3-1.	Elements properties.....	40
TABLE 3-2.	Natural frequencies of exact and identified model (ERA) .....	50
TABLE 3-3.	Stiffness of structural and identified models. ....	50
TABLE 3-4.	Structural characteristics (1 DOF). ....	58
TABLE 3-5.	Identified and theoretical natural frequencies.....	59
TABLE 3-6.	Exact and identified stiffness (MN/m) of 12 and 120 DOF models. ....	61
TABLE 3-7.	Exact and identified natural freq. of 12 and 120 DOF models. ....	61
TABLE 4-1.	Natural frequencies for the undamaged structure and cases 1 and 2. ....	65
TABLE 4-2.	Identified Natural Frequencies for cases 1 through 3. ....	73
TABLE 4-3.	Identified stiffness coefficients (Cases 1, 2 and 3). ....	74
TABLE 4-4.	Loss in Stiffness Values for Cases 1 through 3. ....	76
TABLE 4-5.	Natural Frequencies for Cases 4 and 5. ....	78
TABLE 4-6.	Identified stiffness coefficients (cases 4 and 5).....	79
TABLE 4-7.	Natural Frequencies and Identified Stiffness Values in Case 6.....	82
TABLE 5-1.	Natural Frequencies of the Experimental and Analytical (Lumped Mass) Systems. ....	96
TABLE 5-2.	Identified Stiffnesses to Construct Analytical Model.....	96

# Figures

FIGURE 1-1. Hormiguero Bridge .....	6
FIGURE 1-2. Diagram of the Monitoring System. ....	7
FIGURE 2-1. Example of Random Process Ensemble .....	13
FIGURE 2-2. Lumped mass model of an n-story structure.....	29
FIGURE 2-3. Finite element .....	31
FIGURE 2-4. Bar element.....	33
FIGURE 2-5. Transformation of coordinates.....	34
FIGURE 2-6. Transformation of coordinates in the space.....	36
FIGURE 3-1. Benchmark structure .....	38
FIGURE 3-2. Analytical model.....	40
FIGURE 3-3. Force record (First floor) .....	42
FIGURE 3-4. Typical acceleration records. ....	43
FIGURE 3-5. Identification model .....	44
FIGURE 3-6. Cross-spectral density functions .....	46
FIGURE 3-7. Cross-spectral density functions of accelerations (1024 points) .....	47
FIGURE 3-8. Correlation functions .....	48
FIGURE 3-9. Singular values of Hankel matrix. ....	49
FIGURE 3-10. Mode shapes of structural and identified model (ERA). ....	49
FIGURE 3-11. Sensitivity of identified natural frequencies to implementation. ....	51
FIGURE 3-12. Sensitivity of natural frequencies .....	52
FIGURE 3-13. Sensitivity of mode shapes .....	53
FIGURE 3-14. Sensitivity of identified damping to implementation. ....	54

FIGURE 3-15. Sensitivity of damping ratio.....	55
FIGURE 3-16. Sensitivity of identified damping to implementation. ....	56
FIGURE 3-17. Sensitivity of stiffness.....	57
FIGURE 3-18. Sensitivity of total stiffness error to noise level. ....	59
FIGURE 4-1. Damage patterns .....	66
FIGURE 4-2. Asymmetric mass distribution .....	68
FIGURE 4-3. Excitations. ....	69
FIGURE 4-4. Representative Cross-spectral Density Function and Cross-correlation Functions (Case 1, Undamaged). ....	72
FIGURE 4-5. Stiffness Reduction of Each Floor in Damage Patterns for Cases 1 through 3. ....	75
FIGURE 4-6. Stiffness Reduction of Each Floor in Damage Patterns for Cases 4 and 5	77
FIGURE 4-7. Description of the Iterative Technique Used in Case 6. ....	80
FIGURE 4-8. Stiffness Reduction of Each Floor in All Damage Patterns for Case 6. ....	81
FIGURE 4-9. Conversion of Natural Frequencies for Damage Pattern 1. ....	82
FIGURE 5-1. Sample Component Transfer Functions of a Two Story Structure.....	86
FIGURE 5-2. Flow Chart for the Component Transfer Function Technique. ....	88
FIGURE 5-3. Column Distribution (Damaged Case). ....	91
FIGURE 5-4. Typical acceleration records. ....	93
FIGURE 5-5. Experimentally Determined Component Transfer Functions. ....	94
FIGURE 5-6. Frequency response function .....	95

## **Acknowledgments**

Many people have collaborated in one way or another to the development of this thesis. I express my gratitude to Dr. Shirley Dyke for her constant and unconditional support in the development of this work, and Dr. Erik Johnson for his valuable comments about the methods discussed in this thesis.

I also thank Gian Pietro Picco and Amy Murphy for their unchanging friendship. Without them my life in St. Louis would never have been the same. Finally I would like to thank all my family and Sinique Betancourt. They have been the motivation to complete my graduate studies.

# Chapter 1

## Structural Health Monitoring

After a major earthquake, hurricane, or other natural disaster, significant resources are required for inspecting the structural state of buildings and bridges. The predominant inspection method is manual, visual inspection. However, visual inspection is often complicated as structural elements are often covered by non-structural elements like walls and facades. Detecting damage in structural elements can also be performed using localized experimental methods such as radiographs, magnetic or ultrasonic methods. These methods are designed to detect localized damage, requiring that approximate damage locations be known *a priori*. Structural health monitoring (SHM) of civil structures using dynamic properties of structures has received significant recent attention by researchers.

Structural health monitoring is a new and exciting field. This class of methods are used to identify damage in structures using specialized sensors and computers. Two different types of methodologies are available to assess the health of structures, localized and global techniques. Localized techniques are used to identify the health of a structural member using technology such as X-rays and ultrasound. To use these techniques previous knowledge of the location of damage and direct access to the structural member are required. Global techniques use the dynamic characteristics of the structure to identify damage, its approximate location and its severity, reducing the need for manual inspection. Global techniques are very attractive to civil engineers because they can be used

without direct access to the structural members and no previous knowledge of damage of the structure is needed, reducing the time and cost to assess damage in a structure.

This thesis focuses on global techniques. From this point on the term structural health monitoring will refer to global techniques to identify damage in structures.

Structural health monitoring techniques can be categorized depending in various ways. For example, these techniques may be assigned one of 4 different levels based on their capabilities [34]. Level one techniques determine whether or not damage exists in a structure. Level two techniques determine the existence of damage, as well as its' location. Level three techniques identify the existence, location and severity of damage. Level four techniques identify the existence, location and severity of damage, as well as characterizing the remaining life of the structure. Health monitoring strategies may also be classified according to the data that they use, the user's knowledge of the excitation, or if an identification model is assigned. Table 1-1 describes some of the classes of techniques based on different parameters.

**TABLE 1-1. Classification of Structural Health Monitoring Techniques.**

<b>Parameter</b>	<b>Classification</b>
Level of identification	Level I: Existence of damage
	Level II: Existence of damage and location
	Level III: Existence of damage, location and quantification of damage
	Level IV: Existence of damage, location, quantification and life expectation of the structure
Data used	Time domain
	Frequency domain
Excitation	Known excitation
	Unknown excitation
Identification model	Structural model needed for identification
	No structural model needed for identification

Numerous techniques have been applied in the literature for health monitoring of structures. The report written by Doebling *et al* [14, 15] provides a thorough literature review in the field of structural health monitoring to 1996. Several methodologies are described in the report, including methods that use changes in the natural frequencies, changes in the mode shapes, measurements of flexibility, probabilistic measures, model-updating techniques, and neural network approaches. The report also discuss the application of structural health monitoring techniques to several structures including simple beams, trusses, plates, shells, frames, bridges, offshore platforms, and other civil and aerospace structures. Other overview papers on structural health monitoring techniques are provided by Ghanem and Shinozuka [20], Shinozuka and Ghanem [38], and Salawu [35].

The following sections provide a literature review of the most relevant techniques for this thesis. First, the background of the Natural Excitation Technique is discussed. Then, papers on the development and implementation of the Eigensystem Realization Algorithm are presented. Finally the IASC-ASCE Benchmark Problem in Structural Health Monitoring and some preliminary results from various researchers is provided.

## **1.1 Natural Excitation Technique**

Structural health monitoring and system identification techniques have been applied to a variety of structures such as airplanes, space shuttles and offshore oil platforms. Civil structures are a special subset of the systems on which these methodologies are applied. Unlike certain other systems, full-scale civil engineering structures can not easily be tested in a laboratory environment. Additionally, during on-site testing of full scale structures the excitation forces are difficult, if not possible, to measure. Using probabilistic approaches and signal processing techniques, researchers have been able to develop methodologies that are capable of identifying modal parameters (frequencies and mode shapes) of civil structures when the excitation is unknown. An example of such methodologies is the Natural Excitation Technique (NExT) developed by James *et*

*al* [21,22,23]. NExT is based on the fact that the cross correlation function of the acceleration responses and a reference acceleration signal satisfies the homogeneous differential equation of motion. Using this technique it is possible to obtain correlation functions, from responses to an unknown excitation, which may be treated as free vibration data. The unknown excitation should be broadband and stationary.

In 1993, James *et al* [21] used the technique for modal analysis of various structures. First, an analytical model of the DOE/Sandia vertical axis wind turbine was analyzed. This 34 meter testbed is located in Bushland, Texas, and is used to produce electricity by capturing the energy of the wind. The natural frequencies and damping ratios used to develop the analytical model were compared with the results obtained from NExT. The modal parameters obtained from NExT were in good agreement with the model parameters, demonstrating the capabilities of NExT. The method was also used to obtain modal parameters from the real turbine when the device was rotating. In addition to the analysis of the DOE/Sandia vertical axis wind turbine, modal analysis was also performed on a 19 meter FloWind Corporation vertical wind turbine. Accelerometers were used to collect data from the parked (not rotating) turbine. The results were compared with a recent modal testing and resulted in good agreement between the two tests. NExT was also used to test a tractor trailer vehicle. The method was used to extract modal parameters using acceleration data, obtaining the natural frequencies and damping frequencies of the system. A complete report of these tests and a description of NExT is discussed in references [22] and [23].

Farrar and James [18, 19] used NExT for modal analysis of the I-40 highway bridge over the Rio Grande river. Twenty six accelerometers were used to measure the vertical accelerations on a portion of the west bound bridge. The first six vertical natural frequencies of the bridge were obtained with NExT using ambient vibration induced by traffic. The natural frequencies and mode shapes were compared with the results obtained from a forced vibration test using a hydraulic shaker. The ratio between the

NExT results and the forced vibration test were as low as 0.901 for the first six natural frequencies, showing the capabilities of NExT for civil structures. A more detailed analysis of the bridge can be found in reference [18].

Beck *et al* [2] obtained the natural frequencies of the Robert A. Millikan Library at the California Institute of Technology using NExT and MODE-ID. NExT was used to obtain response data for the structure from ambient vibration data, and MODE-ID was used to estimate the modal parameters from the response data. In the first part of the paper the methods are used to identify the natural frequencies, mode shapes and damping ratios of a numerical model of the 6 story shear building. Base excitation was used in the numerical simulations. The modal parameters identified were in agreement with the modal parameters of the mathematical model. In the second part of the paper the results of the ambient vibration test made to 9 story Millikan Library are discussed. Velocity sensors were used. In the paper the first translational natural frequency in each direction (East-West and North-South) and the first torsional frequencies were found. These test were performed for data obtained as early as 1967 and as late as 1994 showing the changes of the natural frequencies of the structure over this time period.

## **1.2 Eigensystem Realization Algorithm**

The Eigensystem Realization Algorithm (ERA) was developed by Juang and Pappa [24]. This algorithm uses impulse response functions to obtain modal properties of multi-input multi-output (MIMO) systems. The algorithm may also be applied using free response data. Following a rigorous justification of the method the implementation of ERA to the identification of the modal parameters of the Galileo spacecraft is discussed. One hundred and sixty two accelerometers were used as input data to the method. Thirty four natural frequencies, mode shapes and damping ratios were obtained from the tests.

Juang and Pappa investigated the effect of noise on results obtained using the ERA in reference [25]. In this paper the authors used simulated data to show that noise in the data has a stronger effect in the higher modes than in the lower modes. Improvements in the identification process can be achieved by using model reduction. The authors also proposed a method to detect the correct singular value cutoff based on the distribution of the identifying natural frequencies in a set of different data.

The results of three large space structures identified using the ERA are shown in reference [31]. The results obtained in the Galileo spacecraft are discussed as well as the results obtained from a solar array and a space erectable truss model. The solar array had many natural frequencies below 1 Hz, testing the capabilities of ERA for long period structures with high modal density. This system was clearly identified as a nonlinear structure because the natural frequencies changed at different points of the free decay. In all three cases the ERA was able to successfully identify the natural frequencies of the structures.

Currently a bridge in Colombia, South America is being instrumented by the Universidad del Valle (see Fig. 1-1) [39,8]. Researchers will use the ERA and NeXT to identify



Courtesy Prof. Peter Thomson and Johannio Marulanda C.

**FIGURE 1-1. Hormiguero Bridge**

the natural frequencies of the structure using acceleration data. A telemetry system will be used to transmit the acceleration data from the bridge to the Universidad del Valle using FM waves. Figure 1-2 shows a flow chart of the telemetry system used. Initial

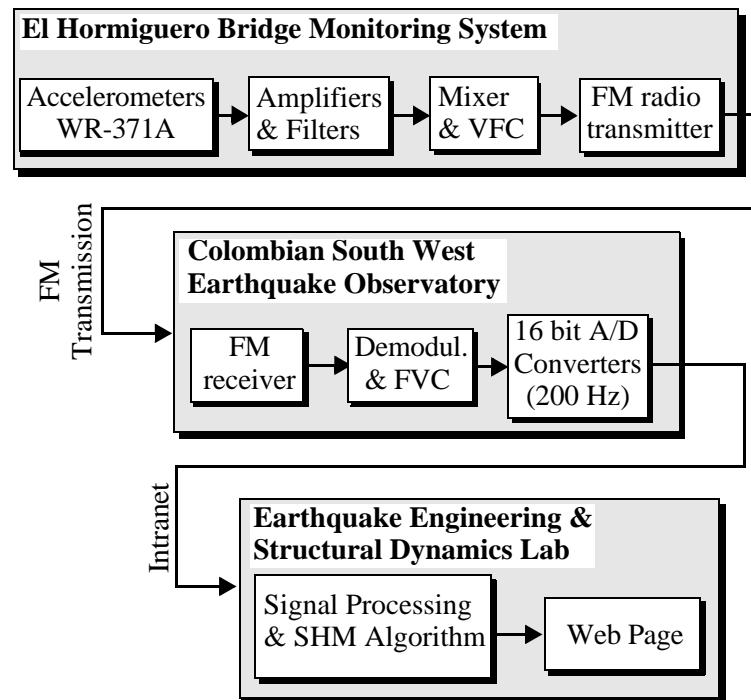


**FIGURE 1-2. Diagram of the Monitoring System.**

measurements with a portable system showed the efficacy of the structural health monitoring techniques by identifying the primary natural frequencies of the bridge [8]. The experience gained in this bridge will be used in the implementation of a structural health monitoring technique of the cable stay bridge located between Pereira and Dos Quebradas in Colombia, South America [39].

### 1.3 Benchmark Problem

The recent technological advances in sensors and computers has led to an interest in structural health monitoring techniques. These techniques have been applied to many structures in various environments, making it difficult to compare the advantages and

disadvantages of each technique. To compare and contrast the pros and cons of these techniques, a task group of the dynamics committee of the American Society of Civil Engineers (ASCE) joined with the International Association for Structural Control (IASC) to develop a benchmark problem in structural health monitoring <<http://wustl.ceel.cive.wustl.edu/asce.shm>> [26].

The first phase of the benchmark is based on analytical models of a 4 story steel building located at the University of British Columbia, Canada [5]. Two finite element models of the structure were developed [26]. Several excitation cases and damage patterns were defined to be solved for the researchers participants in the problem. The second phase of the benchmark problem is based on experimental results obtained from the real structure. The problem definition is currently under development [17].

Several groups of researchers have been working on phase I of the benchmark problem (simulated data). A special session about the problem was held at the 14th ASCE Engineering Mechanics Conference in 2000 and at the Joint ASME-ASCE Mechanics and Materials Conference in 2001. A special issue in the *Journal of Engineering Mechanics* is being prepared on this problem. The following paragraphs describe the work to-date on this problem.

Au *et al* [1] applied a two stage technique to solve the problem. First, NExT was used to obtain the modal properties of the system. Then, the physical parameters of the structure (mass and stiffness) were obtained using a Bayesian statistical approach to update a finite element model. Probability density functions (PDF) of the stiffness of the structure are obtained. Comparing the PDF of the stiffness system before and after damage it is possible to detect damage, its location and the severity in a probabilistic manner.

Katafygiotis *et al* [27] used a statistical modal updating methodology to solve the problem. The authors used a Bayesian methodology to obtain the PDF of the modal

parameters of the structure based on the time domain data. The optimal modal properties are obtained by maximizing the PDF. Then, the process is repeated to obtain the PDF of the physical properties of the structure to reproduce the modal parameters detected.

Bernal and Gunes [4] also solved the problem using a three-step methodology. In the first step the modal characteristics were identified. When the excitation input was available, an ERA with a Kalman observer was used. When the excitation input is not available, the subspace identification algorithm was utilized. The second step identifies the location of damage based on the identified flexibility matrix of the structure. The third step is performed for quantification of the damage. In this model a modal updating methodology is used to quantify the stiffness of each floor of the structure. Damage is quantified by comparing the undamaged with the damaged case.

Corbin *et al* [12] solved the benchmark problem using a wavelet approach. The authors generated a special set of data which spans the point in time at which damage occurs. Using their approach the authors were able to detect when damage occurs by searching for spikes in a wavelet decomposition of the acceleration data. Looking at the distribution of the spikes over the time for the different acceleration measurements the location of damage can be obtained. This paper did not address the quantification of damage.

Dyke *et al* [16] used a combination of NExT and ERA to detect damage in the structure. This thesis contains a greatly expanded version of this study and further details are not provided at this point.

## 1.4 Overview

In this thesis two health monitoring strategies will be developed and verified. The first structural health monitoring technique is developed by utilizing the Natural Excitation Technique and the Eigensystem Realization Algorithm in conjunction with a new

formulation of the least squares solution to the eigenvalue problem. This method is further examined to understand its capabilities and limitations with respect to noise and modeling errors. The second methodology is a new technique developed based on the component transfer functions of the structure. Experimental verification of this technique is performed.

Chapter 2 is dedicated to a description of NExT, ERA and the new formulation of the least square solution of the eigenvalue problem. The chapter begins with a brief introduction to stochastic processes and their properties. The spectral density function and correlation function for stationary processes are discussed, followed by a definition of the limit and derivative of stochastic processes in the mean square sense. In the next section NExT is developed using the concepts of stochastic processes discussed earlier. The ERA methodology is discussed in the following section. The chapter ends with the development of the least square solution of the eigenvalue problem. This section provides a new formulation of the problem used to estimate stiffness values of a structure based on measurements of natural frequencies and mode shapes.

Chapter 3 presents the results of a study of the implementation the first structural health monitoring technique. In this chapter a series of studies are done to study the sensitivity of this technique to various parameters. These studies are developed using the finite element model of the IASC-ASCE structural health monitoring benchmark problem. In the first part of this chapter a description of the finite element models and simulation programs used to generate the acceleration records is provided. In the following sections the different studies are presented. The first study discussed how the number of points in the calculation of the spectral density function affect the natural frequencies, mode shapes, damping ratios and stiffness values identified by the methodology. The second study tests of the results of this method are dependent on the value of the natural frequency as compared to the spectral lines. The effect of noise in the sensors is studied in the following section. The last study considers the effect of modeling errors. These errors are due

to the difference in the number of degrees of freedom in the identification model and the model representing the real structure.

To verify the technique, the methodology is applied to the IASC-ASCE benchmark problem and is presented in chapter 4. In the first part of this chapter a description of the damage patterns and identification cases is given. Then, the results obtained for each identification case are discussed.

The Component Transfer Function Technique is developed in Chapter 5. First the background of this technique is discussed. Then, to experimentally verify the technique, an experiment is performed in the Washington University Structural Control and Earthquake Engineering Lab. A four story structure was tested on the shake table. Damage is simulated by removing columns.

Chapter 6 discusses the conclusions of the research and provides some possibilities for future studies.

## Chapter 2

### Background

This chapter provides background information relevant to the structural health monitoring techniques used in this thesis to detect damage in structures. The methodology developed herein is categorized as level III (identification of the existence, location, and extent of damage). This approach does not require knowledge of the forces exciting the structure. Thus, it is applicable for structures experiencing ambient vibration. Previous knowledge of the mass of the structure is needed to identify stiffness coefficients.

Before discussing the methodology in detail, it is necessary to develop some concepts in stochastic processes. The first section of this chapter provides some background in stochastic processes, their statistical characteristics, and calculus in the mean square sense. These sections provide the necessary background for the subsequent discussion of the Natural Excitation Technique (NeXT) in section 2.2. NeXT is a tool that allows us to obtain crosscorrelation functions from ambient vibration records. Section 2.3 describes the Eigensystem Realization Algorithm (ERA), used to identify modal characteristics. The identification of structural parameters from modal characteristics is achieved through a least-squares optimization, which is discussed in section 2.4.

#### 2.1 Stochastic processes

Data can be classified as deterministic or random. A dynamic process whose value at any point in time is not random is called deterministic. An example of deterministic data

is the displacement of a structure subjected to a known input and initial conditions. This displacement can be calculated as the solution of the differential equation

$$\mathbf{M}\ddot{x}(t) + \mathbf{C}\dot{x}(t) + \mathbf{K}x(t) = F(t), \quad (2-1)$$

where  $\mathbf{K}$  is the stiffness matrix,  $\mathbf{C}$  the damping matrix,  $\mathbf{M}$  the mass matrix,  $F(t)$  the forcing vector, and  $x(t)$  denotes displacement. The operator  $(\dot{\quad})$  indicates the derivative with respect to time. Knowing the mass, damping, and stiffness of the structure, it is possible to obtain the displacements, velocities and accelerations of the structure at every time  $t$  for a specified set of initial conditions.

Processes that have a random value at each point in time are called random, or stochastic. Forces applied to a structure due to ambient vibrations like traffic loads in a bridge or wind forces in a tall structure are modeled as random. One possible realization of a random process is called a sample function. The set of all possible sample functions obtained from a random process is called an ensemble, as shown in Fig. 2-1. Random processes are described in terms of probabilistic expressions.

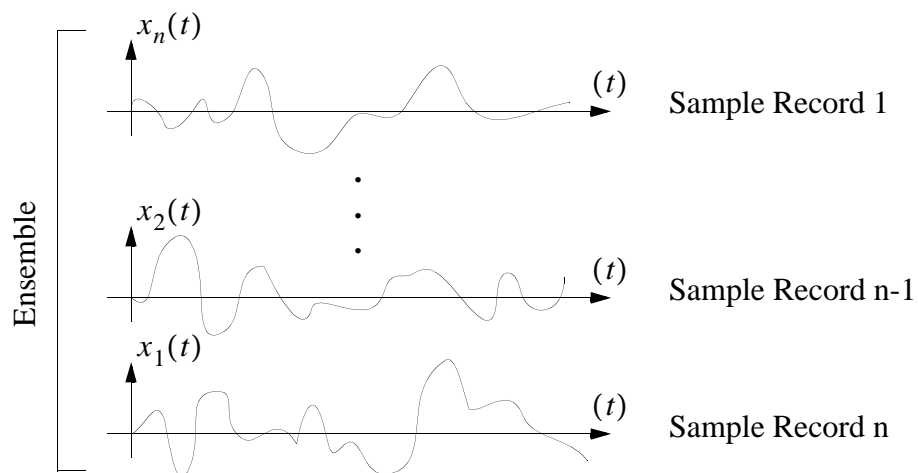


**FIGURE 2-1. Example of Random Process Ensemble**

Stochastic processes are an important tool in the field of system identification and health monitoring of civil structures. The classification of stochastic processes and their basic properties are discussed in next sections. For further details regarding stochastic processes, see Lutes and Sarkani [28], Bendat and Piersol [3], and Papoulis [30].

### 2.1.1 Classification of stochastic processes

Stochastic processes can be classified as either stationary or non-stationary. Stationary random processes have constant statistical properties over time. For example, for the random process,  $X(t)$ , two important statistical properties are the mean,  $\mu_X(t)$ , and the auto-correlation function,  $R_{XX}(t, t + \tau)$ , which are defined as

$$\mu_X(t) = \lim_{N \rightarrow \infty} \frac{1}{N} \sum_{k=1}^N x_k(t), \quad (2-2)$$

$$R_{XX}(t, t + \tau) = \lim_{N \rightarrow \infty} \frac{1}{N} \sum_{k=1}^N x_k(t)x_k(t + \tau). \quad (2-3)$$

When the mean  $\mu_X(t)$  of a stochastic process is constant and less than infinity, and its auto-correlation function  $R_{XX}(t, t + \tau)$  is dependent only on the time interval  $\tau$ , the stochastic process is called weakly stationary. Weakly stationary processes play an important role in the field of structural dynamics, random vibrations, and signal processing. The assumption of weakly stationarity has been used to study many physical processes. Example of weakly stationary processes are band-limited white noise, rectangular pulse, and binary noise [28]. Some natural phenomena can be modeled as stationary over a specific period of time. For example, traffic loads in a cable-stay bridge in rush hour, where the number of cars and speed are almost constant can be modeled as a stationary random process. Another example of stationary random phenomenon is wind loads

applied to a tall building during a storm. An example of a non-stationary random process is the forces applied to structures by earthquakes.

## 2.1.2 Statistical properties of stochastic processes

In this section the spectral density function and the correlation function are discussed. Although all statistical properties are useful in engineering applications, these two are the main properties used in the structural health monitoring methodology described in this thesis.

### 2.1.2.1 Spectral density function

The spectral density function is a powerful tool for the analysis of stationary random processes. For stationary processes, the spectral density function shows the variation of the mean square value  $\psi_X^2$  with respect to the frequency  $f$ . For a weakly stationary random process the cross-spectral density function  $S_{XY}(f)$  between the stochastic processes  $X(t)$  and  $Y(t)$  can be calculated in two ways [3]: i) from correlation functions; and, ii) using finite Fourier transforms of sample records. Using the same procedures it is possible to determine the auto-spectral density functions  $S_{XX}(f)$  and  $S_{YY}(f)$ .

### Spectral density function from correlation function

For two weakly stationary random processes  $X(t)$  and  $Y(t)$ , the two-sided cross-spectral density function  $S_{XY}(f)$  can be defined as the Fourier transform of the cross-correlation function  $R_{XY}(\tau)$

$$S_{XY}(f) = \int_{-\infty}^{\infty} R_{XY}(\tau) e^{-j2\pi f\tau} d\tau, \quad (2-4)$$

In the case of discrete data Eq. (2-4) is expressed as

$$S_{XY}(n) = \frac{1}{N} \sum_{k=1}^N R_{XY}(k) e^{\frac{-j2\pi nk}{N}}, \quad (2-5)$$

where  $N$  is the number of points of the cross correlation function  $R_{XY}(k)$ .

Similarly, the auto-spectral density function  $S_{XX}(f)$  can be defined as

$$S_{XX}(f) = \int_{-\infty}^{\infty} R_{XX}(\tau) e^{-j2\pi f\tau} d\tau, \quad (2-6)$$

or in discrete form

$$S_{XX}(n) = \frac{1}{N} \sum_{k=1}^N R_{XX}(k) e^{\frac{-j2\pi nk}{N}}. \quad (2-7)$$

To obtain spectral density functions from the correlation function it is necessary that the correlation function exist. It is also necessary to satisfy

$$\int_{-\infty}^{\infty} R_{XY}(\tau) d\tau < \infty, \quad (2-8)$$

which is true for finite records.

**Spectral density function from finite Fourier transform of sample records.**

Spectral density functions can be also obtained from finite Fourier transform of sample records. Suppose that  $x_i(t)$  and  $y_i(t)$  are the  $i$ -th sample record of the stochastic processes  $X(t)$  and  $Y(t)$ . For the interval  $0 < t < t_1$  of the sample records define

$$S_{XY}(f, t_1, i) = \frac{1}{T} \hat{X}_i^*(f, t_1) \hat{Y}_i(f, t_1), \quad (2-9)$$

where the  $( )^*$  operator denotes complex conjugate.  $\hat{X}_i(f, t_1)$  and  $\hat{Y}_i(f, t_1)$  are Fourier transform of  $x_i(t)$  and  $y_i(t)$ , respectively, for the interval  $0 < t < t_1$ , given by

$$\hat{X}_i(f, t_1) = \int_0^{t_1} x_i(t) e^{-j2\pi ft} dt, \quad (2-10)$$

$$\hat{Y}_i(f, t_1) = \int_0^{t_1} y_i(t) e^{-j2\pi ft} dt. \quad (2-11)$$

The cross-spectral density function  $S_{XY}(f)$  is obtained as the expectation of  $S_{XY}(f, t_1, i)$  when  $t_1$  goes to infinity. In mathematical format  $S_{XY}(f)$  is

$$S_{XY}(f) = \lim_{t_1 \rightarrow \infty} E[S_{XY}(f, t_1, i)], \quad (2-12)$$

where  $E[ ]$  denotes expectation over the ensemble index  $i$ . Using a similar procedure it is possible to obtain the auto-spectral density functions  $S_{XX}(f)$  and  $S_{YY}(f)$ .

When data records are used to estimate spectral density functions using this method, it is possible to break a record into smaller sections. This results in a better estimation of the spectral density function through averaging.

### 2.1.3 Correlation function

Another important concept for random processes is the correlation function. The cross-correlation function between the stochastic processes  $X(t)$  and  $Y(t)$  is defined as

$$R_{XY}(t, t + \tau) = E[X(t)Y(t + \tau)]. \quad (2-13)$$

Two stochastic processes are uncorrelated when the correlation function  $R_{XY}(t, t + \tau)$  is constant for all  $(t, t + \tau)$  and equal to the product of the means  $\mu_X\mu_Y$ . Similarly, the auto-correlation function of the stochastic process  $X(t)$  is defined as

$$R_{XX}(t, t + \tau) = E[X(t)X(t + \tau)] \quad (2-14)$$

For the case of weakly stationary processes, the auto-correlation and cross-correlation functions are only dependent on  $\tau$ , or

$$R_{XX}(t, t + \tau) = R_{XX}(\tau) \quad (2-15)$$

$$R_{XY}(t, t + \tau) = R_{XY}(\tau). \quad (2-16)$$

Several methods can be used to estimate correlation functions. One of them is through Eq. (2-3), where the correlation function is calculated from data records. Another method to calculate the correlation function is via the spectral density function. Based

on Eq (2-4), the correlation function can be calculated as the inverse Fourier transform of the spectral density function

$$R_{XY}(\tau) = \int_{-\infty}^{\infty} S_{XY}(f) e^{j2\pi f\tau} df, \quad (2-17)$$

where  $S_{XY}(f)$  is the two side cross-spectral density function between the stochastic processes  $X(t)$  and  $Y(t)$ . In the case of discrete data Eq (2-17) can be written using the discrete fast Fourier transform

$$R_{XY}(n) = \frac{1}{N} \sum_{k=1}^N S_{XY}(k) e^{\frac{j2\pi nk}{N}} \quad (2-18)$$

Using cross-spectral density functions to calculate cross-correlation functions has the advantages of filtering and averaging presented in calculation of the cross-spectral density function.

In these sections some important statistical properties of stochastic processes have been described. These concepts are the basic tools used in many structural health monitoring techniques. For a better understanding of the structural health monitoring methodologies described in here it is also necessary to present mean square calculus (the calculus of stochastic processes). The following sections will define the limit, continuity, and derivative of a stochastic process in the mean square sense.

#### **2.1.4 Limit in the mean square**

Mean square calculus is a useful tool for engineering applications involving random processes. The power of mean square calculus lies in the fact that operations similar to

classical calculus can be developed for stochastic processes. This allows engineers to employ the differential equations developed for deterministic data in the solution of stochastic processes. Calculus in the mean square sense can only be applied to second order stochastic processes. These processes have norm squares less than infinity

$$\|X(t)\|^2 < \infty, \quad (2-19)$$

where  $\| \cdot \|$  denotes norm. The norm of the stochastic process  $X(t)$  is defined as

$$\|X(t)\| = \sqrt{E[X(t)X(t)]}. \quad (2-20)$$

Unless otherwise indicated, the stochastic processes discussed in this section will be second order stochastic processes.

The limit in the mean square (l.i.m.) for a stochastic process  $X(t)$  is defined as

$$\begin{aligned} \text{l.i.m. } X_n(t) &= X(t) \\ n &\rightarrow \infty \end{aligned} \quad (2-21)$$

where

$$\begin{aligned} \lim_{n \rightarrow \infty} \|X_n(t) - X(t)\| &= 0. \end{aligned} \quad (2-22)$$

Note that in Eq. (2-22) “lim” (with no periods) denotes limit in the ordinary sense. One important property of the l.i.m. is the fact that the expectation of a l.i.m. is equal to the limit of the expectation of the random process. This is

$$E \left\{ \text{l.i.m.}_{n \rightarrow \infty} X_n(t) \right\} = \lim_{n \rightarrow \infty} E \{ X_n(t) \}. \quad (2-23)$$

This property plays an important role in the relation between the derivative of the correlation function of  $X(t)$  and the correlation function of  $\dot{X}(t)$ , which will be determined in a later section.

#### 2.1.4.1 Continuity in the mean square sense.

Before defining the derivative in the mean square sense of a stochastic process, it is necessary to define continuity in the mean square sense. Let  $R(t, t + \tau)$  be the correlation function of a second order stochastic process  $X(t)$ . If  $R(t, t + \tau)$  is continuous at  $(t, t)$  in the ordinary sense, the stochastic process  $X(t)$  is mean square continuous at  $t$ . For the case of a weakly stationary process, the correlation function is

$$R(t, t + \tau) = R(\tau). \quad (2-24)$$

Using this equation, it is clear that weakly stationary process are continuous in the mean square sense if  $R(\tau)$  is continuous at  $\tau = 0$ .

#### 2.1.4.2 Differentiation in mean square

For the continuous second order stochastic process  $X(t)$  the derivative in the mean square sense is defined as

$$\text{l.i.m.}_{\varepsilon \rightarrow 0} \frac{X(t + \varepsilon) - X(t)}{\varepsilon} = \dot{X}(t). \quad (2-25)$$

For the purpose of this thesis, we are especially interested in the derivative of the correlation function of random processes. Consider the correlation function between two stochastic processes  $\dot{X}(t)$  and  $Y(t)$ ,

$$R_{\dot{X}Y}(t, t + \tau) = E\{\dot{X}(t)Y(t + \tau)\}. \quad (2-26)$$

Using Eq. (2-25) we can write Eq. (2-26) as

$$R_{\dot{X}Y}(t, t + \tau) = E\left[\text{l.i.m.}_{\varepsilon \rightarrow 0} \left[ \frac{X(t + \varepsilon) - X(t)}{\varepsilon} \right] Y(t + \tau) \right]. \quad (2-27)$$

Using Eq. (2-23) it is possible to write Eq. (2-27) as

$$R_{\dot{X}Y}(t, t + \tau) = \lim_{\varepsilon \rightarrow 0} \frac{1}{\varepsilon} E[X(t + \varepsilon)Y(t + \tau) - X(t)Y(t + \tau)]. \quad (2-28)$$

Using the property  $E[A(t) + B(t)] = E[A(t)] + E[B(t)]$  for the stochastic processes  $A$  and  $B$ , Eq. (2-28) can be written as

$$R_{\dot{X}Y}(t, t + \tau) = \lim_{\varepsilon \rightarrow 0} \frac{1}{\varepsilon} (E[X(t + \varepsilon)Y(t + \tau)] - E[X(t)Y(t + \tau)]), \quad (2-29)$$

using Eq. (2-14)

$$R_{\dot{X}Y}(t, t + \tau) = \lim_{\varepsilon \rightarrow 0} \frac{1}{\varepsilon} [R_{XY}(t + \varepsilon, t + \tau) - R_{XY}(t, t + \tau)], \quad (2-30)$$

$$R_{\dot{X}Y}(t, t + \tau) = \frac{\partial}{\partial t} R_{XY}(t, t + \tau) . \quad (2-31)$$

It is clear that Eq. (2-31) can be expanded to the general equation

$$R_{X^{(n)}Y^{(m)}}(t, t + \tau) = \frac{\partial^{(n+m)}}{\partial t^n \partial s^m} R_{XY}(t, t + \tau) . \quad (2-32)$$

In the case of stationary processes the correlation function is described by the following equation

$$R_{XY}(\tau) = E[X(t)Y(t + \tau)] = E[X(t - \tau)Y(t)] . \quad (2-33)$$

Using the derivative of  $X(t)$  we obtain

$$R_{\dot{X}Y}(\tau) = E[\dot{X}(t)Y(t + \tau)] = E[\dot{X}(t - \tau)Y(t)] \quad (2-34)$$

$$R_{\dot{X}Y}(\tau) = - \frac{\partial}{\partial \tau} R_{XY}(\tau) \quad (2-35)$$

Extending this idea to weakly stationary random process, the correlation function of the derivative in the mean square can be written as

$$R_{X^{(n)}Y^{(m)}}(t, t + \tau) = R_{X^{(n)}Y^{(m)}}(\tau) = (-1)^m \frac{\partial^{(n+m)}}{\partial \tau^{(n+m)}} R_{XY}(\tau) \quad (2-36)$$

The last derivation is an important concept for the understanding of the Natural Excitation Technique (NExT). This technique allow us to calculate correlation functions from forced vibration records. NExT is described in the following section.

## 2.2 Natural Excitation Technique (NExT)

The Natural Excitation Technique was developed by George H. James III *et al.* in 1992 [21]. This technique has been effective in the identification of structural modal parameters in different type of civil structures using ambient vibration. Numerical studies have been conducted by Dyke *et al.* [16] and Caicedo *et al.* [7] showing the capabilities of the technique on the benchmark structure proposed by the IASC-ASCE Task Group on Structural Health Monitoring Benchmark Problems [26] (see also: <http://wusceel.cive.wustl.edu/asce.shm/>).

Experimental studies have also demonstrated the advantages of the technique. Beck *et al* [2] used NExT to obtain the modal parameters of the Robert A. Millikan Library located on the California Institute of Technology. In this study two lateral and one rotational natural frequencies of the nine story building were found, using a total of six accelerometers. Farrar and James [19] used NExT to determine natural frequencies and mode shapes of a portion of a highway bridge. This bridge spans the Rio Grande river along the former I-40 highway.

NExT is used to obtain correlation functions from forced vibration records, which constitute the first step of the structural health monitoring methodology discussed in this thesis. NExT is based on the fact that a structure excited with ambient vibration, the correlation function between different sensors with respect to a reference sensor solve the homogeneous differential equation. This requires that the excitation force as well as the response of the structure can be modeled as second order stationary random processes. Also, the reference signal should be uncorrelated with respect to the excitation of the structure.

Consider the differential equation of motion for a multiple degree of freedom structure

$$\mathbf{M}\ddot{\mathbf{x}}(t) + \mathbf{C}\dot{\mathbf{x}}(t) + \mathbf{K}\mathbf{x} = \mathbf{f}(t) \quad (2-37)$$

where  $\mathbf{M}$  is the mass matrix,  $\mathbf{C}$  is the damping matrix and  $\mathbf{K}$  is the stiffness matrix that describe the structure,  $\mathbf{x}(t)$ ,  $\dot{\mathbf{x}}(t)$  and  $\ddot{\mathbf{x}}(t)$  are vectors of displacement, velocity and acceleration, and  $\mathbf{f}(t)$  is a vector describing the forces applied to the structure.

Assuming that the forces applied to the structure as well as its displacement, velocity and acceleration are second order stationary random processes, we can write Eq. (2-37) as

$$\mathbf{M}\ddot{\mathbf{X}}(t) + \mathbf{C}\dot{\mathbf{X}}(t) + \mathbf{K}\mathbf{X}(t) = \mathbf{F}(t) \quad (2-38)$$

where  $\mathbf{X}(t)$ ,  $\dot{\mathbf{X}}(t)$ ,  $\ddot{\mathbf{X}}(t)$  are vectors of stochastic process describing the displacement, velocity, acceleration of the structure, and  $\mathbf{F}(t)$  is a vector of stochastic process of forces applied to the structure. Post multiplying Eq. (2-38) by a reference signal  $x_i(t)$  and obtaining the expectation of the differential equation we obtain

$$\mathbf{M}\ddot{\mathbf{X}}(t)x_i(t-\tau) + \mathbf{C}\dot{\mathbf{X}}(t)x_i(t-\tau) + \mathbf{K}\mathbf{X}(t)x_i(t-\tau) = \mathbf{F}(t)x_i(t-\tau), \quad (2-39)$$

$$\begin{aligned} \mathbf{M}E[\ddot{\mathbf{X}}(t)x_i(t-\tau)] + \mathbf{C}E[\dot{\mathbf{X}}(t)x_i(t-\tau)] + \mathbf{K}E[\mathbf{X}(t)x_i(t-\tau)] = \\ E[\mathbf{F}(t)x_i(t-\tau)] \end{aligned} \quad (2-40)$$

Assuming that  $\mathbf{F}(t)$  is a white noise process (delta-correlated) [28],  $\mathbf{F}(t)$  and  $x_i(t-\tau)$  are uncorrelated for all  $\tau > 0$ , and the means of  $x_i(t-\tau)$  and  $\mathbf{F}(t)$  are zero, we can write Eq. (2-40) in the following form

$$\mathbf{M}\mathbf{R}_{XX_i}(\tau) + \mathbf{C}\mathbf{R}_{XX_i}(\tau) + \mathbf{K}\mathbf{R}_{XX_i}(\tau) = 0 \quad (2-41)$$

for  $\tau > 0$ , where  $\mathbf{R}_{XX_i}(\tau)$  is a vector of correlation functions between the displacement vector, and the reference signal. Using the property of the derivative of the correlation function described in Eq. (2-36) we can write Eq. (2-41) as

$$\mathbf{M}\dot{\mathbf{R}}_{XX_i}(\tau) + \mathbf{C}\dot{\mathbf{R}}_{XX_i}(\tau) + \mathbf{K}\mathbf{R}_{XX_i}(\tau) = 0 \quad (2-42)$$

Equation (2-42) shows that the vector of correlation functions between the displacements and one reference signal satisfies the homogeneous equation of motion for positive  $\tau$ . This result is valid when input forces and the displacements are uncorrelated. It can be shown that this is also valid for records of accelerations. Taking the fourth derivative with respect to time of Eq. (2-42) we obtain

$$\frac{\partial}{\partial t^4}[\mathbf{M}\ddot{\mathbf{R}}_{XX_i}(\tau) + \mathbf{C}\dot{\mathbf{R}}_{XX_i}(\tau) + \mathbf{K}\mathbf{R}_{XX_i}(\tau)] = 0 \quad (2-43)$$

$$\mathbf{M}\ddot{\mathbf{R}}_{\ddot{X}\ddot{X}_i}(\tau) + \mathbf{C}\dot{\mathbf{R}}_{\ddot{X}\ddot{X}_i}(\tau) + \mathbf{K}\mathbf{R}_{\ddot{X}\ddot{X}_i}(\tau) = 0. \quad (2-44)$$

Thus, the matrix of correlation functions satisfies the homogeneous differential equation of motion for a multiple DOF system. In other words, the correlation functions between the acceleration signals and a reference signal can be treated as free vibration data. This correlation function can be obtained from forced vibration records if the force is uncorrelated with the acceleration measurements and the acceleration is stationary. Once free vibration data is obtained from the structure it is possible to determine modal characteristics of the structure using the Eigensystem Realization Algorithm (ERA).

## 2.3 Eigensystem Realization Algorithm

Numerous techniques available for identifying the modal parameters from the free response data [14,15]. Here the eigensystem realization algorithm (ERA) [24,25,31] is adopted because it is quite effective for identification of lightly damped structures and is applicable to multi-input/multi-output systems. In the eigensystem realization algorithm, the Hankel matrix is formed

$$\mathbf{H}(p-1) = \begin{bmatrix} \mathbf{x}(p) & \mathbf{x}(p+1) & \dots & \mathbf{x}(p+m) \\ \mathbf{x}(p+1) & \dots & & \\ \dots & & & \\ \mathbf{x}(p+r) & \dots & & \mathbf{x}(p+m+r) \end{bmatrix} \quad (2-45)$$

where  $x(p)$  is the response vector at the  $p$ -th time step. The parameters  $m$  and  $r$  correspond to the number of columns and rows (of response vectors) in the matrix. For good results,  $r$  should be selected to be approximately 10 times the number of modes to be identified, and  $m$  should be selected to be approximately 5 times  $r$  [25]. The Hankel matrix is evaluated for  $\mathbf{H}(0)$  and a singular value decomposition is performed as

$$\mathbf{H}(0) = \mathbf{P}\mathbf{D}\mathbf{Q}^T. \quad (2-46)$$

Relatively small singular values along the diagonal of  $\mathbf{D}$  correspond to computational modes. The rows and columns associated with computational modes are eliminated to form the condensed version of these matrices  $\mathbf{D}_N$ ,  $\mathbf{P}_N$ , and  $\mathbf{Q}_N$ . The state space matrices for the resulting discrete-time system are found using [24]

$$\hat{\mathbf{A}} = \mathbf{D}_N^{-\frac{1}{2}} \mathbf{P}_N^T \mathbf{H}(1) \mathbf{Q}_N \mathbf{D}_N^{-\frac{1}{2}}, \quad \hat{\mathbf{B}} = \mathbf{D}_N^{-1/2} \mathbf{Q}_N^T E_m, \quad \hat{\mathbf{C}} = \mathbf{E}_n^T \mathbf{P}_N \mathbf{D}_N^{-\frac{1}{2}}, \quad (2-47)$$

where  $\mathbf{E}_r^T = [\mathbf{I}_r \ 0]$  and  $\mathbf{E}_m^T = [\mathbf{I}_m \ 0]$ .  $\mathbf{I}_m$  and  $\mathbf{I}_r$  are identity matrix of order  $m$  and  $r$  respectively.

The imaginary part of the eigenvalues of the associated state matrix are the identified damped natural frequencies of the system. The  $\hat{\mathbf{C}}$  matrix is used to transform the computed eigenvectors of the state matrix corresponding to the non-physical states in the identified model, to displacement output shapes at the floors of the structure

$$\mathbf{j} = \hat{\mathbf{C}}\hat{\mathbf{F}} \quad (2-48)$$

where  $\mathbf{j}$  is the matrix of output shapes and  $\hat{\mathbf{F}}$  is the matrix of eigenvectors of the state matrix  $\hat{\mathbf{A}}$ .  $\hat{\mathbf{B}}$  is not required for this analysis. The ERA method was implemented in MATLAB<sup>®</sup> [29].

## 2.4 Determination of the Stiffness Values

Several methods may be applied to obtain the stiffness values from natural frequencies and mode shapes. The method described in here uses a least square approach of the eigenvalue problem to obtain an estimate of the stiffness values of the structure from the differential equation of motion.

### 2.4.1 Least squares solution of eigenvalue problem

The next step is to identify an appropriate model for the structure from the modal parameters identified in the ERA method. For the lumped-mass system shown in Fig. 2-2 with  $n$  degrees of freedom, the  $n$ -th order mass and stiffness matrices are assumed to be of the form

$$\mathbf{M} = \begin{bmatrix} m_1 & 0 & 0 & 0 \\ 0 & m_2 & 0 & 0 \\ 0 & 0 & \ddots & 0 \\ 0 & 0 & 0 & m_n \end{bmatrix}, \quad \mathbf{K} = \begin{bmatrix} k_1 + k_2 & -k_2 & 0 & 0 \\ -k_2 & k_2 + k_3 & -k_3 & 0 \\ 0 & 0 & \ddots & -k_n \\ 0 & 0 & -k_n & k_n \end{bmatrix}. \quad (2-49)$$

Consider the eigenvalue problem [10]

$$(\mathbf{K} - \lambda_i \mathbf{M})\mathbf{f}_i = 0 \quad \text{or} \quad \mathbf{f}_i^T \mathbf{K} = \mathbf{f}_i^T \lambda_i \mathbf{M} \quad (2-50)$$

where  $\lambda_i$  and  $\phi_i$  are the  $i$ -th eigenvalue and eigenvector of the structure, respectively.

Because we have specified the form of the stiffness and mass matrices, this equation can be expanded to allow the stiffness coefficients to be assembled in a vector. For the  $n$ -story shear structure shown in Fig. 2-2 we can rewrite Eq. (2-50) as

$$\mathbf{D}_i \mathbf{k} = \mathbf{L}_i \quad (2-51)$$

where

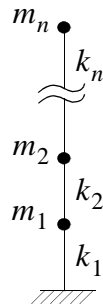


**FIGURE 2-2. Lumped mass model of an  $n$ -story structure.**

$$\mathbf{D}_i = \begin{bmatrix} \phi_{1i} & \phi_{1i} - \phi_{2i} & 0 & 0 \\ 0 & \phi_{2i} - \phi_{1i} & \phi_{2i} - \phi_{3i} & 0 \\ 0 & 0 & \ddots & \\ 0 & 0 & \phi_{(n-1)i} - \phi_{(n-2)i} & \phi_{(n-1)i} - \phi_{(n)i} \\ 0 & 0 & 0 & \phi_{(n)i} - \phi_{(n-1)i} \end{bmatrix}, \quad (2-52)$$

$$\mathbf{k} = \begin{bmatrix} k_1 \\ k_2 \\ \vdots \\ k_n \end{bmatrix}, \quad \mathbf{L}_i = \begin{bmatrix} \phi_{1i}\lambda_i m_1 \\ \phi_{2i}\lambda_i m_2 \\ \vdots \\ \phi_{ni}\lambda_i m_n \end{bmatrix}. \quad (2-53)$$

Equation (2-51) can be written for each of the  $n$  eigenvalues and eigenvectors identified. Assembling all of the eigenvector matrices.

$$\mathbf{D}\mathbf{k} = \mathbf{L} \quad (2-54)$$

where

$$\mathbf{D} = \begin{bmatrix} \mathbf{D}_1 \\ \mathbf{D}_2 \\ \vdots \\ \mathbf{D}_m \end{bmatrix} \text{ and } \mathbf{L} = \begin{bmatrix} \mathbf{L}_1 \\ \mathbf{L}_2 \\ \vdots \\ \mathbf{L}_m \end{bmatrix}. \quad (2-55)$$

This equation represents a total of  $m \times n$  equations which can be used to solve for the vector of stiffnesses  $\mathbf{k}$ . The stiffnesses are computed by

$$\mathbf{k} = \mathbf{D}^{-1}\mathbf{L}. \quad (2-56)$$

In general the matrix  $\mathbf{D}$  is not square. A pseudo-inverse of this matrix is computed and the solution corresponds to a least squares estimate of the stiffnesses [33].

### 2.4.1.1 General formulation

The method discussed in the previous section can be generalized so that it is applied to a wider variety of structures. From finite element analysis we can consider only one finite element with transversal degrees of freedom (see Fig. 2-3)

$$\begin{bmatrix} v_1 - v_2 \\ v_2 - v_1 \end{bmatrix} k = \begin{bmatrix} P_1 \\ P_2 \end{bmatrix} \quad (2-57)$$

where  $v_1$  and  $v_2$  are the displacement of nodes 1 and 2,  $P_1$  and  $P_2$  are the forces applied to these nodes as shown in Fig. 2-3.

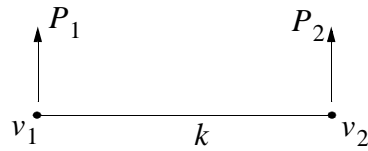


**FIGURE 2-3. Finite element**

It is possible to assemble the displacements matrix of a structure from the displacements of each finite element. For the shear model shown in Fig. 2-2, the displacement matrix should first be written for each element

$$\begin{bmatrix} v_0 - v_1 \\ v_1 - v_0 \end{bmatrix} k_1; \begin{bmatrix} v_1 - v_2 \\ v_2 - v_1 \end{bmatrix} k_2; \dots; \begin{bmatrix} v_{n-1} - v_n \\ v_n - v_{n-1} \end{bmatrix} k_n \quad (2-58)$$

where  $v_0$  correspond to the displacement at the base of the structure. Assembling the complete deformation matrix of the structure it is possible to obtain

$$\begin{bmatrix} v_0 - v_1 & 0 & 0 & 0 \\ v_1 - v_0 & v_1 - v_2 & 0 & 0 \\ 0 & v_2 - v_1 & v_2 - v_3 & 0 \\ 0 & 0 & \ddots & \vdots \\ 0 & 0 & \cdots & v_n - v_{n-1} \end{bmatrix} \begin{bmatrix} k_1 \\ k_2 \\ \vdots \\ k_n \end{bmatrix} = \begin{bmatrix} p_0 \\ p_1 \\ p_2 \\ \vdots \\ p_n \end{bmatrix}. \quad (2-59)$$

Since  $p_0 = 0$  and  $v_0 = 0$  because of the constraints applied to the structure, we obtain

$$\begin{bmatrix} v_1 & v_1 - v_2 & 0 & 0 \\ 0 & v_2 - v_1 & v_2 - v_3 & 0 \\ 0 & 0 & \ddots & \vdots \\ 0 & 0 & \cdots & v_n - v_{n-1} \end{bmatrix} \begin{bmatrix} k_1 \\ k_2 \\ \vdots \\ k_n \end{bmatrix} = \begin{bmatrix} p_1 \\ p_2 \\ \vdots \\ p_n \end{bmatrix}. \quad (2-60)$$

Note that the assembly process for the  $i$ -th vector consists in assemble the matrix in the same way as the stiffness matrix  $\mathbf{K}$ , filling with zeros the degrees of freedom of the structure not related to the  $i$ -th element.

This approach can also be developed for the case of a beam element in space. Two stiffness values will be needed, one in each direction perpendicular to the beam element. The equation equivalent to Eq. (2-58) is

$$\begin{bmatrix} v_1 - v_2 & 0 \\ v_2 - v_1 & 0 \\ 0 & w_1 - w_2 \\ 0 & w_2 - w_1 \end{bmatrix} \begin{bmatrix} k_y \\ k_z \end{bmatrix} = \begin{bmatrix} P_{1y} \\ P_{2y} \\ P_{1z} \\ P_{2z} \end{bmatrix}, \quad (2-61)$$

where  $v_1$  and  $v_2$  are the degrees of freedom in the  $y$  direction for nodes 1 and 2;  $w_1$  and  $w_2$  are the degrees of freedom in the  $z$  direction;  $P_{1y}$  and  $P_{2y}$  are the forces applied to the element in the  $y$  direction;  $P_{1z}$  and  $P_{2z}$  are the forces in the  $z$  direction (see Fig. 2-4).

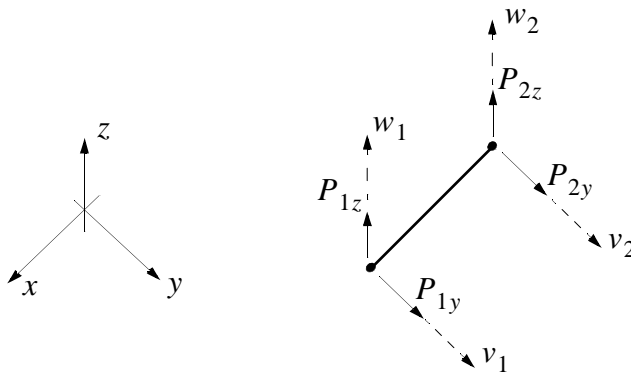


**FIGURE 2-4. Bar element**

#### 2.4.1.2 Local and global coordinates.

In finite element analysis transformation of coordinates is used when elements are not oriented alike. This concept can be applied to this technique as well. It is possible to “rotate” a finite element from its local coordinates to its global coordinates using a transformation matrix. Once all of the elements are expressed in global coordinates it is possible to assemble the displacement matrix for the whole structure as explained before.

Considering the finite element shown in Fig. 2-5 the transformation matrix to rotate the displacement vector an angle  $\alpha$  is

$$\begin{bmatrix} u'_1 \\ v'_1 \\ u'_2 \\ v'_2 \end{bmatrix} = [T] \begin{bmatrix} u_1 \\ v_1 \\ u_2 \\ v_2 \end{bmatrix}, \quad (2-62)$$

where  $[T]$  is the transformation matrix defined as

$$[T] = \begin{bmatrix} \cos(\alpha) & \sin(\alpha) & 0 & 0 \\ -\sin(\alpha) & \cos(\alpha) & 0 & 0 \\ 0 & 0 & \cos(\alpha) & \sin(\alpha) \\ 0 & 0 & -\sin(\alpha) & \cos(\alpha) \end{bmatrix}. \quad (2-63)$$

In system identification and structural health monitoring the acceleration of the structure is used to detect damage. Neglecting the vertical accelerations, and assuming rigid floors on a frame building, the structure can be modeled as beam elements with only transversal degrees of freedom ( $v_1$  and  $v_2$ ). In this case the transformation matrix can be written as

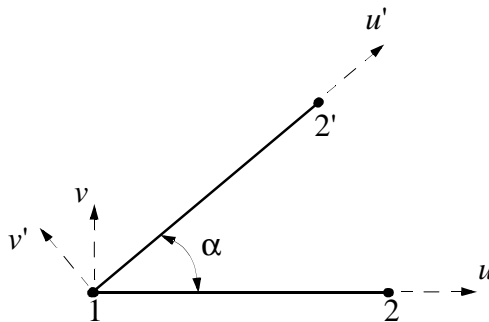


**FIGURE 2-5. Transformation of coordinates**

$$[\mathbf{T}] = \begin{bmatrix} \sin(\alpha) & 0 \\ \cos(\alpha) & 0 \\ 0 & \sin(\alpha) \\ 0 & \cos(\alpha) \end{bmatrix}. \quad (2-64)$$

A total of three translational degrees of freedom ( $u, v, w$ ) per node will exist in a beam element placed in the space. In this case the transformation matrix  $[\mathbf{T}]$  for a bar element can be written as

$$[\mathbf{T}] = \begin{bmatrix} [\mathbf{R}] & 0 \\ 0 & [\mathbf{R}] \end{bmatrix}, \quad (2-65)$$

where the matrix  $[\mathbf{R}]$  is defined as

$$[\mathbf{R}] = \begin{bmatrix} c(\alpha)c(\beta) & s(\alpha)c(\gamma) - c(\alpha)s(\beta)s(\gamma) & s(\alpha)s(\gamma) + c(\alpha)c(\beta)s(\gamma) \\ -s(\alpha)c(\beta) & c(\alpha)c(\gamma) + s(\alpha)s(\beta)s(\gamma) & c(\alpha)s(\gamma) - s(\alpha)s(\beta)c(\gamma) \\ -s(\beta) & -c(\beta)s(\gamma) & c(\beta)c(\gamma) \end{bmatrix} \quad (2-66)$$

where  $s(\alpha) = \sin(\alpha)$ ,  $c(\alpha) = \cos(\alpha)$ ,  $s(\beta) = \sin(\beta)$ ,  $c(\beta) = \cos(\beta)$ ,  $s(\gamma) = \sin(\gamma)$  and  $c(\gamma) = \cos(\gamma)$ .

The angles  $\alpha$ ,  $\beta$  and  $\gamma$  are the angles of rotation with respect to the  $z$ ,  $y$  and  $x$  axes, as shown in Fig. 2-6. To obtain Eq. (2-66) a rotation of  $\alpha$  degrees is done with respect to the  $z$  axis. Then, a rotation of  $\beta$  degrees is done with respect to the  $y$  axis, and finally a rotation of  $\gamma$  degrees is done with respect to the  $x$  axis.

For the case where no axial displacement is present in the element, the matrix  $[\mathbf{R}]$  becomes

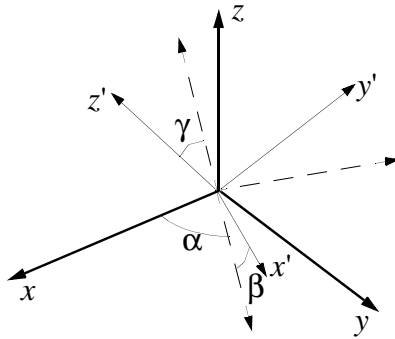


**FIGURE 2-6. Transformation of coordinates in the space.**

$$[R] = \begin{bmatrix} s(\alpha)c(\gamma) - c(\alpha)s(\beta)s(\gamma) & s(\alpha)s(\gamma) + c(\alpha)c(\gamma)s(\beta) \\ c(\alpha)c(\gamma) + s(\alpha)s(\beta)s(\gamma) & c(\alpha)s(\gamma) - s(\alpha)s(\beta)c(\gamma) \\ -c(\beta)s(\gamma) & c(\beta)c(\gamma) \end{bmatrix} \quad (2-67)$$

## 2.5 Summary

This chapter provided the reader with an introduction to stochastic processes, mean square calculus, the NExT approach, and the ERA algorithm were discussed. These concepts will be applied in the subsequent chapters to identify the existence, location, and extent of damage in a benchmark structure.

## Chapter 3

### Implementation of Proposed SHM Methodology

Ideally, implementation of a health monitoring methodology using a large quantity of data will produce exact stiffness values. However, to be useful for health monitoring, a methodology should produce accurate values of the stiffnesses with a limited amount of data. The accuracy of the technique will depend on factors such as the amount of noise present in the system, the linearity and resolution of the sensors used, and if a model is assumed, the error between the assumed form of the model identified and the actual system.

Before applying the structural health monitoring methodology proposed in this thesis, studies were performed to consider various issues in the implementation of the method. This chapter discusses these issues. The numerical models used for these studies are finite element models developed for the benchmark problem in structural health monitoring of the American Society of Civil Engineering (ASCE) in collaboration with the International Association of Structural Control (IASC) [26]. Acceleration records were generated using the benchmark problem structural model. A 12 degree of freedom (DOF) lumped mass model is selected for the *identification model* — that is, the model assumed in the identification process is 12DOF.

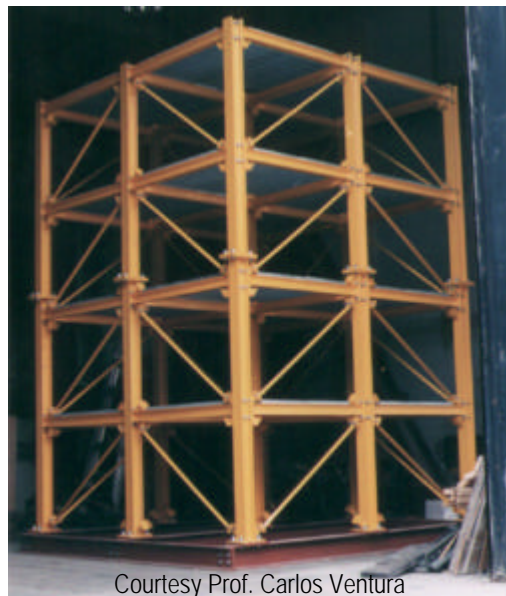
In the first part of this chapter the structural models and the identification model are described. In later sections various questions are investigated, including: i) how much data is required to obtain accurate estimates of the stiffnesses of the structure; ii) the

effect of sensor noise in the identification procedure; iv) the effect of a natural frequency out of the spectral lines of the spectral density functions; and v) modeling errors.

## 3.1 Finite element models

### 3.1.1 Structural model

The finite element models used were developed for the benchmark problem in structural health monitoring [26]. The model was created based on an existing scaled structure located at the University of British Columbia, Canada [5]. Figure 3-1 shows a photograph of the two-bay by two-bay steel structure. Each bay is  $1.25\text{m} \times 0.9\text{m}$ . Hot rolled  $B100 \times 9$  members are used for the columns,  $S75 \times 11$  members are used for the floor beams, and  $L25 \times 25 \times 3$  are used for bracing on each floor. Four slabs are present in each floor. The first floor has four 800kg slabs, the second and third floor has four 600kg slabs and the fourth floor has four 400kg slabs. One of the floor slabs in the fourth floor can be replaced for a 550kg slab to produce an asymmetric mass distribution.



Courtesy Prof. Carlos Ventura

**FIGURE 3-1. Benchmark structure**

For the benchmark problem two reduced order 3D finite element models were created to model the structure based on the same analytical model [26]. The models are constructed using the assumption that each of the floors is rigid. In the first model, the floors are restricted to translation in a plane parallel to the floor and rotation about the vertical axis. Thus, each floor has three DOF per floor, two translational DOF along the longitudinal and transverse axes, and one rotational DOF. A total of 12 DOF are used in this finite element model.

The second model has a total of 120 DOF. This finite element model assumes a rigid floor for each level, restraining only the vertical DOF allowing the floors to rotate with respect to the  $x$ ,  $y$  and  $z$  axes. Both finite element models are provided in Matlab<sup>®</sup> [29], and were modeled with Euler-Bernoulli elements. A 12 DOF shear building was used as identification model.

The investigative studies discussed in this chapter were performed to examine the capabilities of the technique. Thus, most of the studies presented in this chapter used the 12 DOF structural model to obtain acceleration data, making it possible to eliminate modeling errors. However the last study is conducted to specifically examine the effects of modeling errors, and thus the 120 DOF model is used.

Figure 3-2 shows a diagram of the analytical model. In the figure  $\ddot{y}_{ia}$  and  $\ddot{y}_{ib}$  correspond to transverse acceleration measurements and  $w_i$  correspond to applied loads. The properties of each element used to construct the model are shown in Table 3-1, as reported by Johnson *et al* [26]. It is assumed that the braces work only in tension and compression and have zero moment of inertia. The lateral stiffness of each floor is 106.6 MN/m in the strong ( $x$ ) direction, 67.9 MN/m in the weak ( $y$ ) direction and 232.0 MN/rad in the rotational ( $\theta$ ) DOF. The strong direction of the columns is aligned with the  $x$

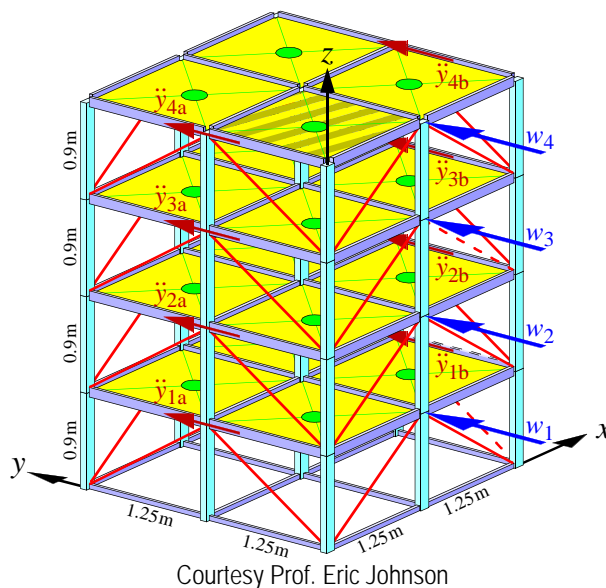


**FIGURE 3-2. Analytical model**

axis, making it 57% stronger than the y-direction. This creates different dynamic characteristics in the two directions.

**TABLE 3-1. Elements properties.**

Property		Columns	Floor beams	Braces
Denomination		B100 × 9	S75 × 11	L25 × 25 × 3
Area	$A$ , [m <sup>2</sup> ]	$1.13 \times 10^{-3}$	$1.43 \times 10^{-3}$	$0.14 \times 10^{-3}$
Inertia (Strong axis)	$I_y$ , [m <sup>4</sup> ]	$1.97 \times 10^{-6}$	$1.22 \times 10^{-6}$	0
Inertia (Weak axis)	$I_z$ , [m <sup>4</sup> ]	$0.66 \times 10^{-6}$	$0.25 \times 10^{-6}$	0
St. Venant torsion constant	$J$ , [m <sup>4</sup> ]	$8.01 \times 10^{-9}$	$38.20 \times 10^{-9}$	0
Young's Modulus	$E$ , [Pa]	$2 \times 10^{11}$	$2 \times 10^{11}$	$2 \times 10^{11}$
Mass per unit length	$r$ , [kg/m]	8.89	11	1.11

Mass is added to each floor with concrete slabs. The total mass of the concrete slabs is 9600kg, including 3200kg at the first floor, 2400kg at the second and third floor, and 1600kg at the fourth floor. The total mass of the structural model, including concrete slabs, beams, columns and braces is 10,567.1 Kg. For the studies described in this

chapter symmetric mass distribution is considered to prevent coupling between translational and rotational modes. A damping ratio of 1% is used for all modes.

The natural frequencies reported by Johnson *et al* [26] for the 12 DOF model are 11.79Hz, 32.07Hz, 48.68Hz and 60.60Hz in the translational strong direction ( $x$ ), 9.41Hz, 25.60Hz, 38.85Hz and 48.37Hz in the translational weak direction ( $y$ ), and 16.53Hz, 45.17Hz, 68.64Hz and 85.51Hz for the rotational degrees of freedom ( $\theta$ ). In this chapter this model is used to study the sensitivity of the proposed methodology to the record length, effect of sensor noise and modeling errors.

The 120 DOF structural model has the same element properties and masses as the 12 DOF model. The natural frequencies reported by Johnson *et al* [26] are 8.53Hz, 24.24Hz, 39.73Hz and 55.16Hz in the strong ( $x$ ) direction, 8.20Hz, 22.54Hz, 35.58Hz and 46.12Hz in the weak ( $y$ ) direction, and 13.95Hz, 39.05Hz, 60.75Hz, and 79.46Hz for the rotational degree of freedom ( $\theta$ ). This model is used to investigate the effect of modeling errors in the identification process.

### **3.1.2 Generating data from analytical model**

To generate data for use in health monitoring studies, the models were excited with random forces applied at every floor in the  $y$ -direction (weak direction) to simulate wind vibration in the structure. Gaussian white noise, filtered with a low-pass Butterworth filter, was used to excite the model. The cutoff frequency of the filter was 100Hz. For the purpose of the investigative studies presented in this chapter, rotation is not taken into account as the mass distribution of each floor is symmetric, and forces are applied in such a way to produce motion in the weak direction only ( $y$ -axis). This simplification allows us to focus on the capabilities of the identification methodology. Figure 3-3 shows 10 seconds of a typical force applied to the structure.

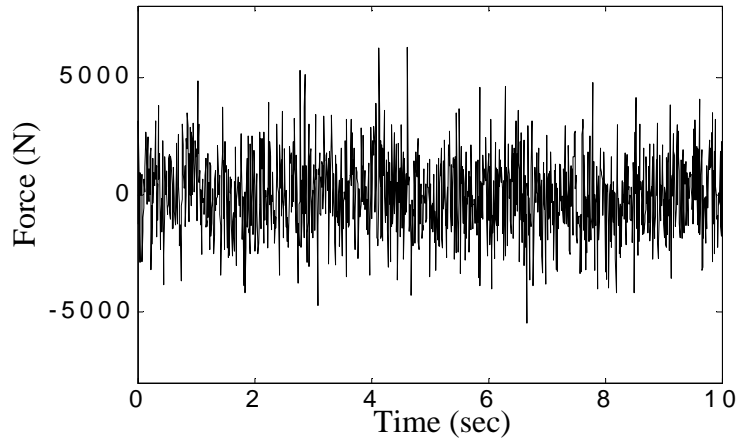


**FIGURE 3-3. Force record (First floor)**

In both models the accelerometers are located on the center columns of each side of the structure, as shown in Fig. 3-2. Gaussian pulse processes are added to the acceleration data to simulate measurement noise in all acceleration signals. The noise was adjusted to have a root mean square (RMS) of 10% of the RMS acceleration at the roof. Figure 3-4 shows typical records of the acceleration obtained from the structural model. The first 10 seconds of each acceleration record are ignored in the identification process to ensure stationary data.

The noisy acceleration data was obtained with the Matlab<sup>®</sup> [29] tool developed by researchers at the Hong Kong University of Science and Technology [26]. The governing equations are integrated at 1kHz and to obtain sensor measurements at this frequency. The acceleration data is downsampled to 125Hz to apply the proposed technique. The purpose of resampling the signal is to reduce the number of points for the identification process, reducing the processing time. All translational modes of both structural models are below 125Hz. The signal was resampled using the Matlab<sup>®</sup> function *resample.m*. Although no aliasing is expected, this function also applies an appropriate low pass anti-aliasing filter to the acceleration record [32].

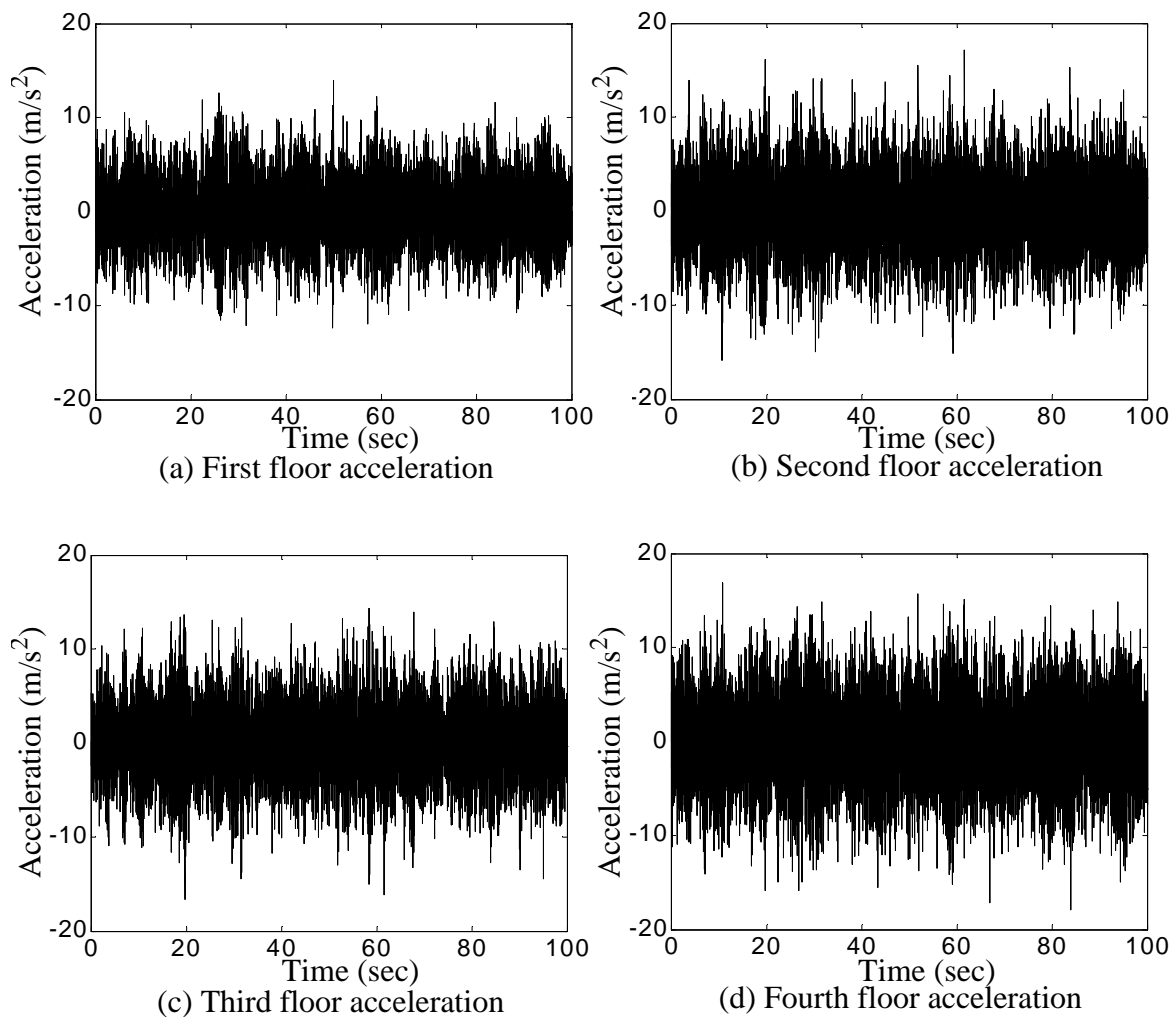


**FIGURE 3-4. Typical acceleration records.**

### 3.1.3 Identification model

Figure 3-5 shows the identification model used to estimate the stiffness coefficients of the structural model. The identification model is a 4 story shear model with DOF matching the 4 translational degrees of freedom of the structural model in the weak direction ( $y$ -axis). This model is specified within the benchmark problem [26]. This 2D model allows the identification of the stiffness of each floor using the least squares solution of

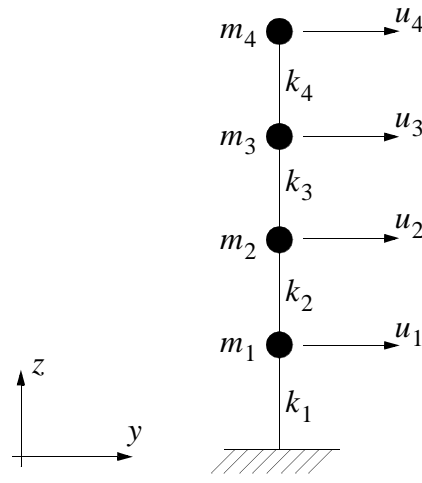


**FIGURE 3-5. Identification model**

the eigenvalue problem discussed in 2.4.1. An estimate of the mass is needed to apply this technique. For this study the mass is assumed to be known and equal to the structural model. Lumped masses are assumed for each floor, producing the following mass matrix

$$\mathbf{M} = \begin{bmatrix} 3452.4 & 0 & 0 & 0 \\ 0 & 2652.4 & 0 & 0 \\ 0 & 0 & 2652.4 & 0 \\ 0 & 0 & 0 & 1809.9 \end{bmatrix} \quad (\text{Kg}). \quad (3-1)$$

The mass matrix of Eq. 3-1 includes the concrete slabs plus the weight of the beams, columns and diagonals.

Thus, for this example the  $\mathbf{D}_i$  matrix and  $\mathbf{L}_i$  vector for the least squares solution of eigenvalue problem will be

$$\mathbf{D}_i = \begin{bmatrix} \phi_{1i} & \phi_{1i} - \phi_{2i} & 0 & 0 \\ 0 & \phi_{2i} - \phi_{1i} & \phi_{2i} - \phi_{3i} & 0 \\ 0 & 0 & \phi_{3i} - \phi_{2i} & \phi_{3i} - \phi_{4i} \\ 0 & 0 & 0 & \phi_{4i} - \phi_{3i} \end{bmatrix}; \mathbf{L}_i = \begin{bmatrix} 3452.4 \times \phi_{1i} \lambda_i \\ 2652.4 \times \phi_{2i} \lambda_i \\ 2652.4 \times \phi_{3i} \lambda_i \\ 1809.9 \times \phi_{4i} \lambda_i \end{bmatrix}, \quad (3-2)$$

for the  $i$ -th eigenvector  $\mathbf{f}_i$  and its corresponding eigenvalue  $\lambda_i$ . The eigenvectors and eigenvalues were determined with the ERA method.

In this section the structural model and the identification model for the set of studies were described. These models are used in the following sections of this chapter to study the effectiveness and implementation of the structural health monitoring technique discussed in this thesis.

### 3.2 Record length and number of points per frame

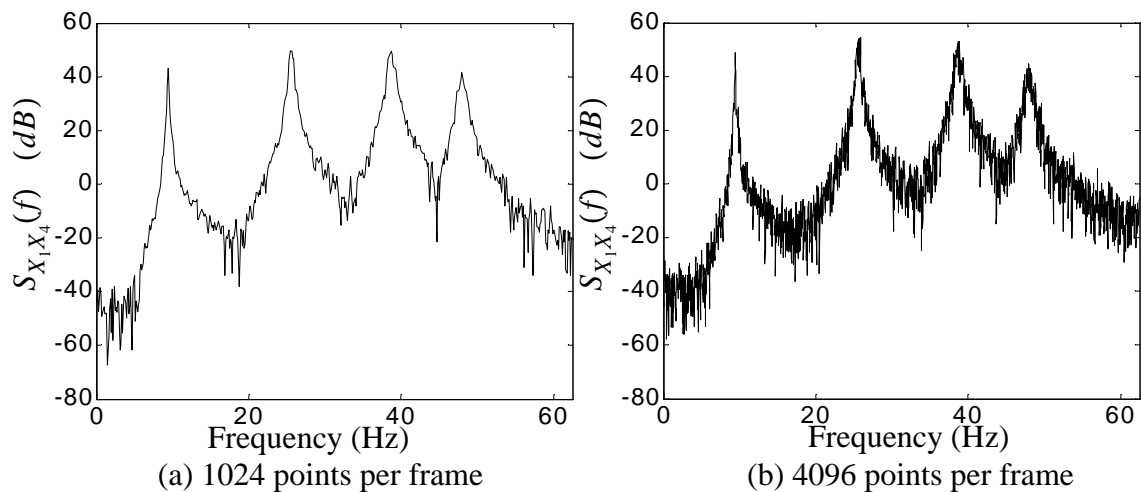
The first study in the implementation of the methodology is to determine an appropriate acceleration record length and number of points per frame. There are trade-offs in the selection of these parameters. With longer records it is possible to do more averages, reducing noise and numerical errors in the spectral density function. Using more points per frame provides more resolution in the spectral density function, but more averages are necessary to average out noise and numerical errors. For example Figure 3-6 shows two spectral density functions in  $m^2/sec^3$  calculated with different points per frame. For the calculation of both spectral density functions 90 seconds of data were used. It is clear that the spectral density function with 1024 points has less noise content than the spectral density function with 4096 points.

The discussed structural health monitoring methodology was used to identify the stiffness values of the structural model using different record lengths. As described in

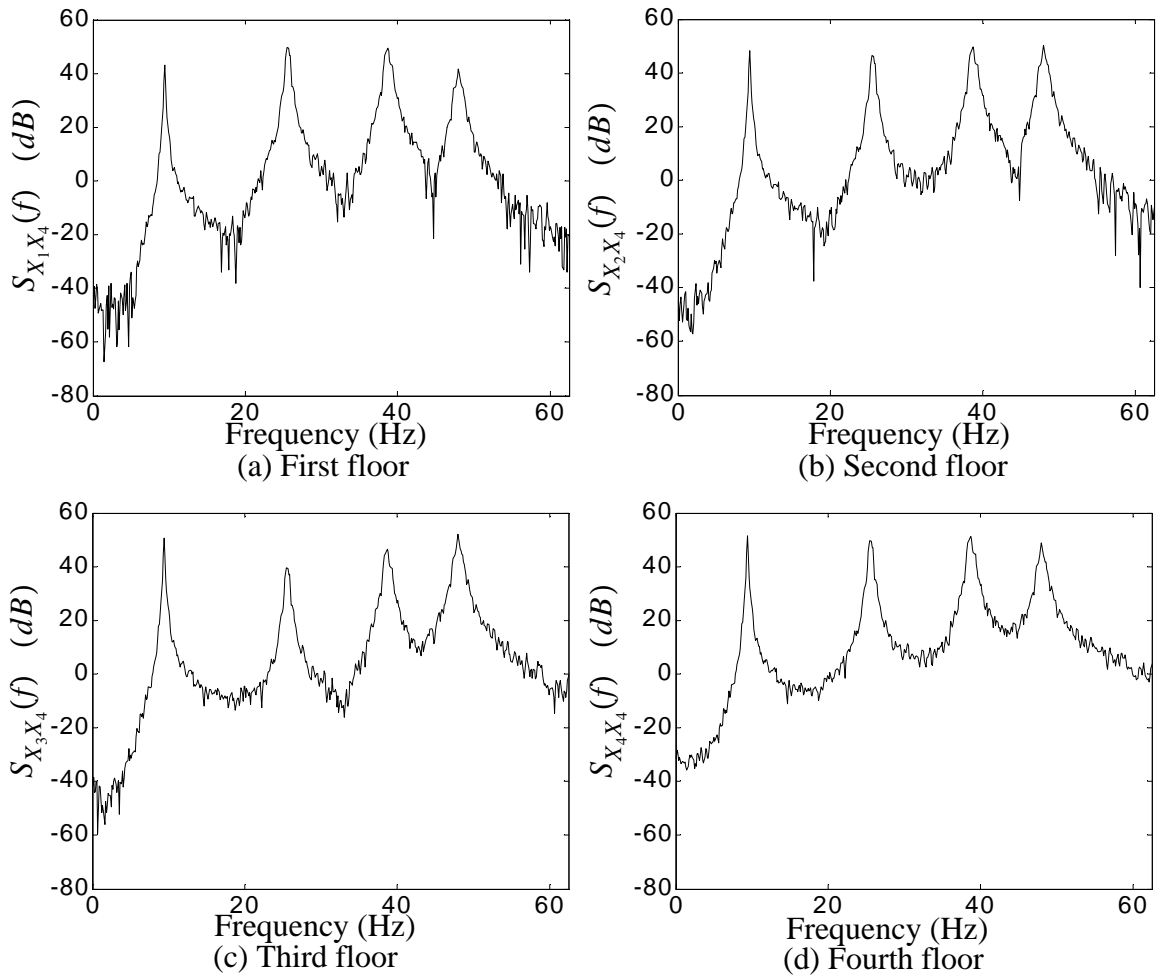
chapter 2, the first step of the methodology is the estimation of the spectral density functions based on acceleration records. Then, the cross correlation functions are calculated from the spectral density functions, obtaining correlation functions of the system. This correlation functions can be treated as free vibration data. The next step is to use the ERA to calculate the modal parameters of the structure. These modal parameters are used in the least squares solution of the eigenvalue problem to determine the translational stiffness values of each floor.

Figure 3-7 shows typical spectral density functions of the acceleration data for each floor using 1024 points per frame. For the calculation of the spectral density functions the acceleration of the roof was selected as the reference signal. This channel was chosen to ensure that all the modes would be observed in the data. A Hanning window is used in each frame to reduce the effects of leakage [32].

The identification procedure was applied using various number of frames to determine the most appropriate value, and to study the influence of the number of points on the results. In the calculation of the spectral density functions, 75% overlap was used for



**FIGURE 3-6. Cross-spectral density functions**



**FIGURE 3-7. Cross-spectral density functions of accelerations (1024 points)**

each frame. Three cases are studied here by varying the frame length. Frame lengths of 1024 points, 2048 points and 4096 points are considered.

After the calculation of the spectral density functions, the correlation functions are obtained as described in 2.1.3 In this calculation the Matlab<sup>®</sup> function *ifft* is used to calculate the inverse fast Fourier transform of the spectral density function. Figure 3-8 shows the sets of correlation functions corresponding to the spectral density functions shown in Fig. 3-7.

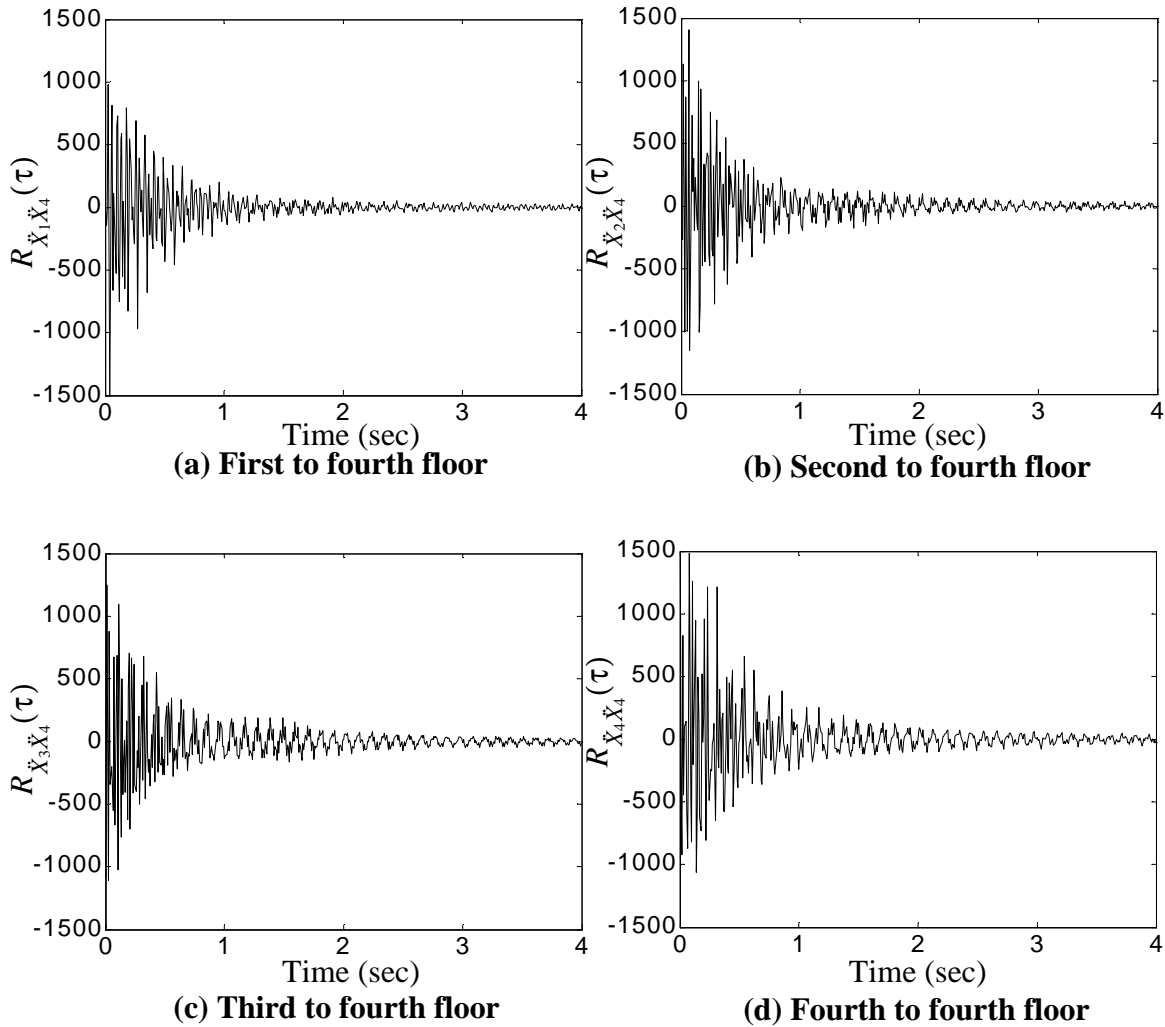


**FIGURE 3-8. Correlation functions**

The next step is to use the ERA method to obtain natural frequencies and mode shapes from the correlation functions. For this operation ERA was programmed in Matlab<sup>®</sup>. The Hankel matrix used in the ERA has 40 columns and 200 rows, using a total time of 0.864 seconds of correlation function. Figure 3-9 shows the singular values of the Hankel matrix. In this figure we can observe that the first 8 singular values are much higher than the other values, indicating that these values correspond to the poles of the structure and all other values are computational modes. After eliminating the computational

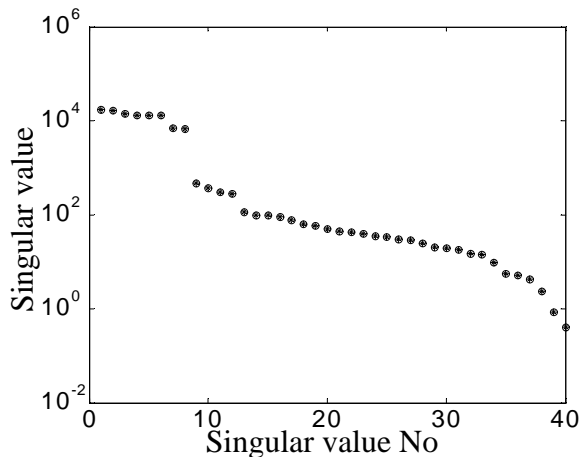


**FIGURE 3-9. Singular values of Hankel matrix.**

modes a discrete-time system is obtained [24]. The natural frequencies of the structural model (y-axis) and the identified with the ERA method are shown in Table 3-2. Figure 3-10 shows the corresponding mode shapes. The identified damping coefficients of the structure were 1.17%, 1.10%, 1.13% and 1.04% for the first, second, third and fourth mode respectively.

The last step of the methodology is estimate the stiffness values of the structure based on the natural frequencies and mode shapes obtained with ERA. For this the least squares

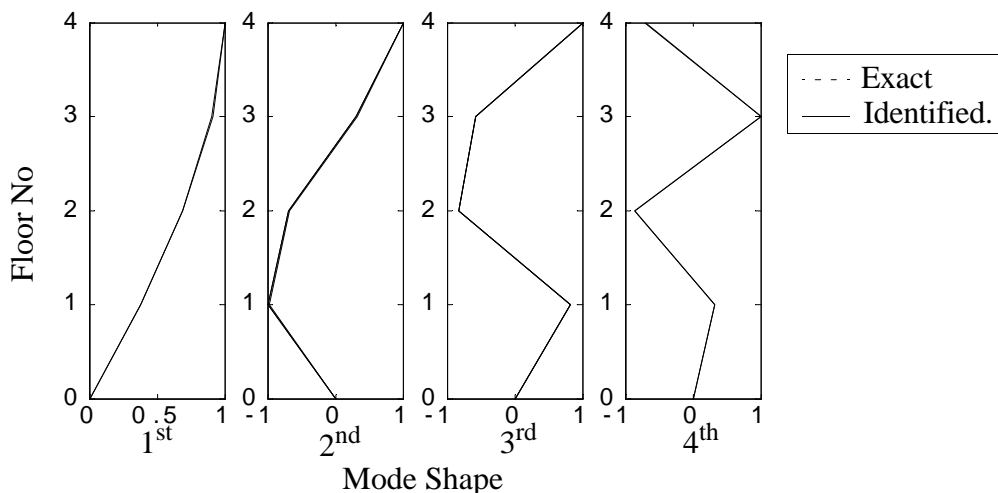


**FIGURE 3-10. Mode shapes of structural and identified model (ERA).**

solution of the eigenvalue problem technique was used. The identified stiffnesses are shown in Table 3-3.

**TABLE 3-2. Natural frequencies of exact and identified model (ERA)**

<b>Natural Freq. No</b>	<b>Exact (Hz)</b>	<b>Identified (ERA) (Hz)</b>	<b>Error (%)</b>
1	9.41	9.40	0.11
2	25.60	25.57	0.12
3	38.85	38.65	0.51
4	48.37	47.99	0.78

**TABLE 3-3. Stiffness of structural and identified models.**

<b>Floor No</b>	<b>Exact (MN/m)</b>	<b>Identified (MN/m)</b>	<b>Error (%)</b>
1	67.9	68.22	0.47
2	67.9	67.98	0.12
3	67.9	67.70	0.29
4	67.9	67.81	0.13

This procedure was applied to data records with different lengths. In the study frames of 1024 points, 2048 points and 4096 points with 75% overlapping are considered. The variation in the identified natural frequencies, mode shapes, stiffness values and damping were studied. The results are discussed in the following sections.

### **3.2.1 Influence of record length on natural frequencies**

Figure 3-11 shows the sensitivity of the natural frequencies obtained with the ERA with respect to the record length. It is clear that the ERA is able to obtain accurate values of the natural frequencies with only a few frames. Increasing the resolution in the window (*i.e.*, using a larger frame size) decreases the number of frames needed to identify the correct natural frequencies. In terms of the number of seconds needed in the identification process about the same time will be needed to obtain similar results with the three frame lengths studied.

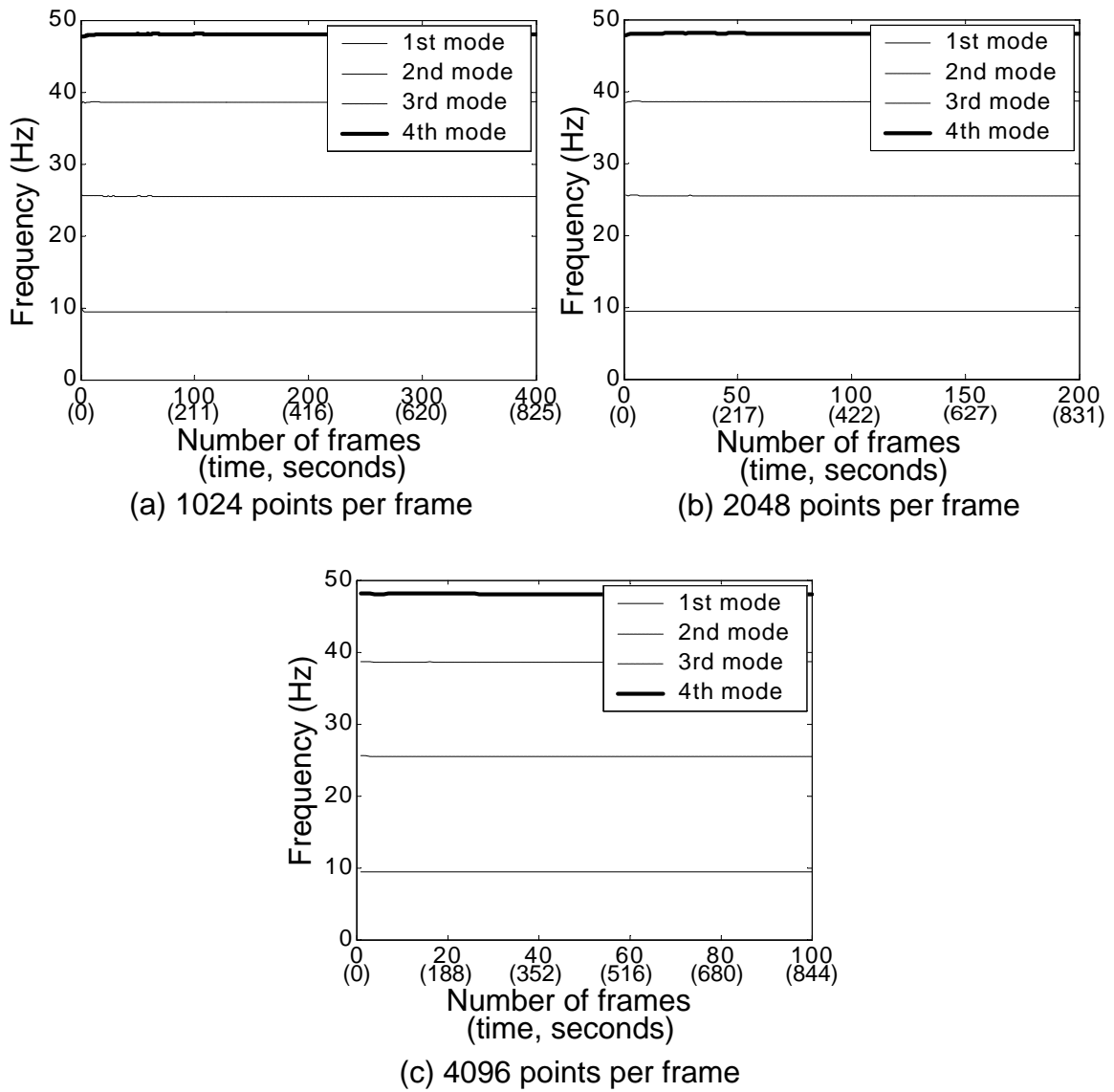


**FIGURE 3-11. Sensitivity of identified natural frequencies to implementation.**

To compare the results obtained in each case define the frequencies total error in the frequency results as

$$E_{\lambda} = \sum_{i=1}^n 100 \cdot \left| \frac{\lambda_{i \text{ identified}} - \lambda_{i \text{ exact}}}{\lambda_{i \text{ exact}}} \right|, \quad (3-3)$$

where  $\lambda_{i \text{ identified}}$  and  $\lambda_{i \text{ exact}}$  are the  $i$ -th natural frequencies from ERA and the structural model,  $|\cdot|$  denotes absolute value, and  $n$  is the number of natural frequencies of the system. In this case  $n$  is equal to 4. Figure 3-12 shows the total error with respect to time

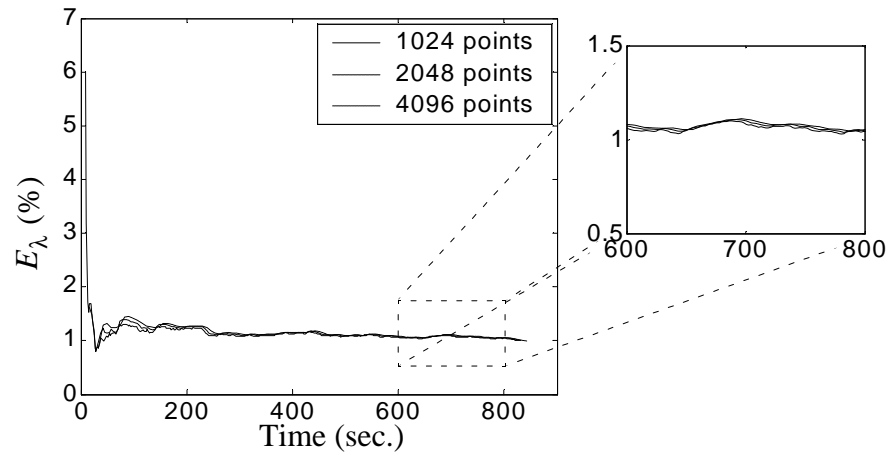


**FIGURE 3-12. Sensitivity of natural frequencies**

record for window length of 1024, 2048 and 4096 points. After 200 seconds the steady state condition for each case is reached. In all three cases the error is similar in magnitude. The lowest error occurs when 4096 points per window are used, and the highest error occurs when 1024 points are used. Note that a bias error was found in the identification of the natural frequencies. This bias error is mostly due to bias errors in the calculation of the spectral density function [36, 37].

### 3.2.2 Influence of the records length on mode shapes

The total error for the mode shapes is defined as

$$E_{\phi} = \sum_{i=1}^n \sum_{j=1}^n 100 \cdot \left| \frac{\phi_{(i,j) \text{ identified}} - \phi_{(i,j) \text{ exact}}}{\phi_{(i,j) \text{ exact}}} \right| \quad (3-4)$$

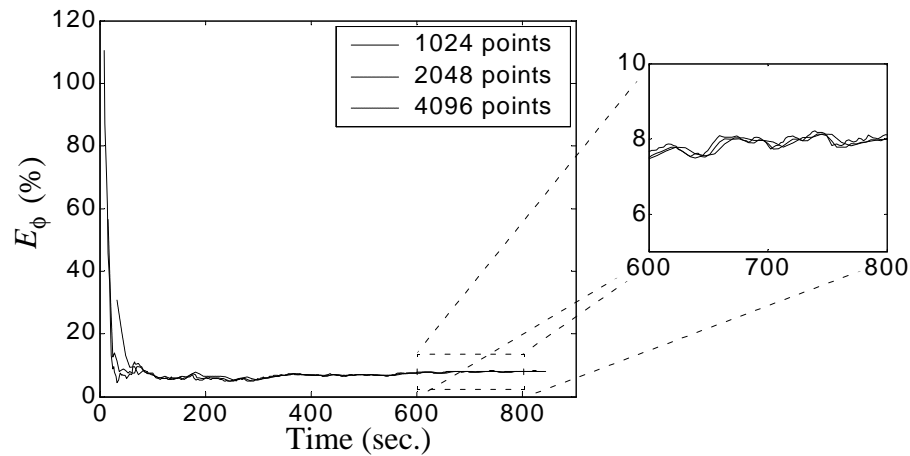


**FIGURE 3-13. Sensitivity of mode shapes**

where  $\phi_{(i,j)}$  is the term of the eigenvector matrix  $\hat{\mathbf{F}}$  located in the  $i$ -th row and  $j$ -th column, and  $n$  is the number of natural frequencies of the structure. In this case  $n$  is equal to 4. The subscript *identified* is used for the identified mode shapes, and the subscript *exact* is used for the exact mode shapes of the structure. All the mode shapes are normalized by setting the maximum deflection equal to 1.

The sensitivity of the mode shapes with respect to the record length is shown in Fig. 3-13. Using about 100 seconds of data produces good results, and using more data does not improve the results. Thus, with short records it is better to use larger frames but with records larger than 100 seconds any of the three frame length studied give similar results.

### 3.2.3 Influence of the record length on damping

The sensitivity of the damping estimate with respect to the record length is shown in Fig. 3-14. As expected, the damping ratios estimated with the ERA method improved when longer windows were used. When short records were used, the damping ratio of the first mode has large errors due to the lack of information about this mode. For the calculation

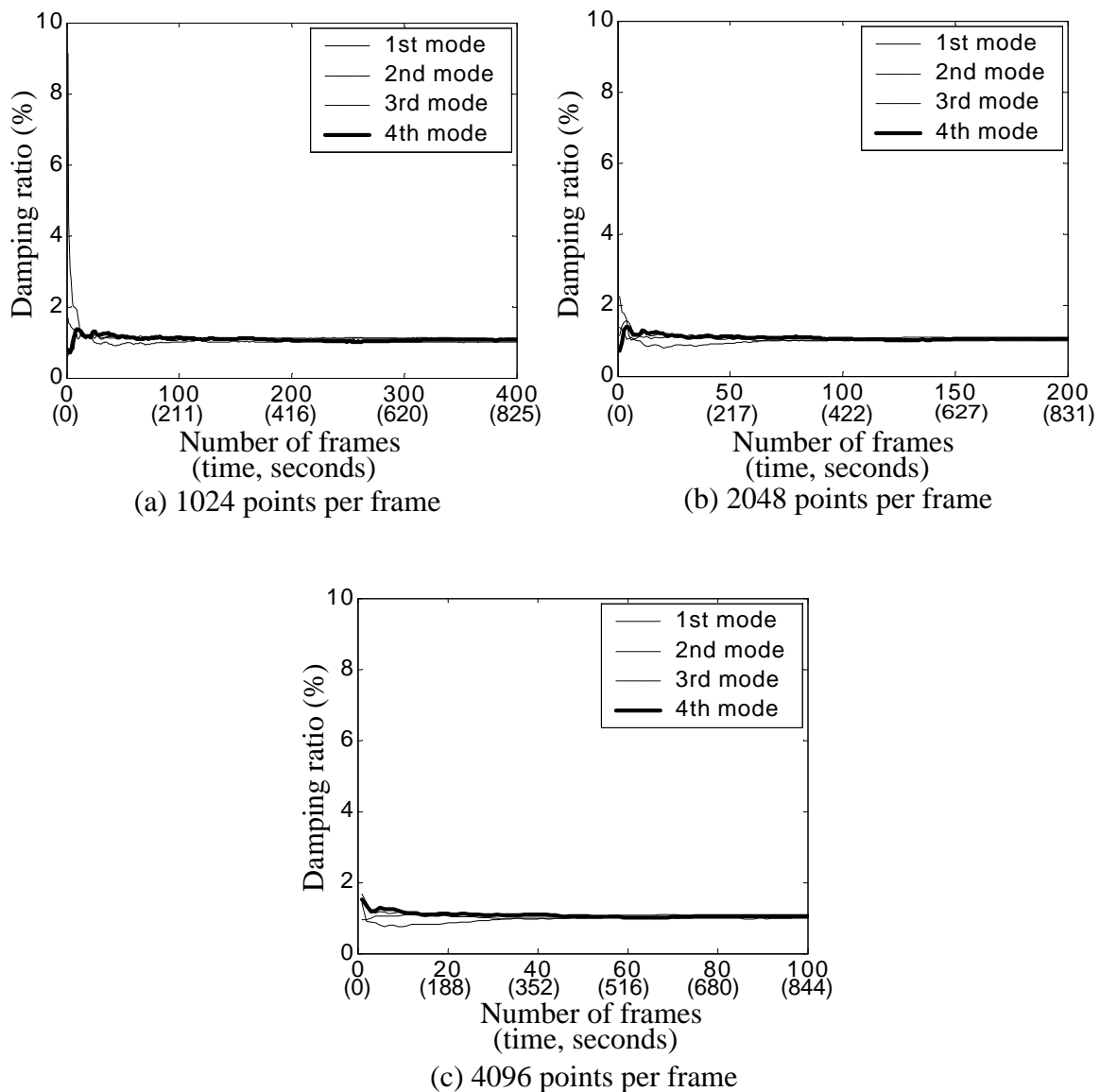


**FIGURE 3-14. Sensitivity of identified damping to implementation.**

of damping in the structure it is more important to use more frames than for the determination of natural frequencies.

To study the error in damping define the total error in the damping ratio as

$$E_d = \sum_{i=1}^n 100 \cdot \left| \frac{\zeta_{i \text{ identified}} - \zeta_{i \text{ exact}}}{\zeta_{i \text{ exact}}} \right| \quad (3-5)$$

where  $\zeta_{i \text{ identified}}$  and  $\zeta_{i \text{ exact}}$  are the identified and exact damping ratios of the  $i$ -th mode. Figure 3-15 shows the variation in the damping error with respect to the record

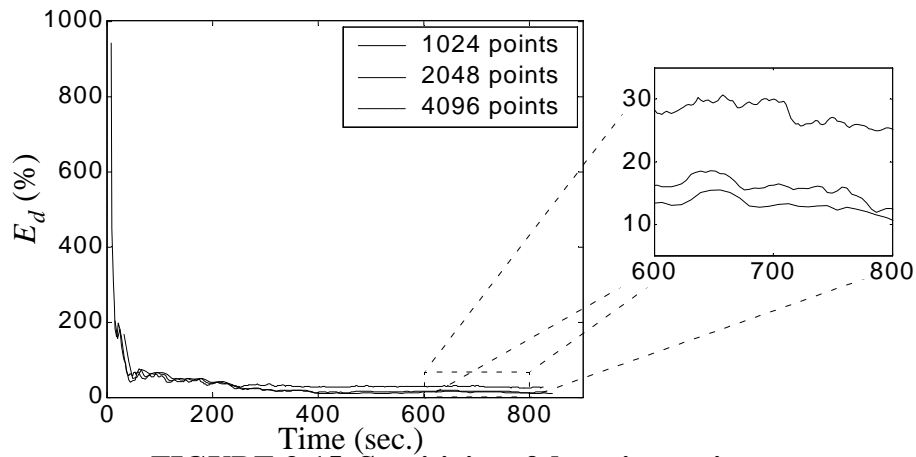


**FIGURE 3-15. Sensitivity of damping ratio**

length. After approximately 500 seconds the steady state in the total error of the damping ratio is reached. Calculated damping ratios have larger errors than calculated natural frequencies, and a better approximation was observed with larger frames.

### 3.2.4 Stiffness coefficients

Figure 3-16 shows the variation of the calculated stiffness coefficients with respect to the number of frames. As expected for this simple problem, all stiffnesses converge to the theoretical horizontal stiffness of 67.9 MN/m. With 200 seconds of data the estimated stiffness values have reached a steady state. The accuracy in the estimate does not increase significantly by increasing the number of points of each frame.

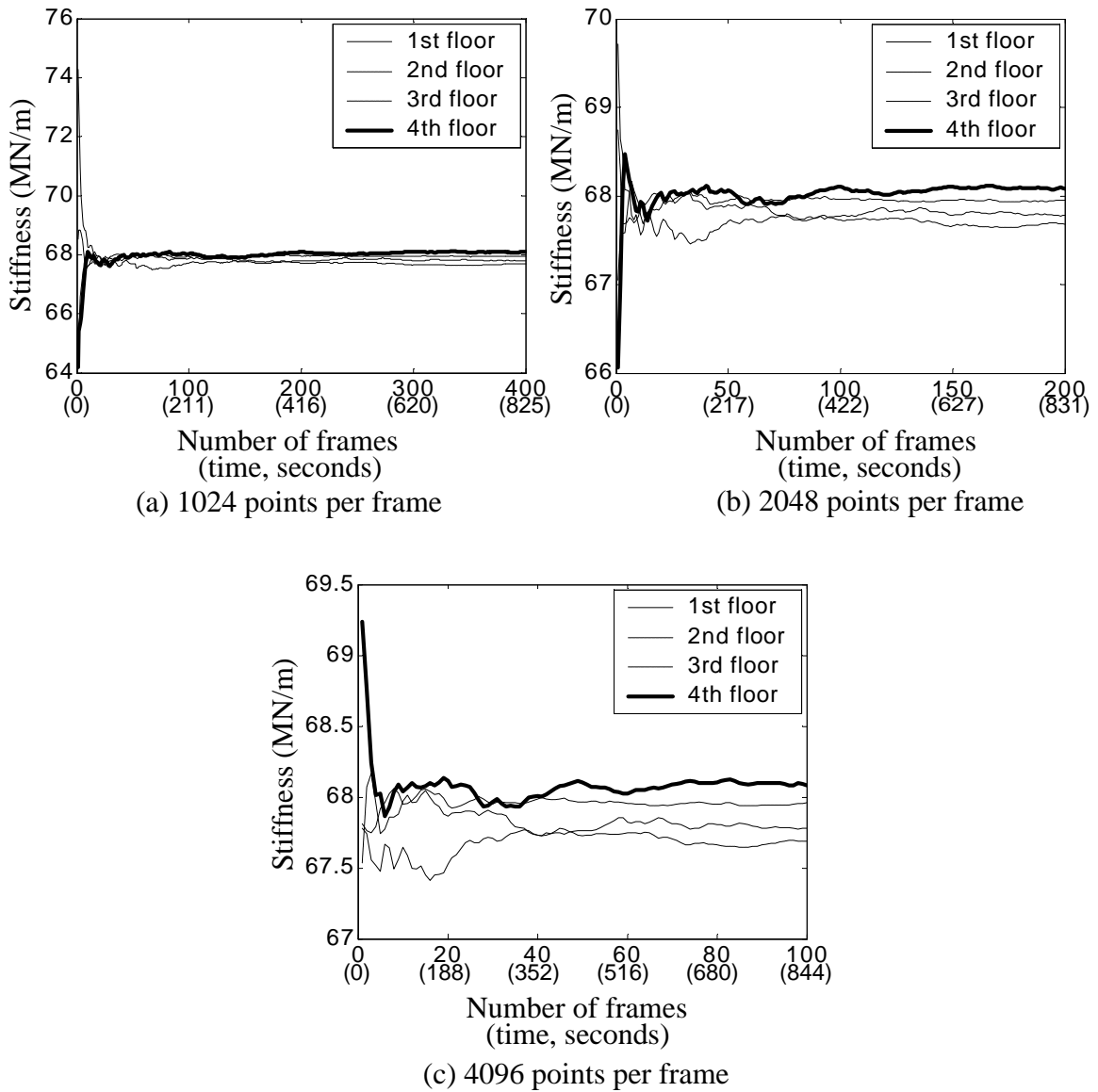


**FIGURE 3-16. Sensitivity of identified damping to implementation.**

To study the error in the stiffness, define the total error in the stiffness as

$$E_k = \sum_{i=1}^n 100 \cdot \left| \frac{k_{i \text{ identified}} - k_{i \text{ exact}}}{k_{i \text{ exact}}} \right| \quad (3-6)$$

where  $k_{i \text{ exact}}$  is the exact horizontal stiffness of the  $i$ -th floor,  $k_{i \text{ identified}}$  is the identified horizontal stiffness for the  $i$ -th floor, and  $n$  is the number of identified stiffnesses. Figure 3-17 provides the variation of the stiffness total error with respect to the record

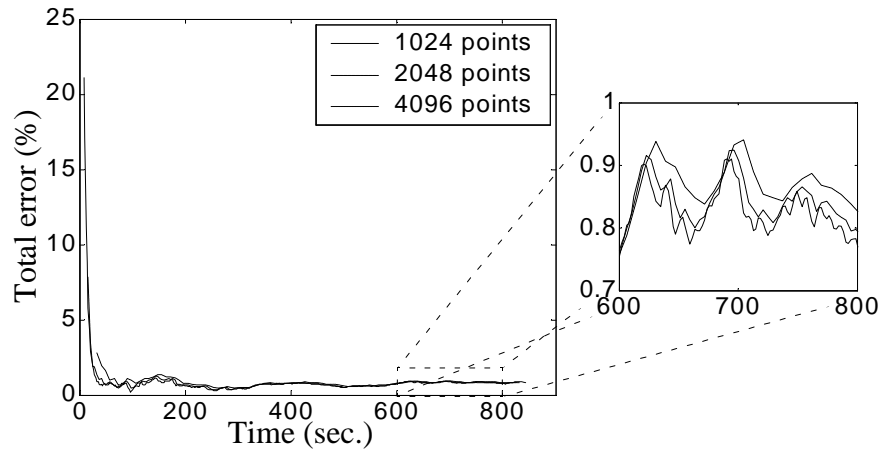


**FIGURE 3-17. Sensitivity of stiffness**

length. With 100 seconds of data a good estimate of the stiffness values is obtained. All 3 frames lengths showed similar behavior, with the same steady state error of 0.85%. This error is due to the sensor noise included in the signal, possible windowing leakage and computational errors.

### 3.3 Spectral lines

When the spectral density function is calculated using a computer, discrete points are obtained from the discrete Fourier transform. The frequencies corresponding to these points are called spectral lines. In this section, the sensitivity of the method is studied to determine if the performance of the ERA method changes if the frequency are on or off the spectral lines. This study considers a one degree of freedom undamped structure. Four structures are studied as shown in table 3-4.

**TABLE 3-4. Structural characteristics (1 DOF).**

<b>Case</b>	<b>Stiffness (MN/m)</b>	<b>Mass (Kg)</b>	<b>Natural frequency (Hz)</b>
A1	106.6	22,877	10.8643
A2	106.6	4,576	24.2920
B1	106.6	22,622	10.9253
B2	106.6	4,553	24.3530

The one DOF structure is excited with the same excitation force used for the study in section 3.2. The system is simulated for 100 seconds but only 90 seconds of stationary data are used for the identification process. Noise is not added to the measurements. Acceleration was obtained using the *lsim* command available in Matlab using 125 Hz as integration frequency. No resampling was applied to the data. Frames with 1024 points (75% overlapping) are used for the calculation of the spectral density functions. The Hankel matrix used in the ERA method had 25 rows and 5 columns of data, using a total of 0.384 seconds of correlation function.

Spectral lines are calculated at 10.8643Hz 10.9863 Hz, 24.2920Hz and 24.4141Hz. Cases A1–2 correspond to natural frequency matching an spectral line, and cases B1–2 correspond to natural frequencies not matching any spectral line.

Table 3-5 shows the identified and theoretical natural frequencies. The results obtained in both cases are extremely accurate. No error is induced in the procedure by having frequencies between spectral lines. This result also indicates that the number of points per frame does not influence the results of the ERA method very much.

### **3.4 Sensor noise**

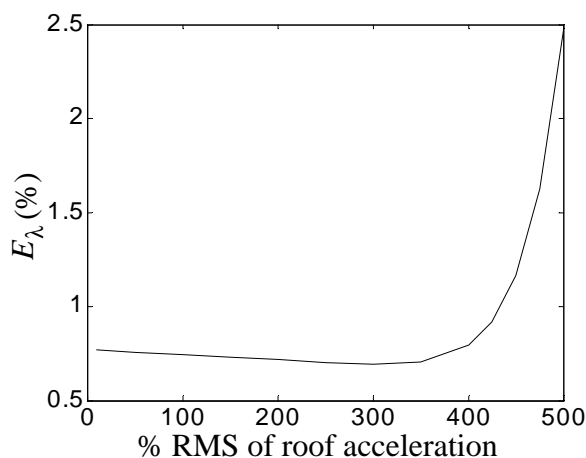
The effect of sensor noise on the results is investigated in this section. In this study the 12 DOF model developed for the health monitoring benchmark problem [26] is used. Sensor noise is included in the acceleration records as a Gaussian pulse process. In this

**TABLE 3-5. Identified and theoretical natural frequencies**

Case	Theoretical N.F. (Hz)	Identified N.F. (Hz)	Error (%)
A1	10.8643	10.8605	0.0350
A2	24.2920	24.2925	0.0022
B1	10.9253	10.9252	0.0091
B2	24.3530	24.3621	0.0373

study 1024 points per frame with 75% overlapping is used for the calculations of the spectral density functions. For the identification process 90 seconds of stationary data at 125 Hz were used. The ERA method was applied using 0.864 seconds of free response data to identify natural frequencies and mode shapes. The Hankel matrix was constructed with 200 rows and 40 columns.

The RMS of the noise is varied from 10% to 500% of the RMS of the roof acceleration. Figure 3-18 shows the resulting variation in the stiffness error with respect to the noise level. The methodology was found noise insensitive up to an RMS of 350% the RMS of the roof acceleration. In this numerical experiment notice that for noise levels lower than 350% the error slightly decreases when the error RMS increases.

**FIGURE 3-18. Sensitivity of total stiffness error to noise level.**

This insensitivity to sensor noise indicates that this methodology will be appropriate for identification using ambient vibration measurements. This will be tested on the experimental phase of the IASC-ASCE benchmark problem [17].

### 3.5 Modeling errors

The sensitivity of the technique due to modeling errors is studied in this section. When a real structure is modeled with a finite number of degrees of freedom (due to oversimplification in the model) errors will result because the  $n$  parameters used in the identification model cannot accurately represent the actual structure. The 120 DOF and 12 DOF models used in the health monitoring benchmark problem of the IASC-ASCE [26] are considered. The identification model is a simple 12 DOF shear building model. The 120 DOF model, used to generate the data, is considered to be the actual structure that is to be identified. The characteristics of the structural model and the identification models are described in detail in section 3.1.

Both models are excited in the weak direction ( $y$ -axis) with four forces, modeled as bandlimited white noise that is filtered with a low-pass Butterworth filter as described in section 3.1. One hundred seconds of acceleration data are generated at 1000Hz and resampled at 125Hz. Sensor noise is added modeled as Gaussian pulse processes with RMS of 10% the RMS of the roof acceleration.

The parameters used in the identification procedure (record length, number of points per frame, *etc.*) were selected based on what was learned in the previous studies. Ninety seconds of stationary data are used in the identification process. Frames of 1024 points with 75% overlapping are used in the calculation of the spectral density functions. The Hankel matrix used in the ERA has 40 columns and 200 rows, using 0.864 seconds of correlation function.

**TABLE 3-6. Exact and identified stiffness (MN/m) of 12 and 120 DOF models.**

Floor No	12 DOF structural model			120 DOF structural model		
	Exact	Identified	Error	Exact	Identified	Error
1	67.9	68.22	0.47%	61.38	63.60	3.61%
2	67.9	67.98	0.12%	55.95	64.69	15.62%
3	67.9	67.70	0.29%	54.45	63.18	16.03%
4	67.9	67.81	0.13%	51.28	55.16	7.57%

The identified stiffnesses of the two structural models are shown in Table 3-7. It is clear that modeling errors have a strong influence on the calculation of the identified stiffnesses. With no modeling errors (12 DOF structural model) a maximum difference of 0.47% is obtained between the identified and the actual stiffnesses. With modeling errors a maximum difference of 16.03% is observed, indicating that the selection of an appropriate identification model plays an important role in the identification process.

The identified and structural natural frequencies are shown in Table 3-7. Here we can observe that the ERA does a good job identifying the natural frequencies of both systems, indicating that the error in the identification process is a result of the choice of identification model.

**TABLE 3-7. Exact and identified natural freq. of 12 and 120 DOF models.**

Nat Freq No	12 DOF structural model			120 DOF structural model		
	Exact	Identified	Error	Exact	Identified	Error
1	9.41Hz	9.40Hz	0.11%	8.20Hz	8.21Hz	0.12%
2	25.60Hz	25.57Hz	0.12%	22.54Hz	22.57Hz	0.13%
3	38.85Hz	38.65Hz	0.51%	35.58Hz	35.55Hz	0.08%
4	48.37Hz	47.99Hz	0.78%	46.12Hz	46.09Hz	0.06%

### 3.6 Summary

In this chapter the sensitivity of the technique to different parameters was studied. Record lengths of 100 seconds at 125 Hz were found to be appropriate for structures

with natural frequencies ranging from 9Hz to 50Hz. The technique was found to be relative insensitive to the number of points per frame used in the calculation of the spectral density function. It was also found to be insensitive to Gaussian noise in the measurements. The ERA method was able to calculate natural frequencies accurately, even when the natural frequency does not lie directly on a spectral line. A bias error was found due to leakage and bias errors in the calculation of the spectral density functions. Modeling errors were found to be the most important source of errors in the numerical studies carried out. These results indicates that this technique has potential as a system identification technique for civil structures using ambient vibration data.

## Chapter 4

# Application of Health Monitoring to Simulated Data

Numerous techniques have been developed for structural health monitoring. These techniques have been applied to many structures in various environments making it difficult to compare the capabilities and deficiencies of each technique. The dynamics committee of the American Society of Civil Engineers (ASCE) joined with the International Association for Structural Control (IASC) to develop a benchmark problem to compare the pros and cons of each technique [26]. The subject of the structural health monitoring benchmark problem is the existing scaled structure located in the University of British Columbia, Canada [5]. The benchmark problem has two phases, a numerical phase and an experimental phase.

For the first phase of the benchmark problem two finite element models based on the structure are developed. The two models, referred to as structural models, play the role of the real structure in the generation of acceleration data. A third model is used to identify the stiffness coefficients of the structure. This model is called identification model. In chapter 3 the structure and the finite element models developed for the benchmark problem were discussed. No further description of the structure and the finite elements is given in this chapter.

The second phase of the benchmark problem will use acceleration records of the real structure as data for researchers to identify damage [17]. This phase is currently under development and it is not discussed in this thesis.

This chapter discusses the application and results of the structural health monitoring methodology discussed in this thesis to the first phase of the ASCE structural health monitoring benchmark problem. A description of the benchmark problem, excitation cases and damage patterns is given in the first section of this chapter. In the second section a discussion of the identification parameters used for the methodology to solve the benchmark problem is provided. Then, the results of the identification process are discussed, followed by a summary.

## **4.1 Benchmark problem definition**

The IASC-ASCE structural health monitoring benchmark problem has a total of six cases to be studied. Each case differs in the excitation forces, structural configuration, and damage patterns. A 12 DOF model and a 120 DOF model are used to obtain acceleration data in the benchmark problem. The mass distribution of these structures is symmetric or asymmetric depending of the identification case. The difficulty of the identification process increases with the case number. For example, in the first case the 12 DOF symmetric structure is used for the identification of 2 damage patterns, and in case 6 the 120 DOF asymmetric structure is used to identify 5 patterns of damage with limited sensors. The different identification cases, damage patterns and excitation cases are described in the following sections.

### **4.1.1 Damage patterns**

Damage in the structure is simulated by removing braces or decreasing the stiffness of the floor beams. The following five different damage patterns were defined in the benchmark problem: i) all braces in the first story are removed; ii) all the braces of the

first and third stories are removed; iii) one brace in the first story is removed; iv) one brace is removed in the first and third stories; and v) one brace is removed in the first and third stories and a floor beam is loosen in the first story. Figure 4-1 shows the different damage patterns.

Johnson et al [26] reported changes in the natural frequencies for damage patterns 1 and 2 for both models. These values are shown in Table 4-1. In this table we can observe that the 120 DOF model has lower natural frequencies than the 12 DOF model. The first natural frequency is in the translational direction of the weak direction (y-axis) in both models. The first natural frequency of the 12 DOF model changes from 9.41 Hz for the undamaged case to 6.24 Hz and 5.83 Hz for the first and second damage pattern. For the 120 DOF model the first natural frequency changes from 8.20 Hz in the undamaged case to 4.91 Hz and 4.36 Hz for the first and second damage patterns.

**TABLE 4-1. Natural frequencies for the undamaged structure and cases 1 and 2.**

Mode Type	12 DOF Model			120 DOF Model		
	Undamaged	Patt. 1	Patt. 2	Undamaged	Patt. 1	Patt. 2
Trans (y)	9.41	6.24	5.83	8.20	4.91	4.36
Trans (x)	11.79	9.91	9.52	8.53	6.61	5.77
Rotat.	16.53	11.84	11.13	13.95	8.82	7.74
Trans (y)	25.60	21.58	14.93	22.54	18.38	10.26
Trans (x)	32.07	28.99	24.98	24.24	21.06	15.22
Trans (y)	38.85	37.56	28.78	35.58	32.56	18.32
Rotat.	45.17	38.75	36.28	39.05	33.98	33.80
Trans (y)	48.37	47.57	41.65	39.73	38.09	37.47
Trans (x)	48.68	48.19	47.06	46.12	45.80	37.83
Trans (x)	60.60	60.45	54.76	55.16	54.68	47.81
Rotat.	68.64	66.46	64.86	60.75	58.11	58.01
Rotat.	85.51	85.20	74.27	79.46	78.80	66.38

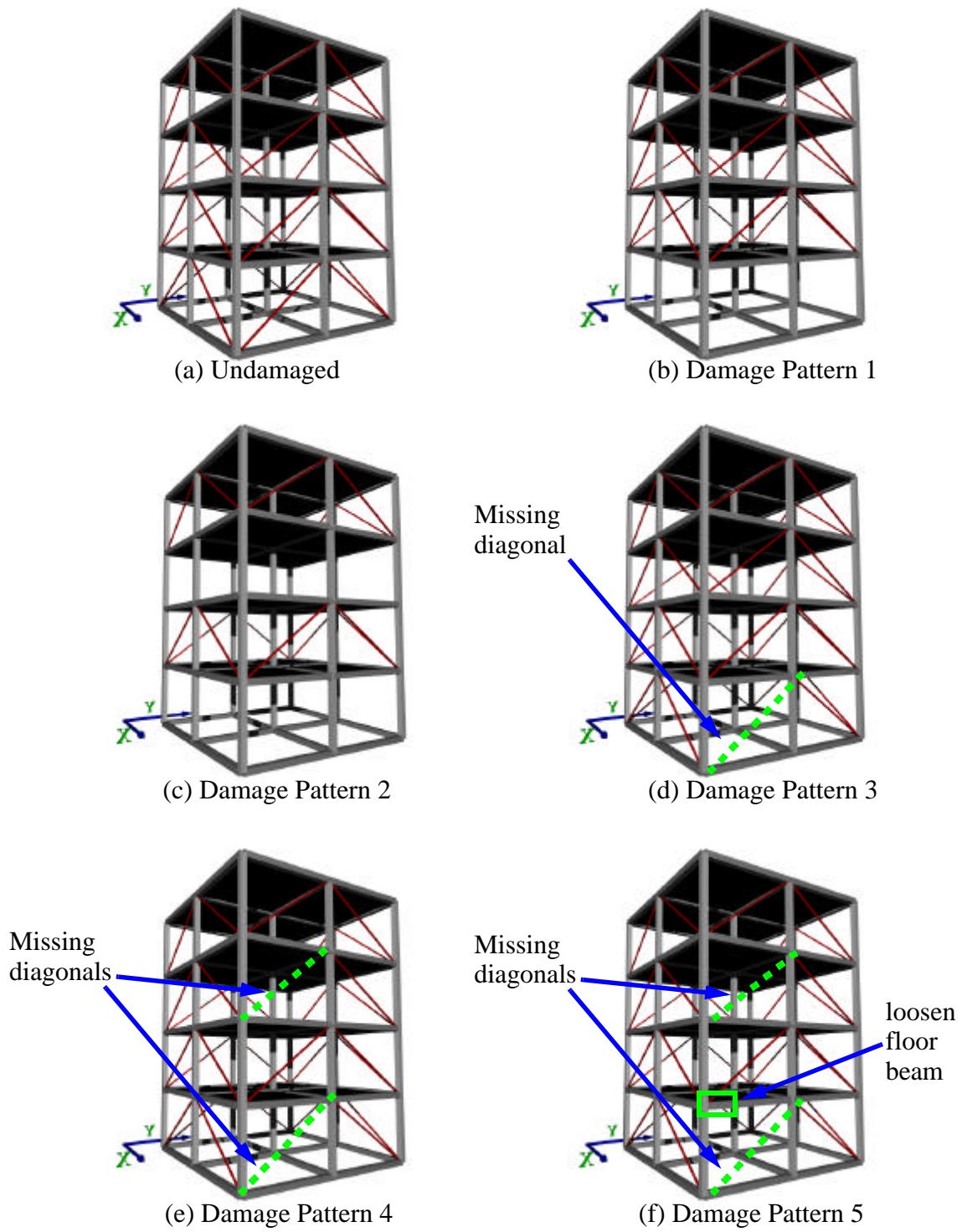


**FIGURE 4-1. Damage patterns**

To identify the occurrence of damage, the stiffness of each floor in the damaged cases are compared to that of the undamaged case. The percent reduction in the stiffness values are defined as

$$\text{Stiffness loss } i\text{-th floor (\%)} = \frac{k_{i \text{ undamaged}} - k_{i \text{ damaged}}}{k_{i \text{ undamaged}}} \times 100, \quad (4-1)$$

where  $k_{i \text{ undamaged}}$  is the undamaged stiffness of the  $i$ -th floor and  $k_{i \text{ damaged}}$  is the damaged stiffness of the  $i$ -th floor.

Johnson *et al.* [26] also reported the theoretical stiffness values for the first 2 damage cases for the 12 DOF structure. In the strong direction ( $x$ -axis) the healthy structure has a original stiffness of 106.6 MN/m in each floor. When the braces are removed, the stiffness in this direction decreases to 58.4 MN/m in the damaged floor, for a stiffness loss of 45.21%. In the weak direction ( $y$ -axis) the healthy structure has a stiffness of 67.9 MN-m. When braces are removed, the stiffness of the damaged floor in this direction is 19.7 MN-m, for a stiffness loss of 70.99%.

#### 4.1.2 Mass distribution

The basic structure has a symmetric mass distribution as discussed in Section 3.1. The total mass of the structure is 10,567.1 Kg including beams, columns, diagonals and concrete slabs. The mass of the concrete slabs is 3,200 Kg at the first floor, 2,400 Kg at the second and third floor, and 1,600 Kg at the fourth floor.

An asymmetric mass distribution was also considered in the benchmark problem. This distribution was obtained by changing one of the four concrete slabs of 400 Kg at the

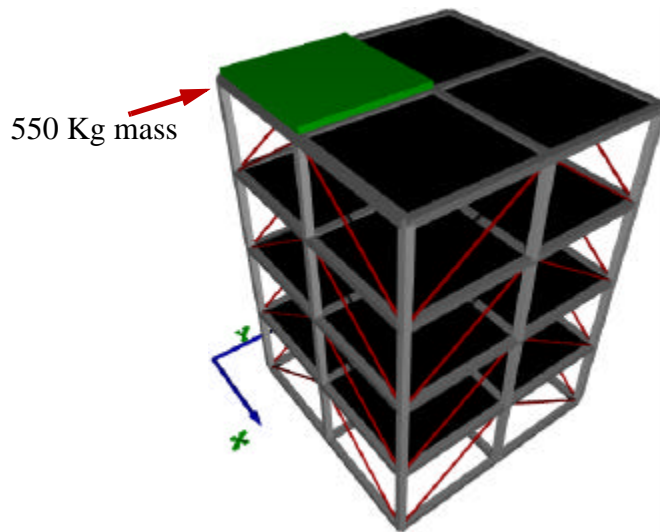


**FIGURE 4-2. Asymmetric mass distribution**

roof to a concrete slab of 550 Kg as shown in Fig. 4-2. This allows coupling between the translational and rotational motions of the structure.

### 4.1.3 Excitation cases

Two excitation cases were used in the benchmark problem (Fig. 4-3.) The first type of excitation is a horizontal force applied to each floor of the structure, modeling ambient excitation or wind excitation (Fig. 4-3a). The forces are modeled as independent Gaussian white noise processes filtered with a 6<sup>th</sup> order low-pass Butterworth filter. This filter has a cutoff frequency of 100 Hz as reported by Johnson *et al.* [26].

The second type of excitation is force at the top of the structure (Fig. 4-3b). This force will simulate the effects of a shaker on the roof. The load applied to the structure is applied along the diagonal. Note that when the mass distribution is symmetric, there is

no rotation due to this force. The force in the shaker was also a Gaussian white noise process filtered with a low-pass Butterworth filter.

#### 4.1.4 Identification cases

Six different identification cases with increasing levels of difficulty were considered. The first three cases used symmetric mass models and identification was performed in the weak direction ( $y$ -axis) of the structure. In cases 4 through 6 the asymmetric mass models were used.

In the first identification case the 12 DOF structure is used to generate acceleration data. The model was excited with the ambient excitation. Four acceleration sensors are available per floor with a sensor noise with RMS of 10% the RMS of the roof. Damage patterns one and two were considered in this case. This is the basic identification case, where only one dimensional damage is considered with no modeling errors.

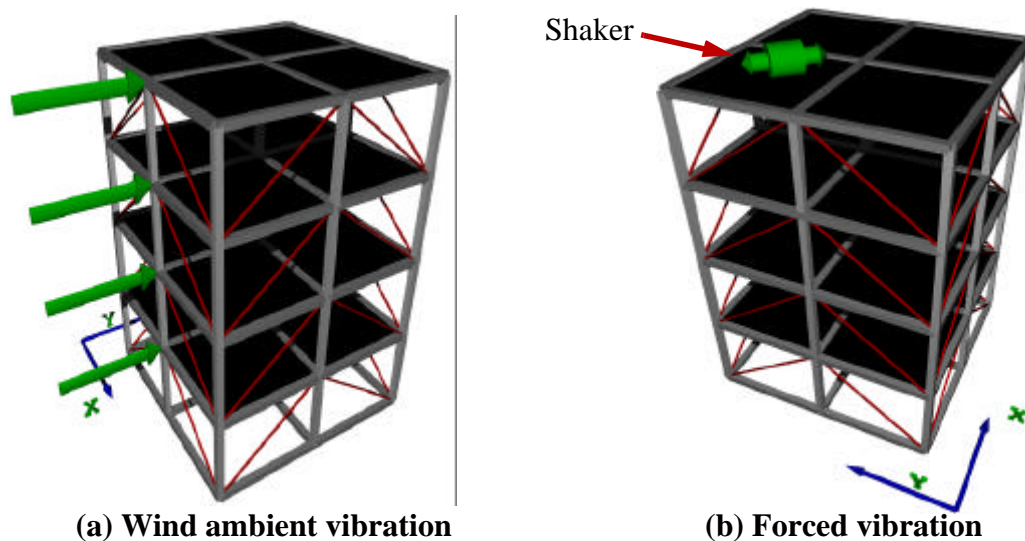


FIGURE 4-3. Excitations.

Modeling errors are included to the structural health monitoring procedure in case two. This case identification case two has the same characteristics as case one but the 120 DOF model was used to generate the data.

Case three is similar to case one but the shaker is used to excite the structure instead of the ambient vibration. Only damage patterns one and two are considered in this case. Because the shaker is located in the roof diagonal, the forces excite the weak and the strong axes of the structure. Thus, damage identification is required for both axes ( $x$  and  $y$  axes).

Case four is the first case where asymmetric mass distribution is considered and coupling between the rotational and translational modes of vibration is studied. The 12 DOF model was used. This model was excited with the shaker forces to generate acceleration data in the 14 sensors. In this case all damage patterns are present.

Case five and six have the same characteristics as case four but the 120 DOF model is used. In case five all of the sensors are used for the identification process. However, in case six limited sensors (at the second and fourth floors) are available.

The proposed structural health monitoring methodology was used to identify damage in each of the cases and damage patterns described in this section using the parameters found in chapter 3. In the next section a description of the parameters used for the methodology for the identification of damage is provided.

## **4.2 Solution to the benchmark problem**

The methodology proposed in this thesis was used to solve the identification cases proposed in the IASC-ASCE structural health monitoring benchmark problem. Based on

the results obtained in chapter 3 the following parameters were used in the identification procedure:

- Acceleration data was resampled to 125 Hz, which is large enough to identify all the translational modes of vibration of the structure.
- In the calculation of the spectral density functions a frame of 1024 points was used with a 75% overlapping. This allows us to maximize the averaging of the points with shorter records.
- A record length of 90 seconds was used, for a total of 40 averages in the calculation of the spectral density function.
- To reduce the effects of leakage a Hanning window was used in the calculations of the spectral density functions [32].
- The reference channel to calculate the spectral density functions is the acceleration at the roof. This channel was selected because all modes are observed at this point.
- The Hankel matrix used in the ERA method has a total of 40 columns and 200 rows. Thus, the ERA method uses 0.864 seconds of the correlation function.
- The first 8 singular values of the Hankel matrix were selected as the poles of the structure. The remaining 32 values are considered computational modes.

Using these parameters the six cases of the benchmark problem were solved. The results of the application is discussed in the next section.

### **4.3 Results**

The results of the benchmark problem are presented in this section. The first part focuses on cases 1 through 3, where only two damage patterns are considered. The second part focuses on the cases 4 and 5, where all five damage patterns are considered. The final part discusses the results of case 6, in which limited sensor data is available.

### 4.3.1 Benchmark Problem Cases 1 through 3

The structural health monitoring technique was applied to the first three cases of the benchmark structural health monitoring problem. A representative cross-spectral density function and cross-correlation function (case 1, undamaged) are shown in Fig. 4-4. The results of cases 1 through 3 are provided in Table 4-2. The first four columns provide the frequencies identified with the ERA algorithm. The last four columns show the natural frequencies of the identified model using the stiffness values obtained with the least squares estimates. The least squares estimates of the stiffness values for each floor are provided in table 4-3.

For the 12 DOF model the ERA results are all within 0.79% of the reported frequencies by Johnson et al [26] shown in table 4-1. The maximum difference between the exact values and those obtained using the resulting identified stiffness values in Table 4-2 is 0.83%. The ERA results are all within 0.17% of the reported frequencies for the 120 DOF structure (Table 4-1).

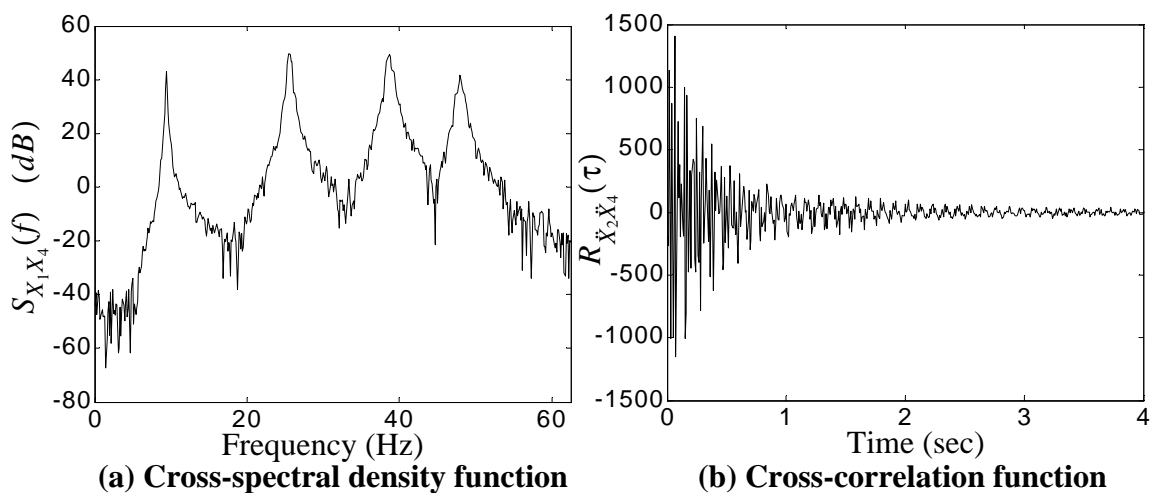


**FIGURE 4-4. Representative Cross-spectral Density Function and Cross-correlation Functions (Case 1, Undamaged).**

**TABLE 4-2. Identified Natural Frequencies for cases 1 through 3.**

Case	Damage Pattern	ERA Nat. Freq. (Hz)				Least Squares Nat. Freq. (Hz)			
		$\omega_1$	$\omega_2$	$\omega_3$	$\omega_4$	$\omega_1$	$\omega_2$	$\omega_3$	$\omega_4$
1 (y-axis)	No damage	9.40	25.57	38.65	47.99	9.42	25.54	38.67	47.97
	Pattern 1	6.25	21.53	37.33	47.79	6.22	21.50	37.36	47.78
	Pattern 2	5.84	14.89	36.14	41.40	5.80	14.77	36.08	41.45
2 (y-axis)	No damage	8.21	22.58	35.55	46.10	9.11	24.34	36.37	45.46
	Pattern 1	4.91	18.35	34.04	45.76	5.71	20.40	35.04	45.21
	Pattern 2	4.36	10.26	33.84	37.40	5.19	12.80	34.31	36.74
3 (x-axis)	No damage	11.75	32.04	48.44	60.10	11.80	32.02	48.37	60.19
	Pattern 1	9.90	28.92	47.24	59.92	9.89	28.91	47.26	59.95
	Pattern 2	9.51	24.87	46.86	54.35	9.49	24.82	46.83	54.39
3 (y-axis)	No damage	9.43	25.57	38.73	48.06	9.40	25.52	38.73	48.04
	Pattern 1	6.22	21.54	37.43	47.89	6.19	21.50	37.46	47.85
	Pattern 2	5.83	14.90	36.17	41.32	5.91	15.22	36.12	41.25

For the 12 DOF model (cases 1 and 3) the identified stiffness values range between 105.20 to 107.79MN/m in the strong direction, and 67.60 to 68.42 MN/m in the weak direction for the undamaged case. These results are within 1.11% and 0.77% of the actual values, respectively. When all the braces are removed, the identified values range from 57.58MN/m to 58.28MN/m in the strong direction and 19.23MN/m to 20.84MN/m in the weak direction which are within 1.40% and 5.6% of the actual values, respectively.

In case 2 the 120 DOF model is used to generate the data. Thus, because we have decided to base the technique on a model of a set order, the identified values of the stiffnesses are equivalent values which correspond to a least squares estimate, and they cannot be compared to exact values. As expected, the identified equivalent horizontal stiffnesses of this model are lower than the stiffnesses of the identified 12DOF.

**TABLE 4-3. Identified stiffness coefficients (Cases 1, 2 and 3).**

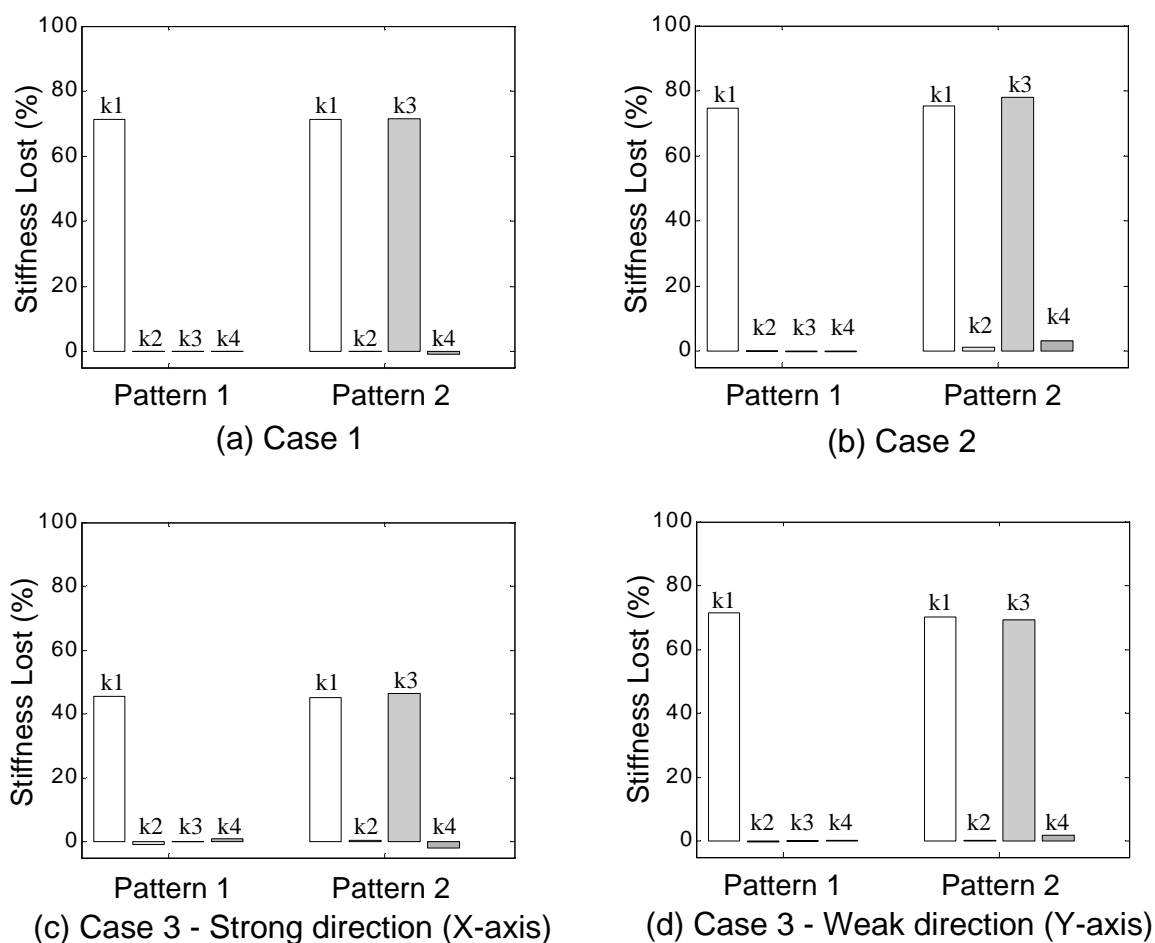
Case	Damage Pattern	Stiffness (MN/m)			
		k1	k2	k3	k4
1 (Y-axis)	No damage	68.12	68.00	67.70	67.82
	Pattern 1	19.50	67.96	67.66	67.79
	Pattern 2	19.59	68.06	19.23	68.41
2 (Y-axis)	No damage	63.63	64.69	63.19	55.14
	Pattern 1	16.08	64.62	63.32	55.27
	Pattern 2	15.77	63.96	13.90	53.36
3 (X-axis)	No damage	106.30	107.25	107.79	105.20
	Pattern 1	57.75	108.15	107.64	104.28
	Pattern 2	58.28	106.69	57.58	107.36
3 (Y-axis)	No damage	67.60	68.03	67.65	68.42
	Pattern 1	19.30	68.23	67.61	68.31
	Pattern 2	20.23	67.91	20.84	67.11

Figure 4-5 shows the stiffness loss for each case. In this figure we can see clearly that damage occurs in the first floor for damage pattern one and in the first and third floor for damage pattern two in all three identification cases.

Table 4-4 provides the values of the stiffness loss in cases 1 to 3. Negative values indicate a identified increase of the stiffness.

Notice from Table 4-4 that the stiffness reduction based on the identified values obtained in cases 1 and 3 are quite accurate. These cases are accurate because the 12 DOF model is used to generate the data. The form of the actual model used to generate the data and the assumed form of the model are identical. Notice also that there is no significant difference in the values of the stiffnesses obtained in the case 1 and the weak direction of case 3. The proposed technique is able to successfully identify damage for the cases in wind excitation is applied to all floors (case 1) as well as when a single excitation is applied at the top floor (case 3).

In case 2 the form of the actual model (120 DOF) and the assumed model are different. However, the frequencies identified by the ERA method are within 0.17% of the theoretical values. Thus the errors in the obtained stiffnesses can be attributed primarily to modeling errors (i.e., the 12DOF model selected cannot represent the 120DOF structure well). Modeling errors due to the computation of an equivalent stiffness appear as a larger reduction of stiffness in damage floors. Further in the 120DOF finite element model, removal of a brace will effect the stiffness of the floors above and below that level. Interestingly, the effects of this damage on the stiffnesses of the other floors in the results obtained for case 2 were observed. Here there is a 1.13% reduction in  $k_2$  and a 3.24% reduction in  $k_4$  for damage pattern 2. Because the magnitude of the damage is



**FIGURE 4-5. Stiffness Reduction of Each Floor in Damage Patterns for Cases 1 through 3.**

significantly larger than the effects of modeling errors in this example we can still identify the damaged floors.

**TABLE 4-4. Loss in Stiffness Values for Cases 1 through 3.**

Case	Damage Pattern 1				Damage Pattern 2			
	k1 (%)	k2 (%)	k3 (%)	k4 (%)	k1 (%)	k2 (%)	k3 (%)	k4 (%)
<b>1-Weak (Y)</b>	71.37	0.06	0.05	0.05	71.24	-0.08	71.60	-0.87
<b>2-Weak (Y)</b>	74.73	0.10	-0.21	-0.23	75.22	1.13	78.00	3.24
<b>3-Strong (X)</b>	45.67	-0.84	0.13	0.87	45.18	0.52	46.58	-2.06
<b>3-Weak (Y)</b>	71.45	-0.30	0.06	0.17	70.08	0.17	69.20	1.92

### 4.3.2 Benchmark Problem Cases 4 and 5

Five patterns of damage are considered in cases 4 and 5. Table 4-5 provides the resulting frequencies determined using the ERA algorithm and the identified stiffness values. The loss in the identified stiffness values is displayed graphically in Fig. 4-6. In case 4 the 12 DOF model is used to generate the data, and in case 5 the 120 DOF model is used to generate the data. Additionally, the mass is distributed asymmetrically in these cases, resulting in a coupling between the  $x$  and  $y$ -motions. Because the floors are assumed to be rigid, we can decouple the motions in these two directions to determine the translational acceleration in the  $x$  and  $y$  direction of the structure. The motions are decoupled using the average of two accelerations on opposite faces of the structure as

$$a_i = \frac{a_{1i} + a_{2i}}{2}, \quad (4-2)$$

where  $a_i$  is the acceleration in the  $i$ -th direction ( $x$  or  $y$ ),  $a_{1i}$  and  $a_{2i}$  are the two accelerations. Because we decouple the motions of the structure, the torsional frequencies are not present in the cross-spectral densities. However, this information is not necessary as it is used in the identification procedure.

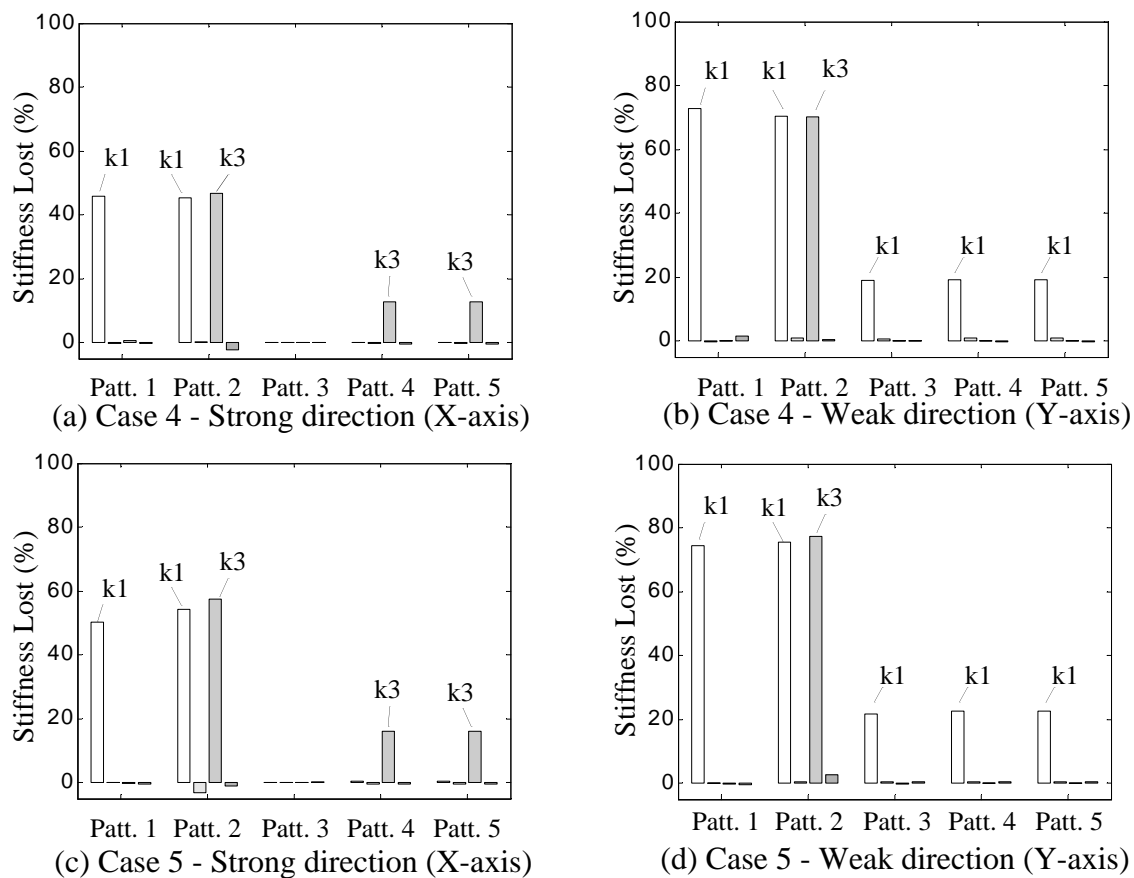


**FIGURE 4-6. Stiffness Reduction of Each Floor in Damage Patterns for Cases 4 and 5.**

Notice that the identified stiffness values resulting from data generated with the undamaged 12 DOF model (case 4) are between 108.11MN/m and 105.06MN/m in the strong direction, and between 67.65MN/m and 68.23MN/m, which are within 1.44% and 0.49% of the actual values. The stiffness values identified in damage patterns 1 and 2 are also quite close to the exact values reported in Johnson *et al.* [26]. Thus, the identification procedure is not affected by the coupling due to asymmetry in the mass distribution.

In case 4, accurate stiffness values are obtained for damage patterns 1 and 2. A smaller reduction in stiffness is observed in damage patterns 3 and 4, although the damage can be clearly associated with the floors which are damaged. Because the loosening of a beam in a 12 DOF model (case 4) does not effect enough the stiffness matrix to change

**TABLE 4-5. Natural Frequencies for Cases 4 and 5.**

Case	Damage Pattern	Natural Freq. (Hz) - ERA				Nat. Freq. (Hz) Least squares			
		$\omega_1$	$\omega_2$	$\omega_3$	$\omega_4$	$\omega_1$	$\omega_2$	$\omega_3$	$\omega_4$
4 (X axis)	No damage	11.62	31.58	48.04	59.73	11.64	31.67	47.82	59.88
	Pattern 1	9.79	28.52	46.86	59.55	9.76	28.56	46.73	59.65
	Pattern 2	9.41	24.69	46.56	53.66	9.36	24.59	46.51	53.71
	Pattern 3	11.62	31.57	48.03	59.72	11.64	31.67	47.81	59.88
	Pattern 4	11.49	30.84	48.03	58.07	11.51	30.86	47.88	58.19
	Pattern 5	11.49	30.84	48.03	58.07	11.51	30.86	47.88	58.19
4 (Y axis)	No damage	9.32	25.25	38.26	47.83	9.29	25.25	38.33	47.75
	Pattern 1	6.16	21.27	36.72	47.49	6.01	21.12	36.86	47.41
	Pattern 2	5.77	14.79	36.03	40.60	5.81	14.95	35.94	40.63
	Pattern 3	8.77	24.43	37.81	47.70	8.79	24.27	37.86	47.66
	Pattern 4	8.77	24.43	37.80	47.70	8.78	24.26	37.85	47.66
	Pattern 5	8.77	24.43	37.80	47.70	8.78	24.26	37.85	47.66
5 (X axis)	No damage	8.40	23.91	39.43	54.99	10.76	27.86	41.17	53.34
	Pattern 1	6.53	20.77	37.68	54.51	8.79	25.08	39.89	52.98
	Pattern 2	5.70	15.11	37.31	47.60	8.05	20.27	39.57	45.96
	Pattern 3	8.40	23.91	39.40	54.99	10.76	27.85	41.15	53.34
	Pattern 4	8.13	22.96	39.16	53.18	10.58	27.09	40.99	51.37
	Pattern 5	8.13	22.96	39.16	53.18	10.58	27.09	40.99	51.37
5 (Y axis)	No damage	8.08	22.26	35.21	45.96	8.98	24.05	35.93	45.30
	Pattern 1	4.86	18.14	33.62	45.61	5.68	20.14	34.57	45.04
	Pattern 2	4.30	10.21	33.52	37.02	5.12	12.83	34.13	36.34
	Pattern 3	7.61	21.34	34.54	45.82	8.43	23.02	35.39	45.16
	Pattern 4	7.60	21.29	34.50	45.82	8.40	22.96	35.37	45.15
	Pattern 5	7.59	21.28	34.50	45.81	8.41	22.96	35.37	45.14

the natural frequencies of the system (the largest change in the frequencies is 0.26%), the stiffness values identified for damage pattern 5 are identical to those identified for damage pattern 4.

In case 5 the identified stiffness values obtained using the data corresponding to damage patterns 1 and 2 are close to the values obtained in case 2. A smaller reduction is observed in damage patterns 3 and 4. Again, although only one brace is removed, the

damage is extensive enough to clearly identify the floors at which damage occurs. However, the additional damage due to the loosened floor beam in damage pattern 5 is not clearly identified. This additional damage results in a very small change in the frequencies of the structure. The modeling errors incurred by the limitation of the 12 DOF identification model are of the same order as the additional stiffness reduction. Perhaps releasing the restriction of the 12 DOF identification model would allow this additional damage to be identified.

**TABLE 4-6. Identified stiffness coefficients (cases 4 and 5)**

Case	Damage Pattern	Stiffness (MN/m)			
		k1	k2	k3	k4
4 (X axis)	No damage	106.14	106.96	108.11	105.06
	Pattern 1	57.58	107.24	107.37	105.37
	Pattern 2	57.93	106.81	57.59	107.32
	Pattern 3	106.13	106.97	108.15	104.97
	Pattern 4	106.14	107.18	94.41	105.54
	Pattern 5	106.14	107.18	94.41	105.54
4 (Y axis)	No damage	67.65	68.21	67.63	68.23
	Pattern 1	18.34	68.42	67.63	67.08
	Pattern 2	20.08	67.58	20.22	67.84
	Pattern 3	54.75	67.72	67.66	68.23
	Pattern 4	54.61	67.60	67.68	68.29
	Pattern 5	54.61	67.60	67.68	68.29
5 (X axis)	No damage	91.59	95.41	89.44	64.10
	Pattern 1	45.53	95.45	89.59	64.38
	Pattern 2	41.92	98.37	38.04	64.87
	Pattern 3	91.52	95.43	89.45	64.01
	Pattern 4	91.21	95.74	75.03	64.32
	Pattern 5	91.20	95.74	75.04	64.31
5 (Y axis)	No damage	63.66	64.31	63.38	55.11
	Pattern 1	16.25	64.33	63.45	55.36
	Pattern 2	15.56	64.04	14.38	53.66
	Pattern 3	49.91	64.04	63.49	54.85
	Pattern 4	49.26	64.08	63.42	54.85
	Pattern 5	49.33	64.02	63.38	54.85

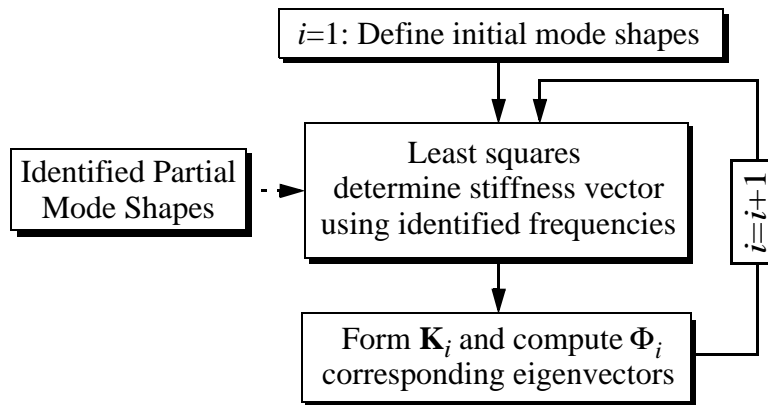


**FIGURE 4-7. Description of the Iterative Technique Used in Case 6.**

### 4.3.3 Benchmark Problem Case 6

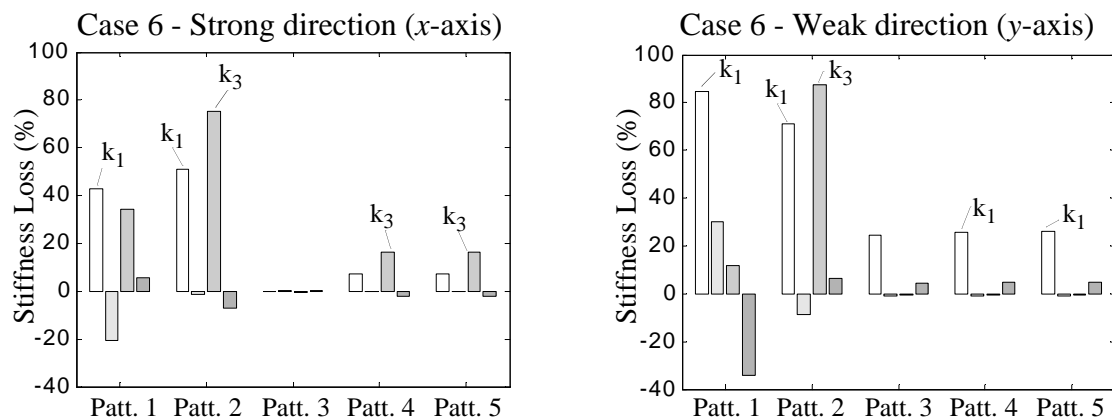
Case 6 of the benchmark problem focuses on the case in which the number of sensors on the structure is limited. Specifically, the sensors on the first and third floors are removed in this case of the benchmark study. Because these sensors are not used, the entire eigenvector matrix cannot be identified. An iterative procedure was developed to determine the eigenvectors and the stiffness terms. A description of the method is provided in Fig. 4-7. The steps in this procedure are as follows:

1. As an initial value, set the mode shape matrix equal to the full mode shape matrix of the undamaged system. Here the mode shapes from the undamaged structure resulting from the modal identification of case 5 were used. Alternatively, one could use a model of the structure to set the initial values.
2. Insert known values from the identified eigenvectors into the eigenvector matrix. This step is optional as indicated by the dashed line in the diagram in Fig. 4-7.
3. Use these mode shapes to determine the stiffnesses of the floors of the structure.

4. Form the stiffness matrix,  $\mathbf{K}_i$ , using the stiffnesses identified in step 3, and compute the corresponding eigenvector matrix,  $\Phi_i$ .
5. Set  $i = i+1$ , and return to step 2 using the eigenvectors computed in step 4.

Note that if, in step 2, the identified components in the eigenvector are not used in this iterative procedure, only the frequencies are required to determine the least squares estimate of the stiffness. Thus, a single sensor to determine the natural frequencies would be adequate to determine the eigenvectors, eigenvalues, and stiffnesses of the structure.

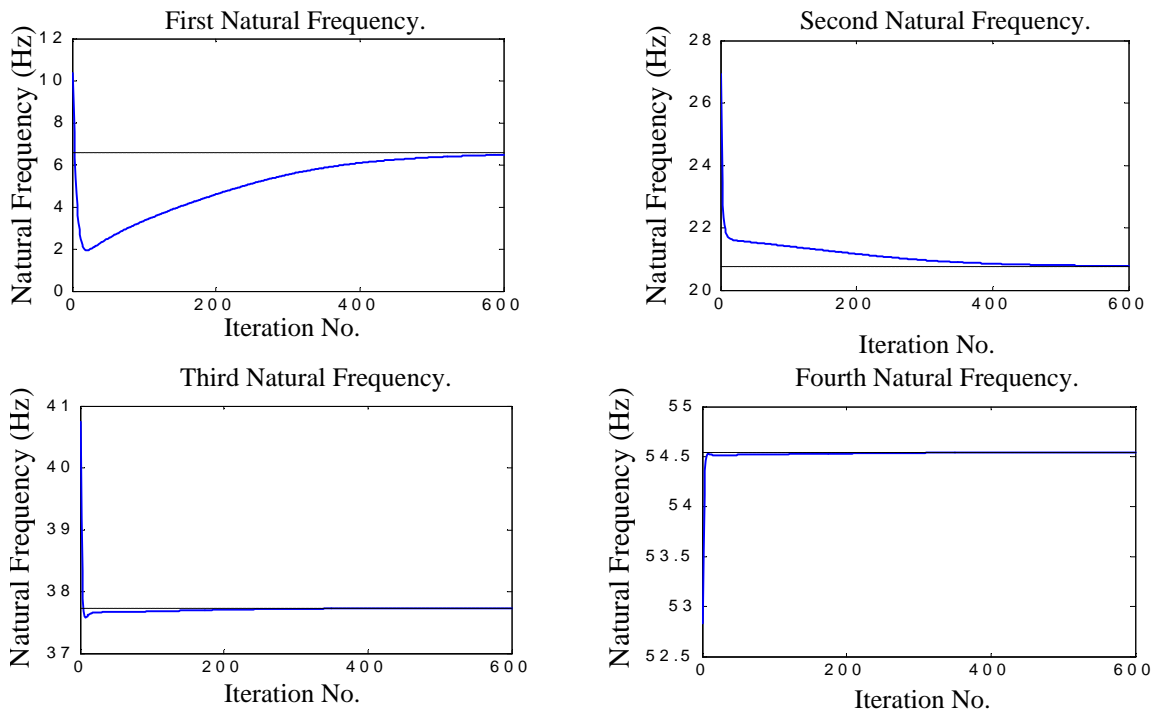
In the damaged structure (damage pattern 1), the eigenvalues of the identified model converge as shown in Fig. 4-9. Based on these plots, a total of 600 iterations were used to identify the stiffnesses and mode shapes for case 6. The results of this analysis are provided in Fig. 4-8 and Table 4-7. Note that the correct damage pattern is obtained in most, but not all, situations. For instance, the loss in stiffness in damage patterns 2–5 corresponds to the actual location of the damage. In some cases some damage is observed at other floors, although this is small relative to the loss in stiffness on the floor with damage. However, in damage pattern 1, the results indicate that the largest loss in



**FIGURE 4-8. Stiffness Reduction of Each Floor in All Damage Patterns for Case 6.**

**TABLE 4-7. Natural Frequencies and Identified Stiffness Values in Case 6.**

Case	Damage Pattern	Natural Frequencies (Hz)				Stiffness (MN/m)			
		$\omega_1$	$\omega_2$	$\omega_3$	$\omega_4$	$k_1$	$k_2$	$k_3$	$k_4$
6 (x-axis)	No damage	8.41	23.88	39.40	54.92	36.01	121.36	87.66	54.28
	Pattern 1	6.56	20.77	37.73	54.55	20.58	146.43	57.60	51.12
	Pattern 2	5.73	15.11	37.38	47.64	17.63	122.85	21.79	58.21
	Pattern 3	8.41	23.88	39.35	54.92	36.06	120.98	88.03	54.04
	Pattern 4	8.13	22.97	39.11	53.14	33.43	121.52	73.47	55.38
	Pattern 5	8.13	22.97	39.11	53.14	33.43	121.52	73.46	55.38
6 (y-axis)	No damage	8.10	22.23	35.16	45.94	38.63	69.54	66.94	51.97
	Pattern 1	4.86	18.17	33.68	45.57	6.00	48.44	59.08	69.77
	Pattern 2	4.31	10.24	33.54	36.97	11.10	75.63	8.46	48.71
	Pattern 3	7.61	21.34	34.55	45.81	29.16	70.09	67.26	49.78
	Pattern 4	7.60	21.28	34.48	45.80	28.72	70.05	67.35	49.53
	Pattern 5	7.59	21.27	34.48	45.79	28.58	70.04	67.29	49.54

**FIGURE 4-9. Conversion of Natural Frequencies for Damage Pattern 1.**

stiffness occurs on level 1, but a significant loss in stiffness is observed on other floors as well. In damage pattern 3 when damage is not present in the  $x$ -direction, the results of the iterative approach also indicate that no loss in stiffness is present in this direction. Thus this approach provides an indication of the location of the damage, but may indicate that damage occurs in some locations where damage is not present. Thus, once this method indicates that there is some damage, further data would be required to investigate the actual damage present in the structure. This additional data could be provided by moving the available sensors around on the structure since the cross-correlation functions do not require all measurements to be made simultaneously and can be obtained with two sensors at a time (one must always be at the reference channel).

#### **4.4 Summary**

The structural health monitoring approach discussed in this thesis was found to be quite effective for detecting damage in the benchmark model. Typical errors in the identified stiffness values were less than 1%. The method was found to be insensitive to noise in the data, and a reasonable amount of data (90 sec.) was required to implement the technique. An additional advantage of this technique is that, although it was not necessary for this example, it may be automated for real-time applications [8]. Additionally it is not necessary to have all of the frequencies and mode shapes, although a minimal number is required to obtain a unique least squares solution.

Further, although a 12DOF model was assumed for the identification model, damage was correctly identified when the data was generated with the 120DOF model. Thus the method was relatively insensitive to modeling errors. Small damage, such as that associated with the loosened beam, was not detected because the stiffness loss was significantly smaller than the modeling errors. Future studies will consider this case when the restriction on the form of the identification model is lifted, reducing the modeling errors and allowing for more accurate identification of the stiffnesses. However, in case 6

(limited sensors are available), the least squares solution of the eigenvalue problem cannot be used directly. An iterative process was developed for this case. This iterative method was successful in finding the location of possible damage. In some cases damage was found where no damage existed. However, for this problem, the method did not miss any damage locations.

## **Chapter 5**

# **Component Transfer Function Technique**

The previous chapters of this thesis described a structural health monitoring methodology using NeXT and ERA techniques. This chapter discusses the Component Transfer Function Technique (CTF), a new methodology for structural health monitoring. The Component Transfer Function technique is a level III methodology based on absolute acceleration measurements at various locations. To implement the CTF one does not need a model of the structure to detect damage and its location. Transfer functions between the sensors are computed to determine if damage is present in the structure, and identify the location. However, with this technique a structural model is needed to quantify the damage through an iterative process where stiffness coefficients are obtained.

In the first part of this chapter the motivation and approach to the Component Transfer Function Technique is described. The remainder of the chapter focuses on an experiment that was conducted to verify this technique. This verification was performed in the Washington University Earthquake Engineering Laboratory using a four-story building. In the last section of this chapter some concluding remarks are presented discussing the advantages and disadvantages of this technique.

### **5.1 Motivation for the CTF Technique**

Consider a seismically excited two-story structure as shown in Fig. 5-1. A lumped mass idealization of this structure is governed by the equations of motion

$$\begin{bmatrix} m_1 & 0 \\ 0 & m_2 \end{bmatrix} \begin{bmatrix} \ddot{x}_1 \\ \ddot{x}_2 \end{bmatrix} + \begin{bmatrix} k_1 + k_2 & -k_2 \\ -k_2 & k_2 \end{bmatrix} \begin{bmatrix} x_1 \\ x_2 \end{bmatrix} = - \begin{bmatrix} m_1 \\ m_2 \end{bmatrix} \ddot{x}_g. \quad (5-1)$$

where  $x_1$  and  $x_2$  are displacements of the floors relative to the ground. For a linear system the transfer function is defined as the Laplace transform of the output divided by the Laplace transform of the input [13]. Taking the Laplace transform of Eq. (5-1) and determining the transfer function from the ground acceleration to the first and second floor relative displacements yields

$$\frac{X_1(s)}{\ddot{X}_g(s)} = \frac{-[k_2 m_2 + m_1 m_2 s^2 + k_2 m_1]}{[(m_1 m_2) s^4 + [k_2 m_1 + m_2 (k_1 + k_2)] s^2 + k_2 k_1]} \quad (5-2)$$

$$\frac{X_2(s)}{\ddot{X}_g(s)} = \frac{-m_1 m_2 s^2 - m_2 k_1 - m_2 k_2 - m_1 k_2}{[(m_1 m_2) s^4 + [k_2 m_1 + m_2 (k_1 + k_2)] s^2 + k_2 k_1]}. \quad (5-3)$$

Knowing that the absolute acceleration of each floor is given by

$$\ddot{X}_{ia}(t) = \ddot{X}_i(t) + \ddot{X}_g(t), \quad (5-4)$$

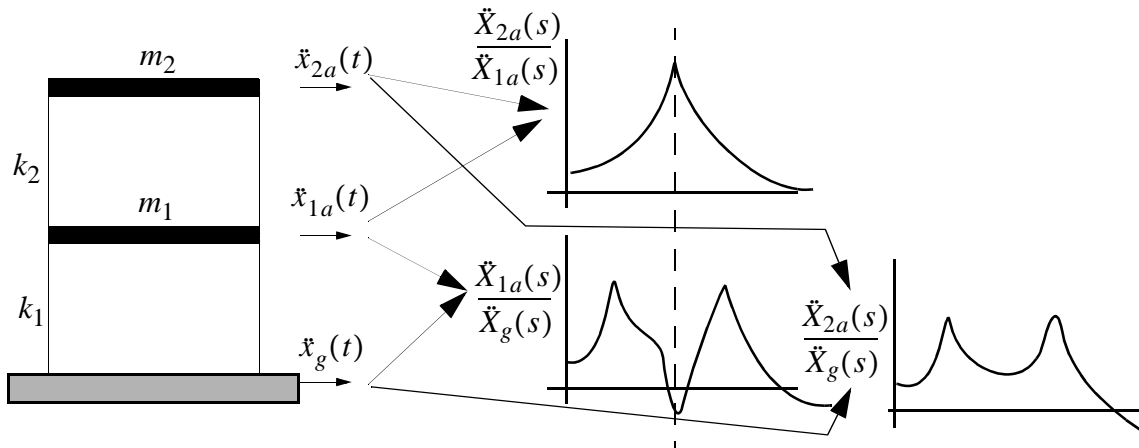


**FIGURE 5-1. Sample Component Transfer Functions of a Two Story Structure.**

one can determine the transfer functions from the ground acceleration to the  $i$ th floor absolute accelerations using the relationship

$$\frac{\ddot{X}_{ia}(s)}{\ddot{X}_g(s)} = \frac{s^2 X_i(s)}{\ddot{X}_g(s)} + \frac{\ddot{X}_g(s)}{\ddot{X}_g(s)} \quad (5-5)$$

which yields the transfer functions

$$\frac{\ddot{X}_{1a}(s)}{\ddot{X}_g(s)} = \frac{m_2 k_1 s^2 + k_1 k_2}{m_1 m_2 s^4 + (m_1 k_2 + m_2 k_1 + m_2 k_2) s^2 + k_1 k_2} \quad (5-6)$$

$$\frac{\ddot{X}_{2a}(s)}{\ddot{X}_g(s)} = \frac{k_1 k_2}{m_1 m_2 s^4 + (m_1 k_2 + m_2 k_1 + m_2 k_2) s^2 + k_1 k_2} \quad (5-7)$$

The *poles* and *zeros* are defined as the roots of the numerator and denominator of a transfer function respectively [13]. For light damped structures, poles come in complex conjugates pairs and correspond to the peaks of the plots shown in Fig. 5-1. Zeros correspond to depressions in the same figure. This model of the structure will have four poles.

Note that the zeros of the transfer function in Eq. (5-6) are the poles of the top floor of the structure,  $\sqrt{k_2/m_2}$ . Additionally the transfer function in Eq. (5-7) has no zeros. Using Eqs. (5-6) and (5-7), the component transfer function (CTF) of the upper floor of the structure (the transfer function from the first floor absolute acceleration to the second floor absolute acceleration) is

$$\frac{\ddot{X}_{2a}(s)}{\ddot{X}_{1a}(s)} = \frac{k_2}{m_2 s^2 + k_2} \quad (5-8)$$

Note that this transfer function has two poles (one peak) and no zeros. The poles of this system correspond to the natural frequency of the top floor of the structure ( $\sqrt{k_2/m_2}$ ), and are also the zeros of the transfer function from the ground acceleration to the first floor of the structure. This is due to the interaction between the first and second floors of the structure. This effect is portrayed in the diagram in Fig. 5-1. We can extend this observation to larger systems of lumped masses and springs.

## 5.2 Component Transfer Function Technique.

The component transfer function method is based on the observations described in the previous section. Because the peaks in the CTFs are determined by the mass and stiffness of the corresponding component, each component can be identified sequentially. The algorithm uses the CTFs to identify the location and severity of the damage. The steps in this approach are: *i*) determination of experimental component transfer functions; *ii*) identification of natural frequencies of component transfer functions; and, *iii*) determination of unknown structural stiffnesses. The stiffness of each floor of the structure is obtained sequentially from the top down. A flow chart describing the approach is shown in Fig. 5-2.

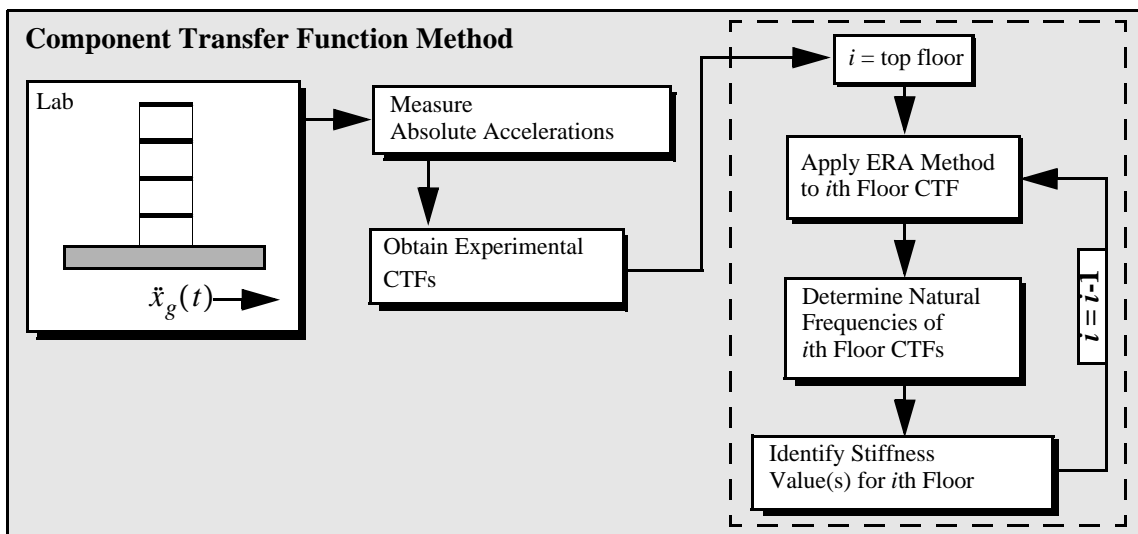


**FIGURE 5-2. Flow Chart for the Component Transfer Function Technique.**

Note that this approach can be automated to run on-line without user intervention which is an important requirement of any health monitoring technique. Additionally, an advantage of this technique is that the component transfer functions may be initially determined and examined for damage. If the peaks in these transfer functions do not shift, then there is no observable damage in the structure. Additionally, if the peaks in the CTFs for a number of upper stories do not change, then there is no damage at these levels and one may begin the identification procedure at the first level at which damage is present. Furthermore, sensors are not required at every floor of a structure. CTFs may be determined between adjacent sensors to obtain an indication of damage within that portion of the structure. This technique appears to be best suited for structures which can be modeled as lumped mass systems. Further studies are necessary before applying this technique to distributed systems.

### 5.2.1 Determination of Experimental Component Transfer Functions

Determination of the experimental transfer functions can be computed via one of two expressions [3] given by

$$H_{VU}(jf) = \frac{S_{UV}(f)}{S_{UU}(f)} \quad \text{and} \quad H_{VU}(jf) = \frac{S_{VV}(f)}{S_{VU}(f)} . \quad (5-9)$$

where  $H_{VU}(jf)$  is the transfer function for a stationary input signal,  $u(t)$  and a corresponding output signal,  $v(t)$ .  $S_{UV}(f)$  denotes the cross spectral density function between the processes  $U$  and  $V$ . The first of these equations is more commonly used. However, the second expression is usually applied when there is input noise [3]. The second approach was found to yield a less noisy transfer function in the experimental verification. The corresponding discrete frequency transfer function is

$$H_{VU}(jk\Omega) = \frac{S_{VV}(k\Omega)}{S_{UU}(k\Omega)}, \quad (5-10)$$

were  $S_{VU}(k\Omega)$  is the discrete cross spectral density function between the processes  $V$  and  $U$ .

### 5.2.2 Identification of Natural Frequencies.

Once the transfer function data is obtained there are numerous techniques available for identifying the modal parameters. The Eigensystem Realization Algorithm ERA [24] was used, as described in section 2.3. For the implementation of the ERA the impulse response function (or free response data) is needed. Here the impulse response function is calculated from the discrete frequency transfer function in Eq. 5-10 using the inverse Fourier transform [3]

$$h(t) = \int_{-\infty}^{\infty} H(jf) e^{j2\pi ft} df \quad (5-11)$$

The corresponding inverse discrete fourier transform is

$$h(n) = \frac{1}{N} \sum_{k=0}^{N-1} H(jk\Omega) e^{\frac{j2\pi kn}{N}} \quad n = 0, 1, 2, \dots, N-1 \quad (5-12)$$

### 5.2.3 Identification of stiffness coefficients

Using the natural frequencies obtained with the ERA, the stiffness of each floor is obtained using the least square solution of the eigenvalue problem as described in section 2.4.1. The stiffness coefficients are obtained sequentially from the top down. The

masses are assumed to be known. Once the stiffness of the undamaged structure are identified, damage can be measured comparing the stiffnesses of the potentially damaged structure to the stiffnesses of the healthy structure or structural models.

### 5.3 Experimental Verification

An experiment was performed in the Washington University Structural Control and Earthquake Engineering Laboratory <<http://wusceel.cive.wustl.edu/quake>> to verify the technique. This laboratory houses a uniaxial earthquake simulator. The simulator consists of a  $1.7 \times 1.7 \text{ m}^2$  ( $5 \times 5 \text{ ft}^2$ ) aluminum sliding table mounted on high-precision, low-friction, linear bearings.

The subject of the experimental study is the four-story test structure shown in Fig. 5-3. The structure is 120 cm (49 in) tall and has a total mass of 98 kg (216 lb) which is distributed uniformly between the floors. The structure is modular such that columns can

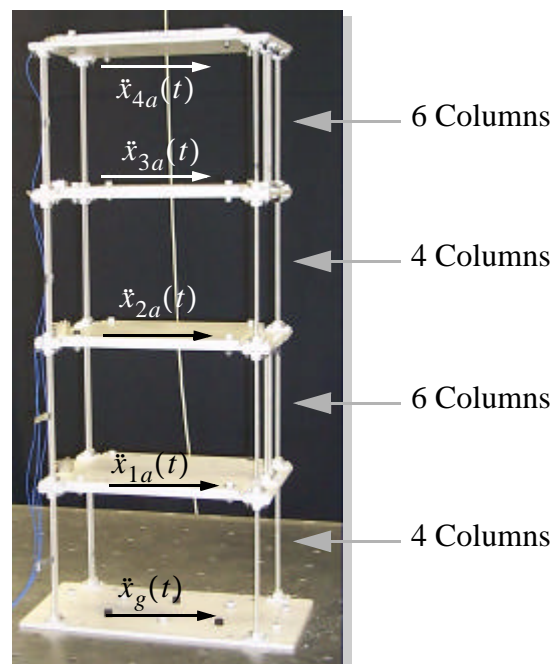


**FIGURE 5-3. Column Distribution (Damaged Case).**

be replaced or removed to study variations in the structural parameters. To experimentally verify this technique, members were removed from the structure to simulate damage. For the baseline (undamaged) structure six columns were placed on each level of the structure (see figure 5-3). Damage was induced in the structure by removing the two supplemental columns on the first and third floors of the structure. This change in the number of columns correspond to approximately a 33.3% loss in the stiffness between the undamaged and damaged cases on floors 1 and 3.

One capacitive accelerometer from PCB Piezotronics was used on each floor. A DSP Technologies Siglab 20-42 data acquisition system was used to obtain the absolute acceleration of all floors simultaneously. The acceleration of each floor is measured as shown in Fig. 5-3. Data is collected using a sample frequency of 128 Hz. Antialiasing filters were used to prevent aliasing. The data was later resampled to 32 Hz using the Matlab tool *resample.m* [29].

A 20 Hz band-limited white noise is used to excite the earthquake simulator table. Sets of 240 seconds of excitation were used to test the structure.

### 5.3.1 Experimental Results

Figure 5-4 shows 50 seconds of typical acceleration records for each of the accelerometers in the experiment. The experimental component transfer functions of the test structure are shown in Fig. 5-5. Notice that the peaks of the transfer function from the third to the fourth floors are the same for the damaged and the undamaged cases, indicating that no damage is present on the top floor. However, the component transfer functions demonstrate a shift in the peak between the undamaged and damaged cases. This is evidence of damage in the 3rd story.

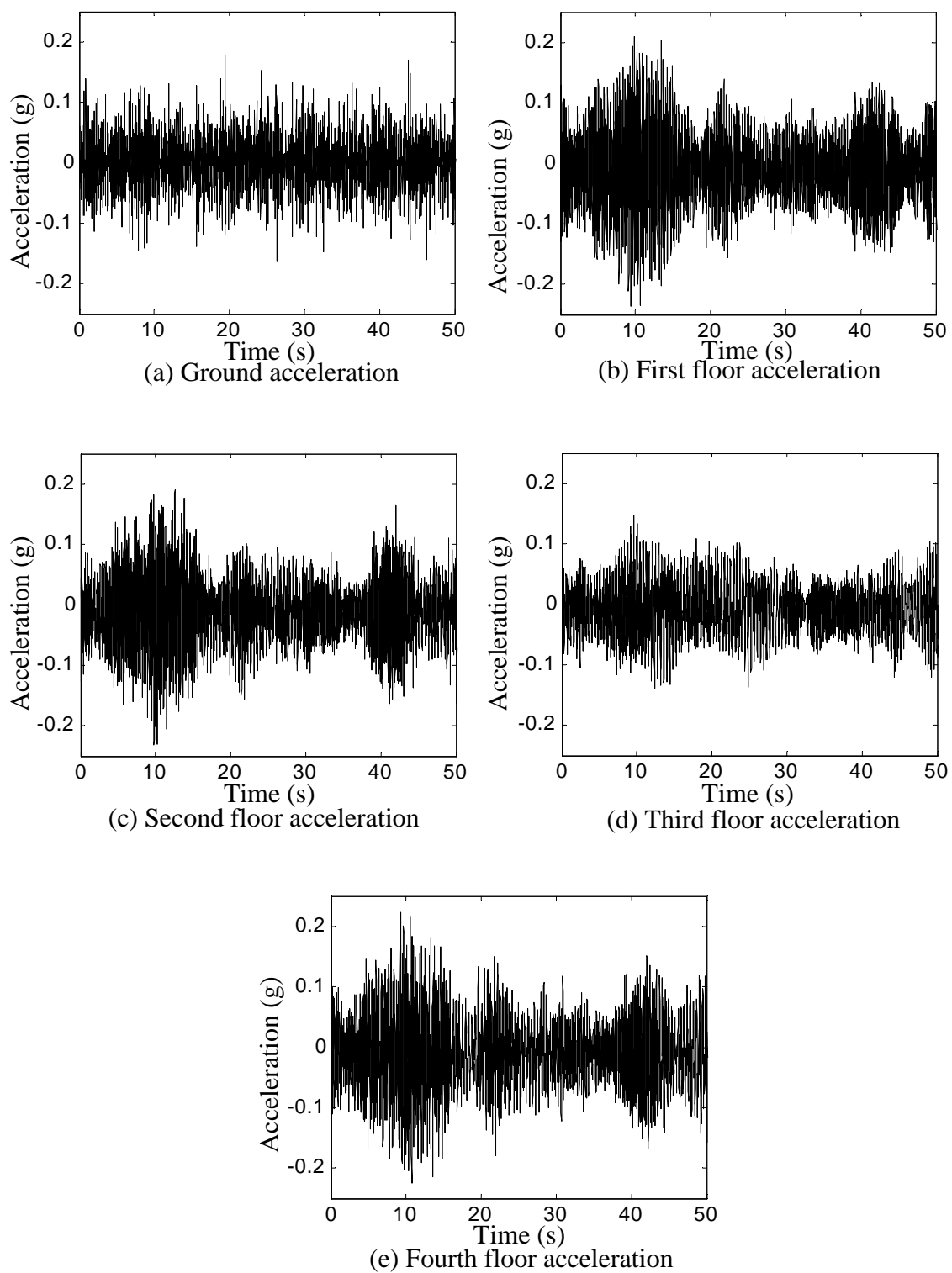


**FIGURE 5-4. Typical acceleration records.**

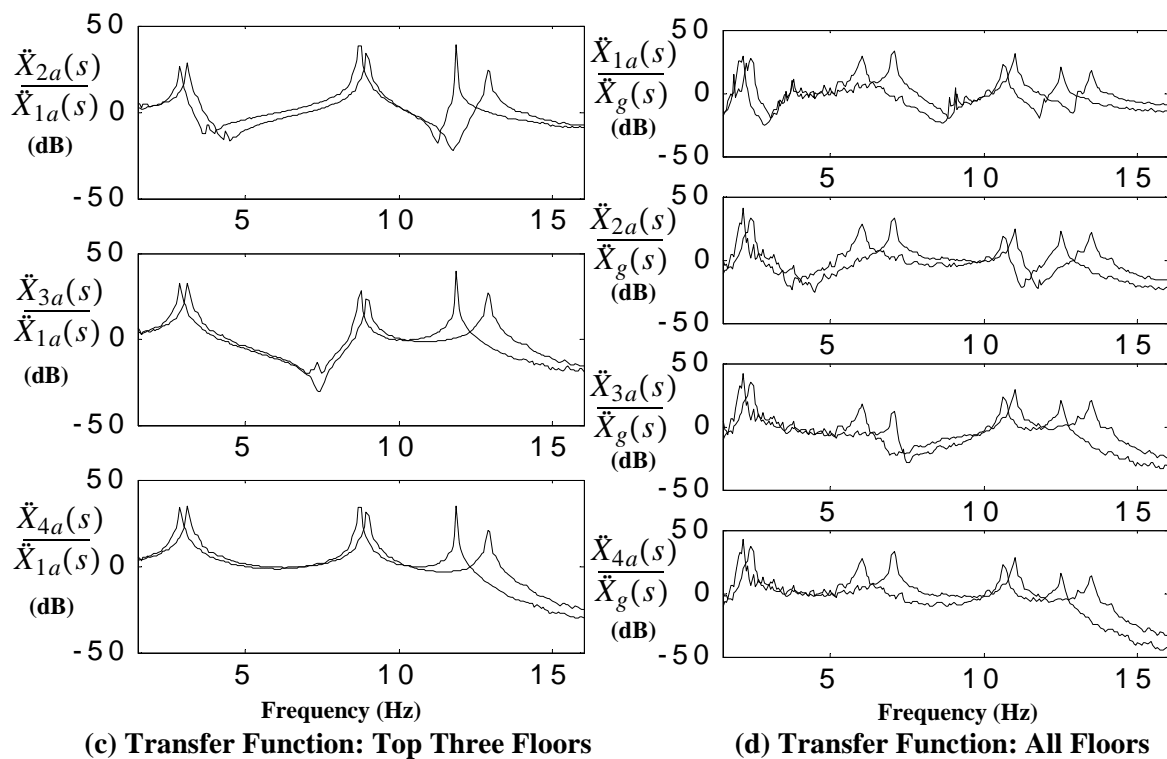
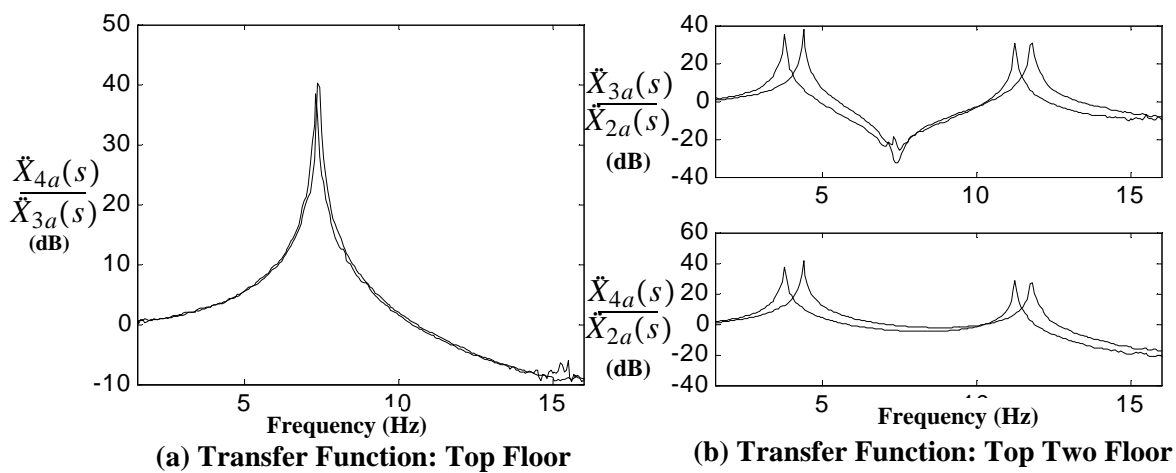
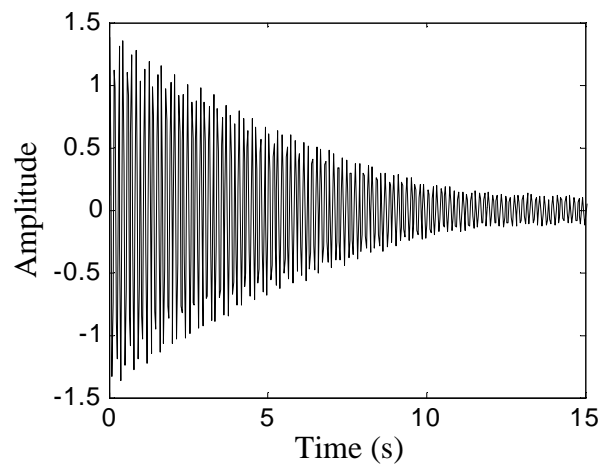


FIGURE 5-5. Experimentally Determined Component Transfer Functions.



**FIGURE 5-6. Frequency response function**

Although observation of the shifts in the peaks of the transfer functions may be used for initial inspection of the structure to identify the presence of damage, it is not appropriate for quantifying damage or identifying multiple damaged points. Thus, the ERA method is applied to the frequency response function obtained from the transfer functions. Figure 5-6 shows a typical frequency response function of the system. Using ERA the modal frequencies of the component systems are identified. Then, an optimization is used to determine the stiffness parameters.

The ERA method was applied to identify the natural frequencies of each component transfer function. The natural frequencies computed from the ERA state matrix are presented for the undamaged case in Table 5-1, in the rows designated “Experimental.” A lumped mass model is assumed and the nonlinear optimization is used to estimate the stiffness in each story. The resulting stiffnesses are provided in Table 5-2 for both undamaged and damaged cases, and the percent of stiffness loss estimated with this method. The component transfer function method yields a 33.9% and 32.8 % reduction the stiffness of the first and third floors, respectively. This correlates well with the approximately 33.3% loss in stiffness in the experimental structure by removing the

columns. A small change in the stiffness of the other floors is also observed. This result is primarily due to modeling errors associated with the assumption of a lumped mass model.

Using the identified stiffnesses for the undamaged case, the natural frequencies are recomputed and are shown in Table 5-1 in the rows designated “Model.” The high correlation between these natural frequencies and those directly from the ERA state matrix eigenvalues indicates that the nonlinear optimization performs adequately.

**TABLE 5-1. Natural Frequencies of the Experimental and Analytical (Lumped Mass) Systems.**

Floor	Source	1st Natural Freq. (Hz)	2nd Natural Freq. (Hz)	3rd Natural Freq. (Hz)	4th Natural Freq. (Hz)
4th	Experimental	7.3248	–	–	–
4th	Model	7.3248	–	–	–
3rd	Experimental	4.3625	11.6907	–	–
3rd	Model	4.3625	11.6961	–	–
2nd	Experimental	3.1185	8.9061	12.8700	–
2nd	Model	3.1109	8.9061	12.7902	–
1st	Experimental	2.3666	7.0220	10.9447	13.3859
1st	Model	2.3993	7.0220	10.8488	13.2089

**TABLE 5-2. Identified Stiffnesses to Construct Analytical Model.**

	1st Story (kN/m)	2nd Story (kN/m)	3rd Story (kN/m)	4th Story (kN/m)
Undamaged	44.933	46.690	46.971	51.936
Damaged	29.688	48.540	31.570	50.460
Stiffness Loss	33.9287%	-3.9610%	32.7892%	2.8423%

## 5.4 Summary

In this section the component transfer function method was discussed and experimentally verified. This method provides a means of identifying the existence of damage in a structural system. The method is based on component transfer functions, which are transfer functions between two sensors on the structural system. One advantage of this method is that the component transfer functions can be examined to first determine if damage is present in the structure. Damage identification and quantification is only needed if damage is indicated. A systematic procedure is applied to identify the stiffnesses of the structure based on the component transfer functions. By comparing the identified stiffnesses to those of the baseline structure the damage is quantified. Note that this technique appears to be best suited for lumped mass systems. Further studies are necessary before applying this technique to distributed systems. An experiment is performed to verify the technique. The loss in stiffness determined in the experiment matches the actual loss in stiffness of the experimental structure.

## Chapter 6

### Conclusions and Future Work

This thesis focuses on the development and implementation of two techniques for structural health monitoring. The first methodology is a three step methodology which uses the Natural Excitation Technique (NExT) in conjunction with the Eigensystem Realization Algorithm (ERA) to obtain the modal parameters. A least squares solution of the eigenvalue problem is employed to obtain stiffnesses of the structure. The second health monitoring technique uses component transfer functions to detect damage in the structure. This chapter will summarize the important contributions of the thesis and provide some directions for future work.

The effectiveness of the first technique was examined by applying it to phase I of the IASC-ASCE structural health monitoring benchmark problem. First, various issues relevant to the implementation of this methodology are investigated using a shear model of the four story building. The first study considered the accuracy of the methodology when different frame lengths were used in the calculation of the spectral density functions. This study showed that the methodology was not sensitive to the length of the frame for the spectral density function calculation. Frame lengths of 1024–4096 were considered in this study. However, there was a small bias error in the stiffnesses identified which was attributed to leakage in the spectral density function calculations. These bias errors were found to be small relative to the damage. Also, the technique was found to be relatively insensitive to noise in the measurements. Damage levels were accurately determined even with noise levels of up to 350% RMS of the RMS value of the roof

acceleration. The effect of modeling errors were also considered by using a 120 DOF model of the same structure to generate the response data. Some leakage of the loss in stiffness was observed in the undamaged floors of the structure. Although the location of the damage was identified correctly, this issue was found to be the most significant source of error.

Based on what was learned in these implementation investigations, the technique was applied to the damage cases delineated in phase I of the IASC-ASCE benchmark problem. The methodology was used to find damage in the structure for all six cases. The technique was applied directly in cases 1 through 5. The method performed well, and the location and extent of damage was accurately determined. However, in case 6 (limited sensors are available), the least squares solution of the eigenvalue problem cannot be used directly. An iterative process was developed for this case. This iterative process was successful in identifying the location of possible damage locations. In some cases damage was indicated where no damage existed (*i.e.*, there were some false positives in the results). However, for this problem, the method did not miss any damage locations (*i.e.*, there were no false negatives).

The second health monitoring strategy developed in this thesis is the component transfer function technique. This technique allows one to identify damage in the structure by examining the transfer functions of acceleration records between floors. Observing changes in the component transfer function provides an indication of the existence and location of damage in the structure. An iterative approach is described to determine the precise location and the extent of the damage. The extent of damage is determined by comparing stiffness values before and after damage. These stiffness values are calculated using a nonlinear optimization. Experimental verification of this technique was conducted using a 4 story structure subjected to a ground excitation. Damage was induced in the structure by removing columns at the first and third floors. The

component transfer function technique was successfully applied to determine the location and extent of the damage.

### ***Future Work***

The two structural health monitoring techniques discussed in this thesis were found to be applicable for the studies herein. The methods have not been investigated for more complex structures and different loading scenarios. The following paragraphs provide some suggestions for further study of these techniques.

As discussed in chapter 2 the Natural Excitation Technique is developed for an ideal stationary white noise excitation. Various researchers have successfully applied this technique in the case of non-stationary, non-white excitations. Future investigations could be conducted to determine the efficacy and limitations of the technique in these situations. This might involve a combination of theoretical and experimental studies. This study would allow the implementation of the technique for cases such as earthquake excitation.

The least squares solution of the eigenvalue problem works well when the points of the mode shapes are identified (full sensors). For the case in which a limited number of sensors are available, an iterative procedure was developed. Further investigation is needed in this iterative procedure to establish if the method converges in all situations, and to improve the results obtained.

Bias errors were observed in the calculations of the natural frequencies with ERA from the correlation functions obtained with NExt in the studies discussed in chapter 3. Additional work is necessary to a better understanding of the causes and possible solutions of this bias errors.

Experimental verification of the first structural health monitoring technique would be useful to establish the applicability of the technique. This is planned as part of the phase II IASC-ASCE structural health monitoring benchmark problem.

Further investigation is also necessary for the component transfer function technique. As defined in this thesis this technique requires a measurement of the ground excitation to identify damage in the first floor. Thus, as formulated, damage in the first floor cannot be identified when the excitation is due to wind or other forms of forced excitation. Additional work is necessary to adapt this methodology for this situation.

The component transfer function technique was found to be very effective for the study of a structure that behaves as a lumped parameter model. In the case of a distributed system, the method is not applicable as yet. Further study is needed before this technique could be applied to a distributed system.

## References

- [1] Au, S.K., Yuen, K.V. and Beck, J.L., “Two-stage System Identification Results for Benchmark Structure”, *Proceedings of the 14th ASCE Engineering Mechanics Conference*, Austin, Texas, May 21-24, 2000.
- [2] Beck, J.L., May, B.S., and Polidori, D.C., “Determination of modal parameters from ambient vibration data for structural health monitoring”, *First World Conference on Structural Control*, California, USA, 3-5 August 1994.
- [3] Bendat, J.S. and Piersol, A.G., “Random Data. Analysis and Measurement Procedures”, John Willey and Sons, Inc, 2000, New York City, NY., 2000.
- [4] Bernal, D. and Gunes, B., “Observer/Kalman and Subspace Identification of the UBC Benchmark Structural Model”, *Proceedings of the 14th ASCE Engineering Mechanics Conference*, Austin, Texas, May 21-24, 2000.
- [5] Black, C.J. and Ventura, C.E. “Blind Test on Damage Detection of a Steel Frame Structure,” *Proceedings of the 16th International Modal Analysis Conf.*, Santa Bar-bara, California, Feb. 2–5, 1998.
- [6] Caicedo, J.M., Dyke, S.J. and Johnson, E.A., “Health Monitoring Based on Component Transfer Function”, *Proceedings of the 2000 International Conference on Advances in Structural Dynamics*, Hong Kong, December 2000.
- [7] Caicedo, J.M., Dyke, S.J. and Johnson, E.A., “NExT and ERA for Phase I of the IASC-ASCE Benchmark Problem: Simulated Data.” *Journal of Engineering Mechanics*, ASCE, (submitted April 2001).
- [8] Caicedo, J.M., Marulanda, J., Thomson, P., and Dyke, S.J. “Monitoring of Bridges to Detect Changes in Structural Health,” *Proceedings of the 2001 American Control Conference*, Arlington Virginia, June 2001.
- [9] Chang, F.K. *Structural Health Monitoring*, Proceedings of the 2nd International Workshop on Structural Health Monitoring, Stanford University, Technomic Publishing Co., Lancaster, PA, September 8-10, 1999.
- [10] Chopra, A.K., *Dynamics of Structures*, Prentice Hall Inc., Upper Saddle River, NJ, 1995.
- [11] Cook, R.D., Malkus, D.S. and Plesha, M.E., *Concepts and Applications of Finite element Analysis*, John Wiley & Sons Inc., New York City, NY, 1989.

- [12] Corbin, M., Hera, A., and Hou, Z., "Locating Damage Regions Using Wavelet Approach", *Proceedings of the 14th ASCE Engineering Mechanics Conference*, Austin, Texas, May 21-24, 2000.
- [13] Dorf, R.C. and Bishop, R.H., *Modern Control Systems*, Addison-Wesley Longman, Inc., Menlo Park, CA, 1998.
- [14] Doebling, S.W., Farrar, C.R., Prime, M.B., and Schevitz, D.W. *Damage Identification and Health Monitoring of Structural and Mechanical Systems from Changes in their Vibration Characteristics: A Literature Review*, Los Alamos Report, LA-13070-MS, May, 1996
- [15] Doebling, S.W., Farrar, C.R., and Prime M.B., "A Summary Review of Vibration-Based Damage Identification Methods", *The Shock and Vibration Digest*, Vol 30, No 2., pp 91- 105, 1998.
- [16] Dyke, S.J., Caicedo, J.M., and Johnson, E.A., "Monitoring of a Benchmark Structure for Damage Detection," *Proceedings of the 14th ASCE Engineering Mechanics Conference*, Austin, Texas, May 21-24, 2000.
- [17] Dyke, S.J., Bernal, D., Beck, J.L., and Ventura, C., "Introducing an Experimental Benchmark Problem in Structural Health Monitoring," *Book of Abstracts, Joint ASME/ASCE Mechanics and Materials Conference*, Arlington, Virginia, June 27-29, 2001.
- [18] Farrar, C.R., Baker, W.E., Bell, T.M., Cone, K.M., Darling, T.W., Duffey, T.A., Eklund, A. and Migliory A., "Dynamic characterization and damage detection in the I-40 brodge over the Rio Grande," *Los Alamos National Laboratory*, Report LA-12767-MS., 1994.
- [19] Farrar, C.R. and James, G. H., "System identification from Ambient vibration measurements on a bridge," *Journal of Sound and Vibration*, 205(1) p 1-18, 1997.
- [20] Ghanem, R. and Shinozuka, M., "Structural-System Identification. I: Theory", *Journal of Engineering Mechanics*, Vol. 121, No. 2, February, 1995.
- [21] James, G.H., Carne, T.G., Lauffer J.P., Nord A.R., "Modal Testing using Natural Excitation", *Proceedings of the 10th International Modal Analysis Conference*, Sant Diego, California, 1992.
- [22] James, G.H., Carne, T.G. and Lauffer J.P., "The Natural Excitation Technique (NExT) for Modal Parameter Extraction From Operating Wind Turbines,"

Experimental Mechanics Department, Sandia National Laboratories Report SAND92-1666, Albuquerque, NM, Feb, 1993.

- [23] James, G.H., Carne, T.G., Mayes, R.L., “Modal Parameter Extraction from Large Operating Structures Using Ambient Excitation,” *Proceedings of the 14th International Modal Analysis Conference*, Darbon, Michigan, 1996.
- [24] Juang, J.-N. and Pappa, R.S., “An Eigensystem Realization Algorithm for Modal Parameter Identification and Model Reduction.” *Journal of Guidance Control and Dynamics*, 8, pp. 620–627, 1985.
- [25] Juang, J.-N. and Pappa, R.S., “Effects of Noise on Modal Parameters Identified by the Eigensystem Realization Algorithm,” *Journal of Guidance, Control, and Dynamics*, Vol. 9, No. 3, pp. 294-303, May-June 1986.
- [26] Johnson E.A., Lam H.F., Katafygiotis L. and Beck J., “A Benchmark Problem for Structural Health Monitoring and Damage Detection”, *Proceedings of the 14th ASCE Engineering Mechanics Conference*, Austin, Texas, May 21-24, 2000.
- [27] Katafygiotis L.S., Lam H.F., Mickleborough N., “Application of a Statistical Approach on a Benchmark Damage Detection Problem”, *Proceedings of the 14th ASCE Engineering Mechanics Conference*, Austin, Texas, May 21-24, 2000.
- [28] Lutes L.D., Sarkani S., “Stochastic Analysis of Structural and Mechanical Vibrations”, Prentice Hall, New Jersey, 1997.
- [29] Matlab<sup>®</sup>. The Math Works, Inc. Natick, Massachusetts, 1997.
- [30] Papoulis, A., “Probability, random variables, and stochastic processes”, McGraw Hill, New York, 1991.
- [31] Pappa, R.S., Juang, J.-N., “Some Experiences with the Eigensystem Realization Algorithm”, *Journal of Sound and Vibration*, pp. 30-34, January 1998.
- [32] Quast, P., Spencer, B.F., Sain, M.K. and Dyke, S.J., Microcomputer Implementations of Digital Control Strategies for Structural Response Reduction, *Microcomputers in Civil Engineering: Special Issue on New Directions in Computer Aided Structural System Analysis, Design and Optimization*, Vol. 10, pp. 13–25, 1995.

- [33] Rao R., Mitra S.K., “Generalized Inverse of Matrices and its Applications”, John Willey and Sons, New York, 1971.
- [34] Rytter, A., *Vibration Based Inspection of Civil Engineering Structures*, Ph. D. Dissertation, Department of Building Technology and Structural Engineering, Aalborg University, Denmark, 1993.
- [35] Salawu, O.S., “Detection of Structural Damage through Changes in Frequency: a review”, *Engineering Structures*, Vol. 19. No. 9., pp. 718–723, 1997.
- [36] Schmidt, H., “Resolution Bias Errors in Spectral Density, Frequency Response and Coherence Function Measurements, I: General Theory”, *Journal of Sound and Vibration*, 101(3), 1985.
- [37] Schmidt, H., “Resolution Bias Errors in Spectral Density, Frequency Response and Coherence Function Measurements, III: Application to Second-Order Systems (White Noise Excitation)”, *Journal of Sound and Vibration*, 101(3), 1985
- [38] Shinozuka, M. and Ghanem, R., “Structural System Identification. II: Experimental Verification”, *Journal of Engineering Mechanics*, Vol. 121, No. 2., February 1995.
- [39] Thomson, P., Marulanda Casas, J., Marulanda Arbelaes, J., Caicedo, J. M., “Real Time Health Monitoring of Civil Infrastructures Systems in Colombia”, *Proceedings of the SPIE 6th Annual International Symposium on NDE for Health Monitoring an Diagnostics*, Newport Beach, California, 4-8 March, 2001.

# Vita

## Juan M. Caicedo

### EDUCATION

- Washington University, St. Louis, MO, M.S: Civil Engineering, 2001
- Universidad del Valle, Colombia, South America: B.S. Civil Engineering, 1998

### PROFESSIONAL HISTORY

- *Research Assistant* – Washington University Structural Control & Earthquake Engineering Laboratory, St. Louis, Missouri (January 1999–present)
- Assistant Engineer – Leca Ingenieros Soc LTDA, Cali, Colombia, South America (September 1997 – December 1998).
- *Undergraduated Teaching and Research Assistant* – Department of Civil Engineering Universidad del Valle, Cali, Colombia, South America (August 1996 – December 1997).
- Undergraduate Assistant – Research/Curriculum Planning Office, Universidad del Valle, Cali, Colombia, South America (August 1995 – August 1996).

### AFFILIATIONS

- Earthquake Engineering Research Institute
- Mid America Earthquake Center Student Leadership Council.

May 2001